The
University
Of
Sheffield.

A dynamic mesh approach to the 2D CFD modelling of ash deposition in solid fuel combustion

---

Yufei Tian

A thesis submitted in fulfilment of the requirements for the degree of
Master of Philosophy

University of Sheffield
Faculty of Engineering
Department of Mechanical Engineering

November 9, 2022

Declaration of Authorship

I, Yufei TIAN, declare that this thesis titled, “A dynamic mesh approach to the 2D CFD modelling of ash deposition in solid fuel combustion” and the work presented in it are my own. I confirm that:

- This work was done wholly or mainly while in candidature for a research degree at this University.
- Where any part of this thesis has previously been submitted for a degree or any other qualification at this University or any other institution, this has been clearly stated.
- Where I have consulted the published work of others, this is always clearly attributed.
- Where I have quoted from the work of others, the source is always given. With the exception of such quotations, this thesis is entirely my own work.
- I have acknowledged all main sources of help.
- Where the thesis is based on work done by myself jointly with others, I have made clear exactly what was done by others and what I have contributed myself.

Signed:

Date:

Abstract

In the foreseeable future, it is anticipated that the use of pulverized solid fuel will continue to grow. Technologies that utilized pulverized solid fuel as a co-firing fuel will prove indispensable to meet electricity demands as well as to combat the ever-increasing threat of global warming, especially in countries where fossil fuels remain the majority of energy source. However, the ash deposition formation remains a very complex process in the furnace, which involves physical and chemical processes that account for: ash-forming, transporting, sticking and consolidating. Each of which is a non-linear process that requires a careful analysis of the temperature-time history of the fuel particles.

In this thesis, the CFD methods are employed to predict the ash deposition for the EI Cerrejon coal and the recycled wood biomass air combustion in 2D mesh. The dynamic mesh model is also employed in the simulation. A new simulation method, combining with dynamic mesh, discrete phase model and mesh partition method, is developed in the parallel ANSYS FLUENT to simulate the accurate and smooth change of the deposit surface during the ash deposition processes. It is noted that the predicted deposit rate matches the experimental data. And this method has more steady simulation and takes one third of time when compared to the current mass redistribution method. The effect of flue gas velocity and the change of the deposition shape are also investigated. The results show that the increase of the flue gas velocity leads to the increase of the ash deposition rate in the coal air combustion case. And the ash deposition rate decreases in the biomass air combustion case when increased the flue gas velocity. It is noted that due to the change of the velocity distribution around tube caused by the change of the deposition shape, the ash particles accumulate at the windward stagnation point of the tube. In addition, the ash deposition for Zhundong lignite combustion is also investigated with this simulation method. The predicted ash deposition thickness is close to the Zhundong lignite experimental data.

Acknowledgements

Firstly, I would like to express my respect and appreciation to my supervisors: Prof. Mohamed Pourkashanian, Prof. Derek B Ingham and Prof. Lin Ma. Thanks to Prof. Mohamed Pourkashanian for providing me with this great opportunity and welcoming me into the Energy2050 research group, Prof. Derek B Ingham for his supports and encouragement during my difficult time and Prof. Lin Ma for his technical assistances and understanding as well as encouragement. Also, I would like to thank Dr. Xin Yang for his insightful discussions about my research. I really appreciate their help, support and understanding during the time when I'm not well. Without their supports and help, I would not be able to finish this thesis.

Secondly, I would like to thank all my colleagues in the research group (Jiaxin, Fangting, Tiantian). I will always remember the days we spent together.

Finally, I would like to thank my parents and my husband for their supports, especially during the Covid-19 pandemic and my sickness.

Contents

List of Figures

List of Tables

List of Abbreviations

AAEM	**A**lkali and **A**alkaline **E**arth **M**etal
AFT	**A**sh **F**usion **T**emperature
CFD	**C**omputational **F**luid **D**ynamics
DO	**D**iscrete **O**rdinates
DPM	**D**iscrete **P**hase **M**odel
DRW	**D**iscrete **r**andom **W**alk
FT	**F**luid **T**emperature
IDT	**I**nitial **D**eformation **T**emperature
JKR	**J**ohnson-**K**endall-**R**oberts
PACT	**P**ilot-scale **A**dvanced **C**apture **T**echnology
RANS	**R**eynolds **A**veraged **N**avier–**S**tokes
RTE	**R**adiative **T**ransfer **E**quation
UDF	**U**ser **D**efined **F**unction
UKCCSRC	**UK** **C**arbon **C**apture and **S**torage **R**esearch **C**entre
WSGGM	**W**eighted-**S**um-of-**G**ray-**G**ases **M**odel

List of Symbols

$\vec{a}$	area vector	
C_L	time scale constant	
C_D	drag coefficient	
d	diameter	m
d_m	maximum spread ratio	
E^*	excess energy normalized by the surface energy	J
E_p	Young's moduli of the particle	$\mathrm{kg/(m\,s^2)}$
E_s	Young's moduli of the surface	$\mathrm{kg/(m\,s^2)}$
$\vec{F}$	force	$\mathrm{kg\,m/s^2}$
f_{melt}	melt fraction of the deposit	
h	height of the ash sample	m
l_m	mixing length of the flow	m
m	deposit mass	kg
R	kinematic restitution coefficient	
Re	Reynolds number	
S	area of the mesh face	$\mathrm{m^2}$
T	temperature	K
u_a	averaged gas velocity	m/s
$\tilde{u}$	instantaneous gas velocity	m/s
$\bar{u}$	time-mean gas velocity	m/s
u'	fluctuating gas velocity	m/s
U_p	normal component of the particle impact velocity	m/s
$\vec{v}$	velocity	m/s

V_{cr}	critical velocity	m/s
We	Weber number	
α	angle coordinate for tube	°
γ_{LV}	liquid-vapour surface tension	N/m
$\Delta\delta_i$	increased thickness of ash deposition	m
$\Delta\bar{\delta}_i$	averaged increased thickness of ash deposition	m
Δm_i	collected deposition mass	kg
η_{stick}	sticking efficiency	
θ	contact angle	°
k	turbulent kinetic energy	J/kg
K	effective stiffness parameter	
μ	dynamic viscosity	Pa·s
ν_p	Poisson's ratios of the particle	
ν_s	Poisson's ratios of the surface	
ν_t	eddy viscosity	$\mathrm{m^2/s}$
ρ	density	$\mathrm{kg/m^3}$
τ	life time of the fluid eddy that the particle is traversing	s
ε	dissipation rate	J/(kg s)
$\varepsilon_{\mathrm{deposit}}$	porosity of the ash deposition	
ς	normally distributed random number	

Dedicated to my parents and my beloved husband

Chapter 1

Introduction

1.1 Background information

1.1.1 Energy consumption

Energy is playing an important role in social development and economy growth. Through the progressive development of technology for harnessing energy, a rich tapestry of human activities and cultural diversity is sustained across the whole spectrum of human history. Since the start of the industrial revolution, the degree of energy utilization has seen a substantial increase in all industrial sectors. This is a trend that is likely to continue for the next few decades due to the continued rise of human population and the need of socio-economic development (B.P. Statistical Review, 2020).

As noted in the B.P. Statistical Review (2020) report, fossil fuels remain the dominant source for energy consumption (accounting for more than 80% of the total (Figure 1.1)), which is partly driven by their high energy density and the relatively inexpensive cost of their production. Fossil fuels come with a rich variety and they can be broadly divided into three types: oil, coal and natural gas. The type of fuel favoured by each community depends on its availability as well as the technological means to extract the fuel. For instance, in south and central American nations, oil accounts for more than

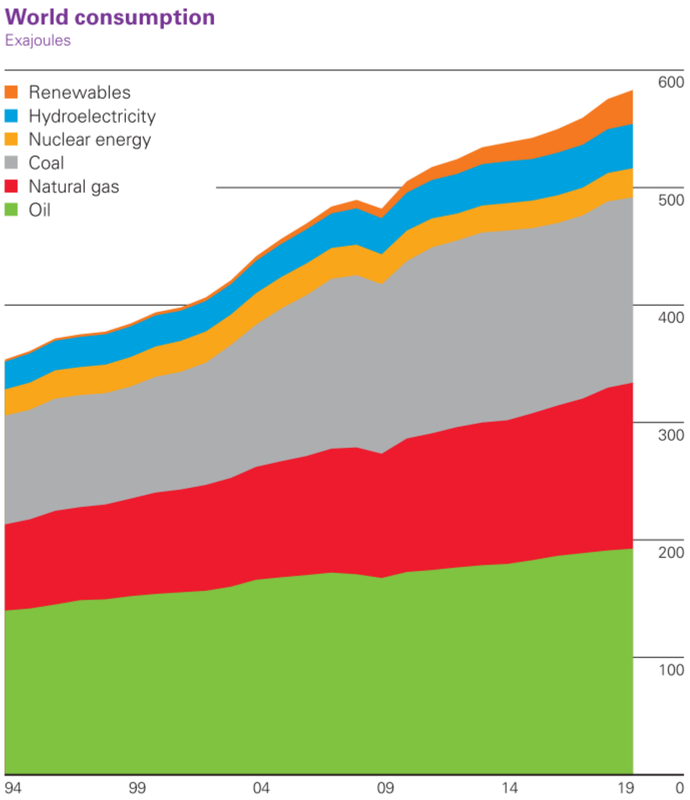

FIGURE 1.1: World energy comsumption(B.P. Statistical Review, 2020)

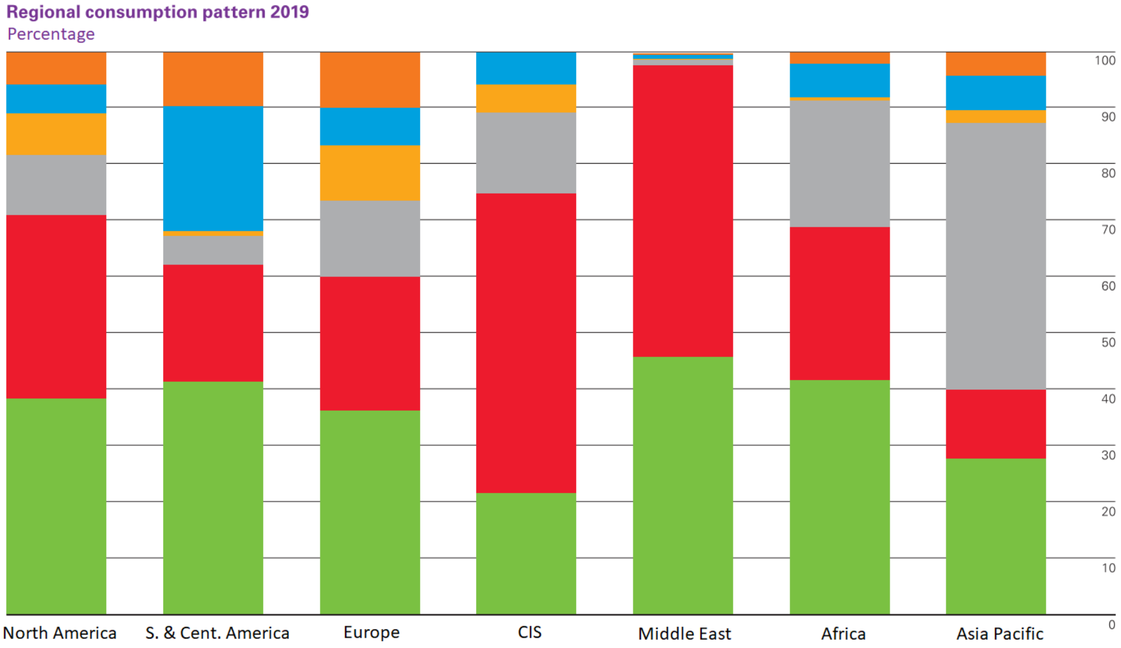

FIGURE 1.2: Regional consumption pattern in percentage 2019(B.P. Statistical Review, 2020)

30% of the energy consumption whereas in Asian Pacific nations, the majority of the energy share comes from coal powered stations (see Figure 1.2). Regardless of the fuel types, however, it is a common knowledge that combusting fossil fuels may result in the release of a variety of toxic chemicals that are detrimental to the local environment. For example, carbon dioxide CO_2 is identified as the main constituent that is responsible for global warming whereas sulphur dioxide (SO_2) and the oxides of nitrogen (NOx) are identified as prime drivers for acid rains and urban smog (Lokare et al., 2006). To mitigate the environmental impact whilst still being able to meet energy demand, two approaches are generally adopted in parallel. One is to shift reliance on fossil fuels to alternative forms of energy such as renewable or nuclear (Saidur et al., 2011) and the other is to improve the existing production techniques so that the toxic chemicals can be suitably isolated and captured prior to being released into atmosphere.

Fossil fuels are formed naturally from deceased plankton and plants under the consistent heating and pressurized condition deep in the Earth's crust over a course of millennium. Driven by the process of photosynthesis, those fossilized plants contain a large reservoir of CO_2 content. If such a large quantity of carbon-based fuels are consumed within a short period of time (over the course of a few decades), then the release of CO_2 into the atmosphere will out-perform the CO_2-absorption capability of the Earth in a typical carbon cycle; resulting in a net increase of CO_2 concentration (Abbasi and Abbasi, 2010). Measurements on the greenhouse gases have revealed that there has been an accelerated growth of the greenhouse gases since the pre-industrial revolution. In fact, Garba (2012) has indicated that an alarming yearly rate of 2.2% increase in CO_2 concentration may be observed currently, which is clearly not sustainable. One promising solution is to use *biomass* as a means to balance the production and absorption of CO_2 content in the atmosphere. Biomass, similar to fossil fuels, is derived from deceased plants but on a much shorter time scale. By carefully cultivating the right amount of vegetation used for biomass fuels, one can theoretically reach a neutrality point where no net addition of CO_2 is released into the atmosphere.

There are several methods for converting biomass into useful forms of energy(McKendry, 2002). The main energy utilization of biomass is combustion, gasification and pyrolysis (Saidur et al., 2011). Biomass is typically burnt along with coal as a partial substitute for a mixture of the fuels used in an efficient coal-fired boiler. The co-firing with biomass proves to be the most cost-effective way of reducing CO_2 emission on existing systems with relatively minor modifications (Loo and Koppejan, 2012).

1.1.2 Ash deposition issues

The burning of solid fuels often gives rise to ash particles that are transported across the combustion system. Depending on the nature of the ash particles, they may deposit along flue gas paths. Commonly, the ash deposition can be identified as either *slagging* or *fouling*.

Slagging deposits are formed when melt or softened ash particles that are not sufficiently cooled to solid state reached the heated walls. The temperature on the walls causes the particles to partially fuse together resulting in a deposit that is characterized by an outer molten ash layer on top of a powdery inner layer. They are commonly found on furnace walls or other regions in the boiler subjecting to a high and consistent radiation impact. If those deposits are left untreated, they may cause the shutdowns of the boilers, which would increase the operational cost and decrease the lifetime of the combustion systems.

Fouling, on the other hand, is typically formed when materials from the flue gas accumulate on solid surfaces that are placed in the convective pass of a boiler. The fouling materials can be organic or inorganic substances and they are usually distinguished from other surface deposits in that the fouling process tends to obstruct the function of the components in the system (such as the superheaters and reheaters). Accordingly, depending on the flue gas temperature, two types of the fouling process can be identified. High temperature fouling, which occurred in the temperature range 900°C to 1300°C, is characterized by the formation of partially fused and sintered ash deposits. Low temperature fouling, on the other hand, is identified by the formation of the loose or slightly sintered deposits, which typically occurs in the temperature range 300°C to 900°C (Weber et al., 2013b; Yang, 2017).

Slagging and fouling occur at different parts of the boiler. For example, Figure 1.3 shows a schematic representation of a conventional pulverized fuel boiler configuration with regions of slagging and fouling. Slagging mainly occupies in the combustion chamber in which the high temperature in the region causes a molten slagging deposit to build up on the refractory wall lining. The slagging deposit behaviour is a major consideration in boiler design. Similarly, fouling deposits affect the proper functioning of the exchange surfaces as in superheaters and reheaters. The build up of the fouling layers could reduce the total thermal efficiency of the boiler and, in some extreme cases, it could also impede the stable operation (Weber et al., 2013b). The effect of the fouling build-up may be mitigated by carefully positioning the convective tube and optimizing the spacing of the heat exchange surfaces (Akar et al., 2013).

1.2 Inorganic constituents in solid fuels

1.2.1 Origin of inorganic constituents

Coal is a major source of fossil fuel for electricity generation. It is derived from the accumulated plant matter on a time scale that spans over millions

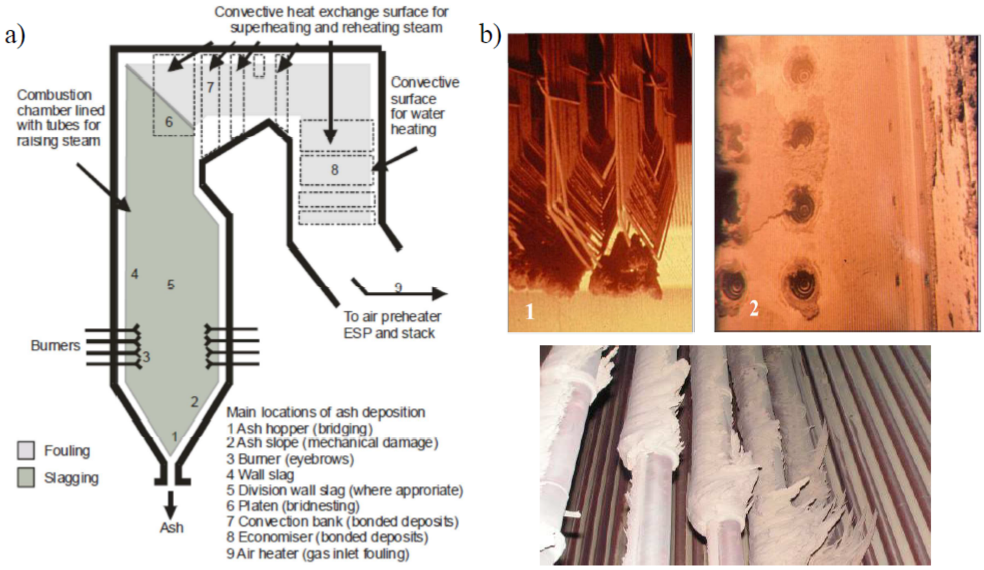

FIGURE 1.3: a) Regions of slagging and fouling in typical boilers, b) Images of ash deposits found in coal-fired boilers: 1 - platen superheater, 2 - furnace wall, 3 - at the entrance to convective pass of boiler (Akar et al., 2013).

of years through a slow coalification process. Due to the extreme conditions during its formation, coal is identified as a combustible sedimentary rock, which may also be contaminated with inorganic impurities. The quality of the coal depends on several factors such as the geological conditions, temperature, pressure and climate. The most common mineral found in coals are clay minerals (such as kaolinite, illite, muscovite and montmorillonite) and carbonates (such as calcite, dolomite and ankerite)(Płaza, 2013; Bradley Adams et al., 1985). Sulphides and Silicon dioxide can also appear in the coal.

Biomass fuels are a type of solid fuel that consist mostly of biodegradable matter. Those matter can derive from a variety of sources such as plant, animal matters or any substances that originate, either directly or indirectly, from them. A wide variety of sources can be used as biomass such as pulverized wood, residues from animals, sewage sludge and dedicated energy crops (Płaza, 2013).

Inorganic constituents of biomass fuels are important factor in determining the combustion efficiency. These substances may accumulate during the various stages of the plant's utilization cycle. In the growing phase of the plants, for instance, the inorganic substances absorbed from the soil enable the proper functioning of the photosynthesis process through which the plant metabolism and physiology are developed. In addition, inorganic substance can also enter the accumulation chain via contamination during the processing stage for the biomass fuel, which may include harvesting, handling and storage. It is noted that for a typical plant-based biomass fuel, such as straw, the main constituent chemical elements are Nitrogen (N), Phosphorous (P), Calcium (Ca), Magnesium (Mg) and Sulfur (S) (Loo and Koppejan, 2012; Vassilev et al., 2010). The use of fertilizer can also boost the concentration of potassium, chlorine and nitrogen to a significant degree.

The mineral composition of different types of biomass varies significantly. In woody biomass, for example, there is a higher content of calcium whereas in agricultural wastes, such as straw, there is more potassium, chlorine and silica. Animal residues, which includes animal bones and meat residues, are rich in phosphorous and calcium (Płaza, 2013). Sewage sludge, a product of the waste water treatment process, contains very high quantities of inorganic materials, which include silicates, aluminates, calcium, magnesium, nitrogen, phosphorous and some heavy toxic metals (Zn, Pb, Cu, Cr, Ni, Cd, Hg and As) (Płaza, 2013; Tortosa Masiá et al., 2007).

1.2.2 Association of inorganic constituents with organic matter

In addition to the organic matter and moisture found in solid fuels, inorganic constituents can also exist. Those can be categorized into three major groups: organically associated inorganic elements, water-soluble slats and mineral

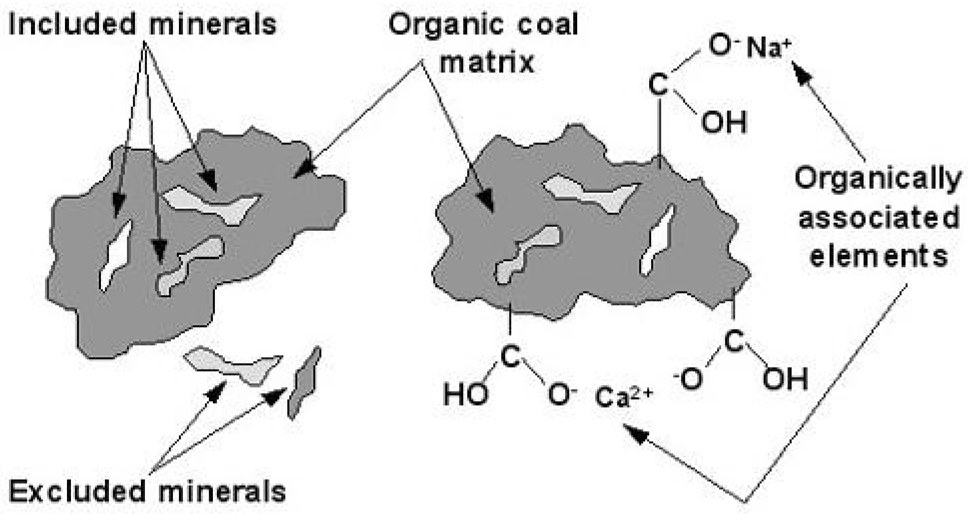

FIGURE 1.4: Types of ash forming elements associated in solid fuels(Płaza, 2013).

inclusions. Mineral inclusions are further divided to *included* and *excluded* minerals (Falcone et al., 1984), as is shown in Figure 1.4. The included minerals are inherent in the organic matrix, but not chemically bound to the fuel matrix, whilst the excluded minerals are individual mineral grains (Yang, 2017).

Organically associated elements are part of the organic structure of a solid fuel, which can be metals and non-metals bound with the fuel matrix. In the case of metals, they are mostly associated with organic functional groups (carboxylic acids and chelates) in the form of metal cations such as Na^+, K^+ and Ca^{2+}(Yang, 2017; Falcone et al., 1984). The organic part of the fuel matrix is commonly associated with organically bound non-metals, such as sulfur, phosphorous and chlorine, which are established by the application of the covalent bonds between the organic matrix and the inorganic constituents. Water-soluble salt includes simple dissolved salt in the pore water of the solid fuels and the salts dissolved in biomass plant fluids. The most common metal cations are potassium, sodium and calcium (Płaza, 2013). Mineral inclusions are divided into included minerals (inherent in the organic matrix) and excluded minerals (individual mineral grains). The minerals can be accumulated during the growth phase of the biomass or during the processing stages such as harvesting, handling and storing of the fuels (Płaza, 2013; Zevenhoven, Yrjas, and Hupa, 2010). Minerals, such as quartz, calcium oxalate, iron oxide or hydroxides, are most common in biomass fuels (Płaza, 2013).

1.3 Ash deposit formation

The mechanism of ash deposition on heat transfer surfaces includes complex physical processes that account for the formation, transportation and accumulation phase of ash particles during a combustion cycle. These processes can be identified by four relevant steps. Those are: 1) the process of breaking and releasing of ash particles from ash-forming elements of the solid fuels during the combustion cycle; 2) the transportation phase of the particles to the deposition surfaces due to the release of the flue gas and the effect of thermal convection; 3) the fusion and adhesion of the particles settled on the heat transfer surfaces; 4) the consolidation of the deposit due to the effect of heat conduction and cooling of the deposition particles (Płaza, 2013).

1.3.1 Release of ash forming elements

The releasing of ash particles from ash-forming elements determines directly the size distribution of fly ash particles observed in the boiler, which is crucial in modelling the deposition process. In a typical cycle, pulverized fuels are injected together with the primary air into the combustion chamber. Due to the high temperature in the chamber, the fuel particles are being rapidly heated up at a heating rate of approximately 10^5 K/s and the moisture is evaporated. As a result, the volatile species are released (devolatilization), which may include combustible gases such as hydrocarbon compounds, hydrogen and carbon monoxide (Chen, 2012). The hot gas pushes the oxygen to react with the volatiles and the chars (mainly consist of fixed-carbons and non-reactive ash) in the fuel in a manner that might or might not occur simultaneously. During both the devolatilization and combustion phase, ionically and organically bound inorganic species (such as K, Ca, Cl, S and P) may release into the hot mixture resulting in the generation of an inorganic vapour, which may further react with the impurities in the fuels such as SiO_2 and Al_2O_3 (Bryers, 1996; Płaza, 2013). Non-reactive minerals in the fuel may remain in the chamber, during which several physical processes could occur to them such as phase transformation, fragmentation, melting and coalescence of the mineral matter. Typically, fragmentation and coalescence of mineral matters tend to produce larger and heavier particles (with a characteristic diameter above 1.0 µm) whereas submicron particles are likely generated during the vaporization and condensation phase of the transformation process (Doshi et al., 2009). For this reason, a bi-model particle size distribution is typically employed to account for those size variations.

1.3.2 Minerals transformation

Slagging is mainly caused by the accumulation of fly ash particles composed mostly of inorganic species. The main constituents of a slagging deposit are the iron-, calcium-, potassium-based minerals, which also include aluminosilicates and alkaline-earth metals (Ca and Mg). Alkali metals, such as sodium and potassium, may enhance the fouling process (Bradley Adams et al., 1985).

Irons are chemically bound in coal minerals, therefore they can exist in the form of a sulphide, carbonate or oxide. Pyrite (FeS_2), in particular, either existing in included or excluded minerals, is regarded as a key mineral in determining the slagging propensity of coal. During coal combustion, the excluded pyrite decomposes to pyrrhotite (FeS) and rapidly forms an iron sulphide melt (Fe-O-S) before full oxidation under reducing conditions

(McLennan et al., 2000; Bradley Adams et al., 1985). Therefore, the excluded pyrite can play a significant role in initiating the formation of slagging deposit. On the other hand, the included pyrite is more likely to be captured by the alumino-silicate to form low melting temperature eutectics, such as Fe-Al-Si eutectics systems, which aggravate the slagging problems (Yang, 2017).

Ca-based minerals are more likely to interact with alumino-silicates to form Ca-Al-Si eutectics with a low melting point, which can significantly increase slagging (Yang et al., 2017a). Moreover, since calcium is associated with the organic part of a coal matrix, they form sub-micron particles as part of the by-product of coal combustion, which may further react with SO_2 in the gas stream. This chemical reaction results in the creation of $CaSO_4$, which is the main constituent of an initial ash deposition layer (Płaza, 2013).

Alkali metals (potassium and sodium) exist in easily soluble forms in biomass fuels. In general, alkali metals are very reactive species and they tend to form sodium/potassium sulphates in the presence of sulphur oxides in the gas stream (Vassilev et al., 2013; Thy et al., 2006). The stickiness found on tube surface is attributed to the presence of those sulphates. Non-sticky ash particles are likely to adhere to the sticky layer - resulting in the acceleration of the fouling process in the convective section of boiler (Bradley Adams et al., 1985).

1.3.3 Ash transport and deposit formation

The formation of deposit on heat exchange surfaces is a direct consequence of the accumulation of fly ash particles. To reach the deposition surface, however, the particles must be transported in the presence of a flow and temperature field of the flue gas as well as the temperature difference on the solid walls. More specifically, once the fuel particles are injected from the burner region, transportation to the deposit surface is initiated and regulated by four main mechanisms. These are: 1) inertial impaction, which determines whether the particles are able to traverse through the streamline of the gas via its own inertial; 2) thermophoresis, which describes an additional transporting force due to the non-zero temperature gradient close to the heat exchange surface; 3) condensation, which is characterized by the production of a collection of vapour species on the surface; 4) diffusion, which is due to the non-zero gradient of localized particle concentrations.

Among the four mechanisms that contribute to the transportation of ash particles, inertia impaction is considered as the prime driver for the ash deposition formation. At higher deposit surface temperature, this mechanism becomes more dominant (McLennan et al., 2000; Taha et al., 2013; Zbogar et al., 2009). When particles are released, they generally have an initial velocity that may be different from the background flow field. This velocity difference propels the particles to traverse the different streamlines of the gas flow field. Impaction with the deposit surface can only occur if the particles have sufficient inertia to overcome the streamline effect, otherwise the particles may follow the streamlines and never reach the solid wall as a result. In addition to the initial velocity of the particles, the impaction rate also depends on the particle properties, gas flow properties and the targeted geometry. Moreover, close to the combustion region where the temperature is usually very high, the effect of condensation of vapour species is typically negligible compared to the inertia effect, thus the inertia impaction is assumed to be the major pathway on which particles are delivered to the deposit surface (Garba et al., 2013).

For small particles (< 10 µm), the effect of thermophoresis becomes important (Zbogar et al., 2009). This is caused by a non-zero temperature gradient close to the heat exchange surface, which produces a thermophoretic force that is opposite to the local temperature gradient. This force is produced when fluid molecules with higher kinetic energy displaces the molecules of lower energy. To this effect, when ash particles moving close to the solid surface there is a constant force directed towards the cooler region induced on the particles. Thermophoresis is more pronounced at initial deposition stage because of the lower deposition surface temperature. However, as the deposition layer grows, the surface temperature approaches that of the outer gas, which then lowers the influence of thermophoresis.

The condensation is the mechanism responsible for alkali deposit collected on the deposit surface. The condensation rate depends on the amount of the vapourised metal species (alkali/alkaline metal) and the temperature condition in the furnace (Yang, 2017). In general, biomass with higher alkali metal content are likely to produce condensation. In addition, the vaporization rate of metal species is also a function of the temperature in the furnace; higher temperature tends to enhance the vaporization capability (Leppänen et al., 2014). Condensation is a key process during the initial stages of the deposition formation on the fouling surfaces. There are three different methods of condensation (Zbogar et al., 2009; Li et al., 2015): 1) The homogeneous nucleation of vapours to form the fume particles and these particles are more likely to deposit on the surface due to the thermophoresis; 2) The direct condensation of vapour on the deposition surface; 3) The vapours condense on the other ash particles. As a result, the condensation can be a significant mechanism for low rank coal or biomass with a large amount of condensable species.

When a collection of vapours or small particles congregate over a localized volume of space, diffusion tends to regularize the buildup by creating a diffusive force that spreads the localized concentration apart. This is characterized by a non-zero particle concentration gradient. Fly ash particles can deposit on the surface via this mechanism. There are three types of diffusion (Zbogar et al., 2009): 1) The Fick diffusion due to the concentration gradient;

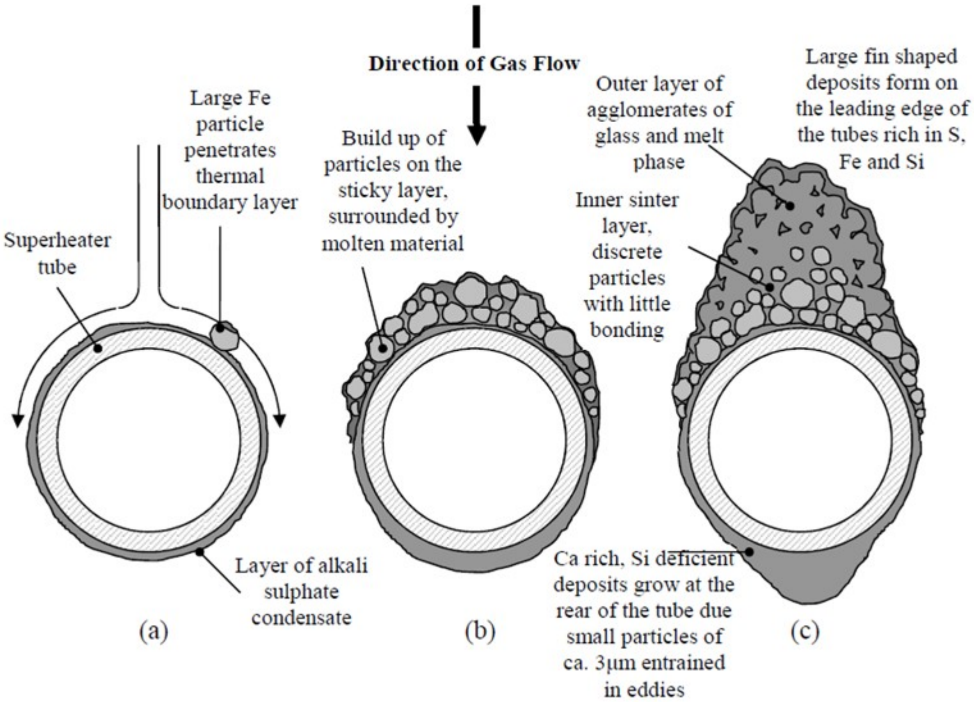

FIGURE 1.5: A schematic of the deposit growth on the superheater tube(Płaza, 2013; Bryers, 1996)

2) The Brownian diffusion-random movement of small particles; 3) The eddy diffusion-movement due to turbulent flow effects.

A schematic of the development of deposit on the superheater tube can be found in Figure 1.5. Once the particles hit the surface, there is a possibility that it may adhere to the surface or rebound. A ratio thus can be defined to quantify this effect. This is known as the *sticking efficiency*. Adhesion occurs as a result of the creation of van der Waals forces established between the deposit surfaces and the ash particles or because of the intrinsic stickiness of the molten particles. Furthermore, alkali vapours can condense directly on to the deposition surface and the ash particles surfaces, which leads to the formation of a sticky inner layer of deposits, which further accelerates the accumulation of other ash particles that impact on the tube (Zevenhoven, Yrjas, and Hupa, 2010).

1.4 Prediction of ash deposition formation

Ash deposition is a major concern in the daily operation of boilers. If the deposition layer is allowed to grow to a sufficient degree, it may impede the effective heat transfer and cause unexpected shutdown of the combustion systems (Weber et al., 2013b; Garba et al., 2013). For this reason, it is necessary to develop numerical models to simulate the ash deposition characteristics, which in turns will guide the choice on design parameters to minimize the risk of unstable operation of the boilers.

The formation of ash deposit results from several key physical processes that account for ash generation, transportation and deposition. The role of the transportation and deposition phase can be predicted by examining the time history of the ash particles, which further involves mechanisms that allow the ash to deposit on solid walls (e.g. particle transportation, particle impaction and sticking, deposit growth and etc). To model these two key processes, computational fluid dynamics (CFD) proves to be an indispensable tool, which allows a detailed temperature and flow field to be constructed. Currently, ANSYS FLUENT, which is a commercially available CFD code, is adopted to simulate the process of transportation and deposition. The code uses a finite volume method to discretize the computational domain for the gas phase. Subjecting to an inlet and outlet boundary condition as well as an initial condition, the transport equations are solved for the mass, momentum and energy balance (Fei, 2015). Since a global field is computed at once, the computational domain is regarded as Eulerian. Meanwhile the fly ash particles, or the discrete phase, are individually tracked and modelled. This is done in a Lagrangian frame (ANSYS Inc., 2020). Moreover, the deposition behaviours, which involves sticking and deposit growth, are simulated via the in-house developed models which are coupled with FLUENT via the User Defined Functions capability.

1.5 Thesis structure

This thesis focuses on using CFD methods to predict the ash deposition behaviours for coal and biomass combustion in the furnace. The ash deposition geometric evolution on the tube is also considered during the simulation. A new simulation method, which includes the implementation of a dynamic mesh model, is developed in order to obtain more accurate results and to stabilise the solution process. In Chapter 2, a literature survey on the state-of-art ash deposition prediction CFD models is presented. Chapter 3 introduces the CFD model adopted in this thesis. Chapter 4 presents a brief overview of the experimental facilities and data collection techniques that are used to develop and validate the ash deposition prediction models. Chapter 5 discusses the CFD modelling of the ash deposition for the EI Cerrejon coal (Coal) and the recycled wood (Biomass) and finally chapter 6 presents the CFD prediction of ash deposition for the Zhundong lignite. A summary of the works being conducted and some recommendations for future work are presented in Chapter 7.

Chapter 2

Literature review

Modelling ash deposition is a challenging task as it needs to account for all the physical processes that may occur during the combustion. An accurate solution requires the correct modelling of the transport process, the deposition process and the correct physical attributes of the medium in both the continuous and discrete phases. This chapter explores some of the state-of-the-art simulation techniques that are being widely used in the literature.

2.1 Overview of ash deposition prediction

The reliable and long-term operation of a boiler relies on mitigating ash build-up on its various subsystems. However, ash deposition is an inevitable process when burning solid fuels. Therefore it is necessary to study and understand how such a process evolves during a fuel's life cycle.

As discussed in section 1.3, the formation of ash deposit arises from four main mechanisms, namely ash generation (i.e. fuel combustion and dissociation of ash-forming elements), ash transportation (i.e. inertia impaction, thermophoresis, condensation and diffusion), ash adhesion or sticking and deposition growth. Various methods have been developed in the past to predict the deposition process in solid fuel combustions. However, they can all be categorized into two major groups. One belongs to the CFD methods, where a global computational domain is constructed to capture the deposition process in macroscopic detail. The other belongs to the empirical methods, where ash deposition indices are utilized. The latter provides a loose estimate of the degree of deposit occurring for certain fuel properties. The indices are mainly derived from experiments and they are useful in dictating the severity of the ash accumulation but lacking in physical and chemical information on how such processes evolve over the operation cycle of the boiler. CFD, on the other hand, is able to model both steady and transient phenomena, which can dynamically model ash transportation and deposition growth to an exceptional high degree of accuracy. Together with the increasing computational power of modern desktop, CFD becomes a preferred option in many high accuracy simulations of the ash deposition behaviour.

In this thesis, the CFD methods are employed to investigate and predict the ash deposition behaviour in the boilers.

2.2 CFD methods

The mechanism for ash particle transport and the aerodynamic behaviour of a boiler can be suitably simulated through the CFD approach. In the continuous phase (gas), the transport equations are solved for the basic flow variables such as temperature, velocity and pressure. Through this backdrop of the flow and temperature field, the ash particles are modelled by means of determining their trajectories either in a one-way interaction (the release of the ash particles does not appreciably affect the gas flow) or a two-way coupling (ash particles may enhance the turbulence diffusion of the gas which in turn may affect their trajectories); depending on the volume fraction of the ash particles present in the domain (Greifzu et al., 2016). The deposition process is initiated when particles impact on the solid surfaces. During this time, the sticking process can take place through which the impacting particle is determined whether it will adhere to the surface or rebound. In addition, other combustion behaviours can also be predicted by the CFD, which include energy and heat transfer (e.g. devolatilisation, volatile combustion, char combustion and etc) (Wang and Harb, 1997).

2.2.1 Solid fuel combustion and heat transfer

Solid fuel combustion is typically modelled as a dilute two-phase reacting flow consisting of a continuous phase (gas) and a discrete phase (fuel particles) (Chen, Lei, 2013). The gas in the boiler acts as a continuous medium in which the solid fuel particles are transported by virtue of fluid kinematic and thermal transport (Yang, 2017). In addition, the concentration of the discrete phase is considered dilute, meaning that the fluid flow in the coal combustion is a particle-laden flow so that both the Euler and the Lagrangian methods are employed simultaneously to solve the kinematic equations of the gas and the solid phases, respectively (Chen, Lei, 2013; ANSYS Inc., 2020).

In the fluid phase, the flow is considered to be turbulent and that the transient part of the gas motion is assumed negligible when the boiler has reached steady operation (Weber et al., 2013b). Therefore, a temporal-average operation can be performed on the Navier-Stokes equations, which result in the so called Reynolds Averaged Navier-Stokes (RANS) equations (ANSYS Inc., 2020). In this approach, the instantaneous flow is decomposed by a time-averaged component and a transient fluctuating part. The effect of turbulence is modelled by assuming that the stress tensor on the mean flow induced by the fluctuation is proportional to the averaged flow strain. This proportionality factor, which is known as the turbulent eddy viscosity, is determined by a closure equation which relates the eddy viscosity to the flow kinematic properties. The choice for the closure equation depends on the nature of the problem as well as computer resource constraints. For example, the zero-equation closure equations relates the eddy viscosity, say ν_t, to the averaged velocity gradient. i.e.

$$\nu_t = l_m^2 \left| \frac{\partial u_a}{\partial y} \right| \tag{2.2.1}$$

where l_m is the mixing length of the flow and u_a is the averaged velocity in the stream-wise direction. Although no additional equation is solved, it is well known that the zero-equation closure possesses severe limits on the types of flow for which the above assumption is accurate (Versteeg et al., 2007). Over the years, turbulence modelling has advanced to the point where additional equations are solved alongside the RANS equations. For instance, one popular one-equation model, known as the Spalart-Allmare model, is calibrated to work well with aerodynamic wall-bounded flows, whereas two-equation models, such as the standard $k - \epsilon$ models, are more suited for general industrial flow scenarios (ANSYS Inc., 2020).

For the discrete phase, the Lagrangian approach is generally adopted to resolve the time-history of the particle trajectories submerged in the fluid medium. The trajectory is determined from solving the kinematic equations of the fuel particles and are subsequently tracked throughout the interaction phase. Coal and biomass combustion modelling is proceeded by four steps: evaporation, devolatilization, volatile combustion and char combustion (Yang, 2017). Evaporation refers to the process of releasing of moisture in the fuel particles while devolatilization is the process of releasing organic compounds into the gas phase from the volatiles in the fuel. Volatile and char combustion are simply the chemical reactions with the oxygen molecules in the gas. The latter is typically initiated after the evaporation and the devolatilization phase (Black, 2014; Yang, 2017). It is noted that the behaviour of each step is quite different, therefore a separate model is usually required in the CFD framework.

The devolatilization process is sensitive to the temperature history of the boiler. In particular, the temperature variation can exert a strong influence on the kinetic and yields of the volatile species (Black, 2014). To account for this effect, the rate of volatile generation can be modelled by a rate equation whereby the rate of release of the volatile content from the particles can be modelled by a variety of empirical functions. The simplest approach is to assume a constant rate whose value depends on the initial mass of the particle, the fraction of the volatiles initially present as well as a tuning parameter. A more refined model uses a linear rate, which is a linear function on the amount of volatiles left in the particles (Garba, 2012). Char combustion is regulated by a diffusion process whereby gaseous oxidants from the gas stream are transferred to the chars' pore for reaction. The combustion rate therefore depends on a pore diffusive coefficient as well as a surface reactivity parameter indicating the chemical rate of the reaction. To characterize the process, the combustion rate is modelled. One of the most popular models for char combustion application is the *intrinsic model* developed by Smith (1982), which assumes that the order of the reaction is equal to unity and the combustion rate is a function of the gas temperature, densities of the reacting agents, surface area, pore diffusion rate and reaction rate.

Radiative heat transfer could account for approximately 90% of the total heat transfer in the radiation section of the boilers and furnaces (Yang, 2017). In CFD, the radiation is modelled by the radiative transfer equation (RTE)(ANSYS Inc., 2020). Solving the full RTE equation is considered an impossible task and there is an enormous body of research dedicated to finding its solution. In practice, however, an approximate solution often suffices to account for the important features in the transfer process. The discrete ordinate method (DO) is one such approach in which the angular variables associated with the radiation field is discretized by a finite number of angular intervals (ANSYS Inc., 2020; Chen, Lei, 2013). The integral contribution due to the scattering in the field is replaced by a weighted sum. Therefore, a linear system of equations may be constructed to obtain the approximate solution. Owing to the large size of the matrix in the system, an iterative method is typically employed such as the Gauss-Jordon elimination. The weighted-sum-of-gray-gases model (WSGGM), which assumes that the flute gas is composed of a transparent gas and several gray gases(Chen, Lei, 2013), is often employed to calculate the radiation characteristics of the gases.

2.2.2 Particle trajectory using DPM

The essential ingredient in modelling the formation of ash deposit is to understand how the ash particles are transported to the deposit sites. In section 1.3.3, we have discussed the main physical mechanisms that contribute to this process, namely the inertia impaction, thermophoresis, condensation and particle diffusions. The arrival rate of the particles on the deposit site depends on a combination of these effects. For modelling purposes, the ash particles can be treated as a Lagrangian particle, which means the ash particles are treated as point masses and whose equations of motion are prescribed in the Lagrangian frame. FLUENT models those particles via the Discrete Phase Model (DPM) module in which the trajectories are determined by the momentum conservation principle. Two modes of interaction can occur during the particle passage through the gas flow field. One is coined one-way coupling, which assumes that the ash particles do not affect the background gas flow field. If this is not the case, then a two-way coupling can occur which enhances the turbulence diffusion rate of the gas. Depending on the value of the volume fraction, a one-way coupling interaction can often be assumed (Greifzu et al., 2016). This then simplifies the calculation pipeline of the underlying solution procedure of FLUENT.

The kinematic equations satisfied by a Lagrangian particle are obtained via the momentum balance in each component. This is an example of Newton's second law. Let $\vec{v}_p$ denote the velocity vector of a Lagrangian particle and $\vec{v}_g$ be the background gas flow velocity, then the rate of change of $\vec{v}_p$ is given by (Yang et al., 2017b):

$$\frac{d\vec{v}_p}{dt} = \frac{18\mu_g}{\rho_p d_p^2}\frac{C_D Re_p}{24}\left(\vec{v}_g - \vec{v}_p\right) + \vec{g}\frac{(\rho_p - \rho_g)}{\rho_p} + \vec{F} \tag{2.2.2}$$

Here, ρ_p and ρ_g denote the density of the particle and gas, respectively. μ_g is the dynamic viscosity, d_p is the characteristic diameter of the particles, C_D is the drag coefficient, Re_p is the particle's Reynolds number and $\vec{g}$ is the acceleration due to gravity. Moreover, other additional forces such as thermophoresis force and Brownian force can be modelled by including a source term, i.e. $\vec{F}$, to the equations.

Although the effect of turbulence is modelled on the gas flow equations by means of the Reynolds averaging procedure, this is typically identified in the modified viscosity factor in the molecular diffusion term of the flow equations, the Lagrangian particles, on the other hand, do not usually experience this stochastic fluctuation due to the turbulent eddies if the mean velocity of the gas flow were to be used to advance the trajectory. Typically, this is corrected by subjecting the particle to interact with the turbulent eddies in succession. To this effect, a Discrete Random Walk (DRW) model is enabled, which includes an additional contribution to the mean velocity of the gas. During each interaction episode, the components of the gas velocity vector are added a pseudo-random number, which is generated from a Gaussian normal distribution with mean zero and a standard deviation $\sqrt{2k/3}$, where k is the kinetic energy of the interacting turbulent eddy. In two-equation models, such as the $k - \epsilon$, this is solved alongside the RANS equations. Therefore, this value is readily available at each volume cells and it only needs to be interpolated to the particle's location at the end of each eddy lifetime, which is characterized by $\tau_e = 2C_L k/\epsilon$, where C_L is a constant that depends on the turbulence model being used (ANSYS Inc., 2020).

At the time of the current research, only a few published articles have utilized the CFD framework to obtain the impaction result relating to the formation of ash deposit (Yang, 2017). A new revised particle impaction model was proposed by Yang et al. (2016), which aims to minimize the numerical discrepancies observed between the predicted and experimental results. The method uses an impaction correction factor and is coupled with the sticking efficiency to obtain a better agreement between the prediction and experimental data. It is noted that an accurate prediction of the ash deposition behavior is possible only if the particle sticking efficiency is taken into account (Weber et al., 2013a; Yang, 2017).

2.2.3 Particle sticking models

Not all ash particles impacting on the deposit site will stick to the surface. The sticking efficiency, defined as the ratio between the number of sticking particles and the total number of impacting particles, depends on several factors such as the physical and kinematic properties of the impacting particles as well as the properties of the deposition surfaces. Wieland et al. (2012) identified the key variables that relate to the sticking process of the ash particles. They are the viscosity of the ash particles, the kinetic energy of the impacting particles and the molten degree of the ash particles.

One of the earliest and most common sticking model is the viscosity-based sticking model introduced by Walsh et al. (1990). In such a model, the ash particles are assumed to always stick to the deposit surfaces whenever their viscosity is smaller than a reference value at a given particle temperature. To be more precise, let $\eta_{\text{stick}}(T)$ denote the sticking efficiency at a particle temperature T, then the model proposes that:

$$\eta_{\text{stick}}(T) = \begin{cases} \frac{\mu_{\text{ref}}}{\mu_p} & \text{if } \mu_p > \mu_{\text{ref}} \\ 1 & \text{if } \mu_p \leq \mu_{\text{ref}} \end{cases} \tag{2.2.3}$$

where μ_p is the particle viscosity and μ_{ref} is the reference viscosity for sticking. The value of the reference viscosity depends on the type of fuels being used in the furnace as well as the temperature range. For example, Table 2.1 presents some commonly used values for the reference viscosity for different types of furnaces.

Work	Boiler	Fuel	Reference viscosity
Walsh et al. (1990)	Pilot scale furnace	Bituminous US coal	8 Pa·s
Srinivasachar et al. (1992)	Lab scale furnace	Bituminous US coal	10^5 Pa·s
Huang et al. (1996)	Lab scale furnace	Bituminous US coal	10^4 Pa·s
Wang and Harb (1997)	Pilot scale and utility scale furnace	Sub-bituminous; lignite US coal	10^5 Pa·s
Rushdi et al. (2005)	Pilot scale furnace	Australian bituminous coal	10^8 Pa·s
Degereji et al. (2012)	Pilot scale furnace	Australian bituminous coal	10^8 Pa·s

TABLE 2.1: The reference viscosities used in the sticking models

The viscosity-based model requires the specification of the reference viscosity. Depending on the furnaces being used, the same fuel (e.g. Bituminous US coal) can result in a vastly different reference value. In fact, Taha et al. (2013) and Wieland et al. (2012) identified the reference viscosity for the Bituminous US coal is anywhere between 8 to 10^8 Pa·s. For instance, the value of 8 Pa·s may be used if molten silicates were present (Walsh et al., 1990).

This suggests that the correct choice for the reference viscosity is extremely sensitive to the temperature present in the particles. Without knowing their exact temperature distribution, the viscosity-based model is always prone to error. Moreover, it is known that the ash particles do not always appear as a molten mixture, instead, the instantaneous temperature of the ash particles can be much lower than their melting point. This presents a particular difficulty in deciding what value should be used for the reference viscosity since the ash particles now exist in a liquid-solid mixture. Fuels, such as the AAEM coals or biomass with a high alkali/alkaline content, when fired, tend to produce a wide variety of inorganic constituents as ash particles which can drastically reduce the predictive value of the viscosity-based models (Yang, 2017).

To circumvent the empirical nature of the viscosity-based approach, a more refined model that takes account of the kinematic properties of the ash particle may be developed. One such approach, based on the Johnson-Kendall-Roberts (JKR) theory, is the Brach & Dunn kinetic energy thresholding sticking model. In this approach, the dissipated energy caused by the impaction is computed. Sticking is thought to occur whenever the dissipated energy is higher than the initial kinetic energy of the particles (Weber et al., 2013b). Thus, based on the law of collision restitution, a single critical speed, normal to the impacting surface, can be identified, say V_{cr}, which is given as follows (Ai and Kuhlman, 2011; Brach and Dunn, 1992):

$$V_{\mathrm{cr}} = \left(\frac{2K}{d_p R^2}\right)^{10/7} \tag{2.2.4}$$

$$K = 0.51\left[\frac{5\pi^2\left(k_s + k_p\right)}{4{\rho_p}^{3/2}}\right]^{2/5} \tag{2.2.5}$$

$$k_s = \frac{1 - {\nu_s}^2}{\pi E_s} \tag{2.2.6}$$

$$k_p = \frac{1 - {\nu_p}^2}{\pi E_p} \tag{2.2.7}$$

where d_p is the characterized particle diameter, R is the coefficient of restitution, E and v are the Young's modulus and the Poisson's ratio, respectively. The subscripts s and p stand for *surface* and *particle*, respectively. A value of 0.9 may be used for R for the applications considered in this study (Ai and Kuhlman, 2011). The model predicts that sticking will occur when the normal component of the impacting velocity of the particle is less than the critical speed V_{cr}. In determining V_{cr}, however, the values of E are required for both the surface and particles, which is taken to be a function of the temperature and the characteristic diameter for the particle case. Those parameters require careful tuning between the experimental data and the simulation result in order to produce an acceptable accuracy (Yang, 2017).

Other sticking model may be developed based on the molten degree of the ash particles. The sticking process is determined by the melting ability of the coal ash particles and the deposit on the deposition surface, which is informed on the basis of an ash fusion temperature (AFT) experiment, which is carried out prior to the simulation. The aim of the experiment is to characterize the melting curve typical of the ash composition. Specifically, the following temperatures are determined: 1) the Initial Deformation Temperature (IDT); 2) the ash Fluid Temperature (FT). The experiment entails subjecting the ash deposit, which is initially in a solid state, to a uniform heating. At some thresholding temperatures, the deposit may undergo softening, deforming and phase transforming. The rough estimate of the temperature may be characterized by the resulting geometry of an initially cone-shaped deposit, as is shown in Figure 2.1, at increasing heating intensity. The IDT corresponds roughly to the initial smoothing of the tip while the FT refers to the complete liquid state of the deposit. A sticking model based on these two observations can be constructed as follows:

$$\eta_{\mathrm{stick}}(T) = \frac{T - \mathrm{IDT}}{\mathrm{FT} - \mathrm{IDT}} \tag{2.2.8}$$

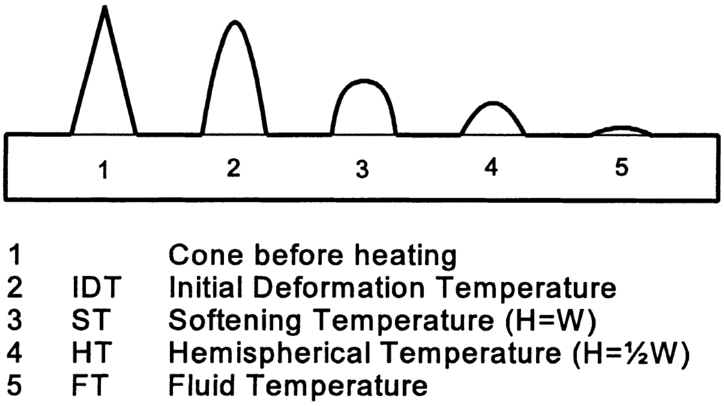

FIGURE 2.1: Schematic of the Ash Fusion test for coal ash (Hansen, Frandsen, and Dam-Johansen, 2005).

where T is the particle temperature. At low furnace temperature, the ash particle temperature may be lower than the IDT, which results in a negative efficiency (Li et al., 2015; Yang, 2017). Therefore, this model is not applicable for these types of furnaces.

Alternatively, the molten fraction of the ash particles can be used instead. In this method, the melt fractions of both the particles and the deposit on the deposition site are computed based on the thermodynamic equilibrium state, which is determined by a minimization process applied to the Gibbs energy in the system with mass balance constraints (Yang et al., 2017b; Cai et al., 2018). Denote $\eta_p\left(T_p\right)$ and $\eta_s\left(T_s\right)$ be the melt fractions of the ash particles and the deposit on the deposition surface at the particle temperature T_p and surface temperature T_s, respectively, then the sticking efficiency may be computed as follows:

$$\eta_{\text{stick}} = \eta_p\left(T\right) + \left(1 - \eta_p\left(T\right)\right)\eta_s\left(T_s\right) \tag{2.2.9}$$

Equation 2.2.9 is used when the biomass fuel contains a high concentration of alkali species (Kær, Rosendahl, and Baxter, 2006).

2.2.4 Prediction of the geometry of deposition

To predict the ash deposition more accurately, the deposit growth phase could be directly implemented into the CFD modelling, which means that the deposit will grow according to the accumulated mass of the particles that has been collected on the deposit surfaces. Simulating such an effect can be divided into two steps. The first step is to calculate the accumulated mass on each of the mesh faces, which can be determined by the ash particles' physical properties, their trajectories and particles impaction and sticking efficiency. The second step is to mimic the deposition growth by morphing the interface geometry so as to simulate the effect of the mass deposit in a continuous manner. To achieve this, one can employ a mesh motion procedure on the deposition surface based on the collected mass on each of the mesh faces. In ANSYS FLUENT, the mesh motion can be realized by translating its nodes where these faces are connected to each other, which can be controlled by a dynamic mesh panel and UDFs (user-defined functions).

García Pérez, Vakkilainen, and Hyppänen (2015) has developed a deposit growth model in which the movement of a given node is defined by a displacement vector $\vec{r}$ (see Figure 2.2). Here, $\vec{r}$ is defined as follows(García Pérez, Vakkilainen, and Hyppänen, 2015; García Pérez, Vakkilainen, and Hyppänen, 2016):

$$\vec{r} = \frac{\vec{a}_1 + \vec{a}_2}{|\vec{a}_1 + \vec{a}_2|} \cdot \frac{m_1 + m_2}{|\vec{a}_1| + |\vec{a}_2|} \cdot \frac{1}{\rho_p \varepsilon} \tag{2.2.10}$$

where $\vec{a}_1$ and $\vec{a}_2$ are the area vectors of each neighbouring faces 1 and 2 towards the direction of the deposit growth; m_1 and m_2 are the total deposit masses at the faces 1 and 2, respectively; ρ_p is the density of ash particles, and ε is the deposit solid fraction.

The effect of turbulence is to introduce a stochastic process that mimics the inherent random nature of fluid flow. As a result, the number distribution of impacting ash particles is not smooth. For example, a given face may

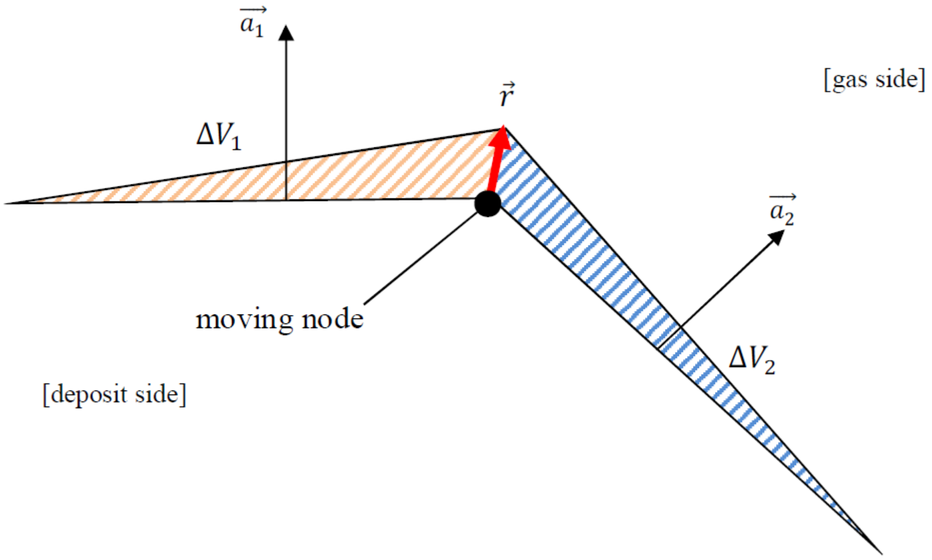

FIGURE 2.2: Schematic of the variables involved in the movement of a node which belongs to the outer interface of the deposit(García Pérez, 2016).

not have collected any ash particles at all whereas its neighbouring face may have collected several. Naive implementation of the node update procedure would lead to a highly discontinuous mass distribution, which could deteriorate the quality of the interface mesh cells to a point where negative volume cells might appear. The CFD solver could not execute on negative cells in the mesh - resulting in undefined behaviour (García Pérez, Vakkilainen, and Hyppänen, 2015). To overcome this problem, a smoothing scheme has to be applied on the mass distribution to ensure the appearance of negative cells is avoided. The smoothing scheme can involve a filtering algorithm, which regulates how the mass is distributed around the surface. To be more precise, suppose a particle of mass m is deposited on a face j. The filtering algorithm then redistribute m over the four neighbouring faces, namely the $j-2, j-1, j, j+1, j+2$ faces with a weight ratio $1:2:3:2:1$ (García Pérez, Vakkilainen, and Hyppänen, 2015). Figure 2.3 shows a schematic of this scheme. The closest face receives a dominant share of the mass.

By implementing this algorithm into the mass distribution, the faces with high collected mass value will share the mass among their neighbouring

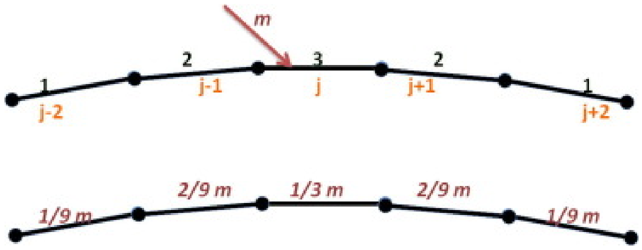

FIGURE 2.3: Schematic of the spreading algorithm when a particle of mass m hits the face j(García Pérez, Vakkilainen, and Hyppänen, 2015).

faces and the faces without any mass can still receive the mass from their neighbours. This way a smoother distribution can be realized (see Figure 2.4). After applying this filtering algorithm in succession, the resulting mass distribution would appear uniform and approach to the average mass collected in the deposit surface (García Pérez, Vakkilainen, and Hyppänen, 2015).

Although the mass-spreading algorithm is reasonably accurate and is able to avoid creating negative cells during the node update, it is, however, quite expensive in terms of parallelizing the implementation across multiple computing processors. Since the redistribution requires access to neighbouring faces (i.e. Equation 2.2.10), a UDF macro needs to be hard-coded into the simulation, which causes extra work for the multiple processors to synchronise (García Pérez, 2016). This will increase the difficulty and the time requirement for a complete simulation case.

2.2.5 Literature survey on CFD prediction of ash deposition

The use of CFD to predict ash deposition phenomena is relatively recent. In this field of research, two broad approaches can be identified, which can be coined as *steady* and *dynamic*. Steady simulations refer to the rate of the deposit accumulation and the deposition behaviours remain constant through the growth period of the deposit, this is in contrast with the dynamic simulations in which those two behaviours are dynamically computed and updated at each time stepping (Yang, 2017). Admittedly, steady simulations provide

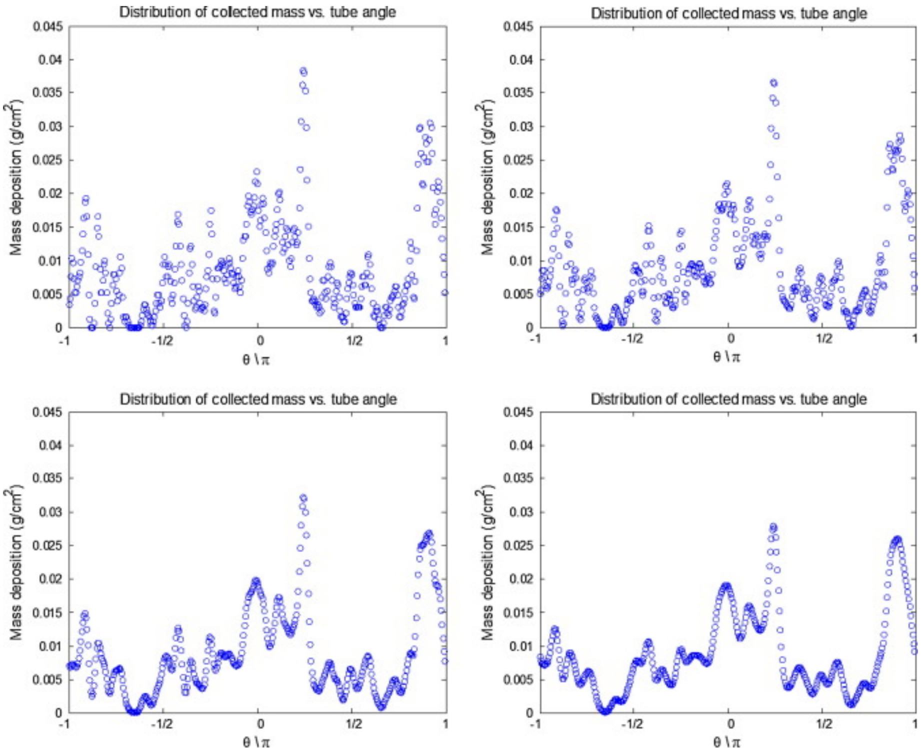

FIGURE 2.4: Resulting mass distributions after (in reading order) 1, 2, 5 and 10 iterations of the spreading algorithm done on the distribution(García Pérez, Vakkilainen, and Hyppänen, 2015).

a good approximation to problems involving uncooled probe, since the temperature on the deposition site is a lot closer to the furnace so that the deposition behavioural difference is minimized due to the temperature variation. On surfaces where there is a large temperature difference (or cooled probe), deposition characteristic is a strong function of the variation in temperature (Taha et al., 2013; Degereji et al., 2012; Mu, Zhao, and Yin, 2012). Therefore, a dynamic approach is generally used where the deposition variables are constantly being updated depending on the growth stage of the deposit.

Huang et al. (1996) simulated the ash deposition formation on the superheater tubes during the coal combustion in a pilot-scale coal boiler and a drop tube furnace using the steady CFD method. Both the effects of the inertia impaction and the thermophoresis were taken into consideration. The viscosity based sticking model was used in the simulation for the prediction of the sticking efficiency. Their simulation showed good agreement with the available experimental data. In particular, the simulated fouling behaviour indicates that ash particles with higher densities are more likely to impact on the surface compared to those with a lower density. Furthermore, they noted that the gas temperature could significantly influence the fouling behaviour.

Formation of ash deposit in a biomass fired fluidised bed boiler was simulated by Mueller et al. (2005). In their work, only the inertia impaction was considered as the dominant process for the ash particle transportation and the sticking efficiency was modelled based on the melt fraction of the ash particles. Their results showed that there is a critical value for the particle's melt fraction above which smaller (< 75 µm) impacting ash particles will always stick to the surface. On the other hand, ash particles with larger diameter exhibit a greater tendency to rebound off the surface at the same melt fraction. This behaviour was found to be in qualitative agreement with the experimental observation.

A 3D steady simulation on the deposition formation for the co-combustion of coal and biomass in a drop tube furnace was carried out by Garba et al. (2013). Their simulation accounted both the effect of thermophoresis and inertia impaction with the inertia impaction being identified as the dominant contribution for the particle trajectories. The sticking efficiency model for the resulting ash is determined empirically based on the mixing ratio of coal and biomass. The viscosity-based model was employed for coal while the molten fraction was used for the biomass. The resulting sticking behaviour is a linear combination of these two models with the ratios controlled by the mixing ratio of the two fuels. The deposition rate was computed and was found to be in good agreement with experiment.

Various sticking efficiency models have been tested by Wieland et al. (2012) for coal combustion in a drop tube furnace. It was found that the viscosity-based approach is highly sensitive to the reference viscosity, whereas models involving the melting characteristic of the ash particles generally showed good accuracy and were less prone to error due to the empiricism in the model parameters.

Utilizing heat transfer, the formation of ash deposition was conducted by Richards, Slater, and Harb (1993) on furnace walls. The deposit growth is modelled and predicted by a heat transfer process on the deposit. In addition, the growth behaviour is also controlled by the volume fractions of the solid and liquid content in the deposit. It was showed that the deposit undergoes a rapid increase in temperature during the initial stage of the growth, this rate, however, starts to drop when the deposit has developed a sufficient thickness at later stages. The cause for this temperature rate variation is attributed to the non-uniform heat conduction occurring in the deposit as a result of a variable heat-flux being applied on the deposit boundary.

Kær, Rosendahl, and Baxter (2006) simulated the slagging formation in a straw-fired grate boiler using an in-house developed dynamic ash deposit model. Li, Brink, and Hupa (2009) and Li, Brink, and Hupa (2013) applied a dynamic slagging model for the prediction of deposition formation in a heat recovery boiler.

García Pérez, Vakkilainen, and Hyppänen (2015) developed a dynamic deposit growth model using dynamic mesh model to predict the deposit shape in a kraft recovery boiler. The flow pattern around a tube array was also resolved in the simulation. In addition, a new algorithm of mass spreading and re-distribution was employed to obtain more accurate results.

Zhou et al. (2019) investigated the shape variation of the ash deposit during the deposit growth on a temperature-controlled probe in a pilot-scale furnace. The dynamic mesh technique was improved upon to avoid negative volume in the Fluent solver. Zheng et al. (2020b) predicted the deposition behaviour on a deposition probe in a 300 kW slagging test furnace fired with Zhundong coal. They used a dynamic numerical method to obtain the shape and surface temperature variation as a function of time.

A dynamic CFD model was employed by Yang, Zhou, and Wu (2022), which considers the effect of particle sticking and erosion. The heat transfer between the flue gas and the deposition was also considered during the simulation. They simulated the formation behaviour under multiple operation conditions in a lab-scale entrained flow reactor with a modelled biomass fly ash species ($K_2Si_4O_9$). To achieve a stable remeshing on the probe surface, a global mass-conserving smoothing scheme was proposed, which uses a multi-point moving averaging algorithm together with a growth scaling factor.

2.3 Summary

The CFD methods, where a global computational domain is constructed to capture the deposition process in macroscopic detail, are able to model both steady and dynamic phenomena. Thus, the ash particles transportation and deposition growth can be predicted with a high degree of accuracy through CFD. Several sub models are also developed and employed while modelling the processes of the ash deposition growth during the solid fuel combustion in the boiler. For instance, the flue gas flow in the boiler is modelled by the RANS approach, while the ash particle trajectories are modelled by DPM module through Lagrangian approach. Ash particle sticking models need to take the viscosity of the ash particles, the kinetic energy of the impacting particles and the molten degree of the ash particles into consideration. Some common sticking models are the viscosity-based sticking model, kinetic energy sticking model and molten fraction sticking model. Additionally, the dynamic mesh model can also be employed to predict the growth of the ash deposition.

In this field of research about the ash deposition prediction, two broad approaches can be identified, which can be coined as steady and dynamic.

Steady simulations refer to the rate of the deposit accumulation and the deposition behaviours remain constant through the growth period of the deposit, this is in contrast with the dynamic simulations in which those two behaviours are dynamically computed and updated at each time stepping. The steady simulations provide a good approximation to problems involving uncooled probe, since the temperature on the deposition site is a lot closer to the furnace so that the deposition behavioural difference is minimized due to the temperature variation. On the contrary, a dynamic approach is generally used where the deposition variables are constantly being updated depending on the growth stage of the deposit.

The research aims are as follow: 1) fully understanding the ash deposition processes during the solid fuel combustion; 2) to develop a novel ash deposit growth model through CFD methods to predict the ash deposition more accurate and more efficient in parallel FLUENT.

Chapter 3

Development of dynamic ash deposition models

To simulate the behaviour of ash deposition, the CFD approach has been selected. A novel approach has been developed to dynamically update the mesh as the ash deposition grows. To achieve this, several modules in FLUENT have been employed. For instance, the realizable $k-\epsilon$ turbulence model is selected to capture the correct turbulent physics. In addition, the flow solver is also coupled with the Lagrangian method for tracking the ash particles(Yang et al., 2019b). The DRW model is also employed to consider the effect of the turbulent diffusion on the particle trajectories. The growth of deposition is based on the sticking efficiency and the arrival rate of the ash particle on the deposition surface. The particle sticking model is based on an energy conservation analysis and considers the particle properties, particle kinetic energy and furnace operation conditions(Yang et al., 2019a; Yang et al., 2019b). The flow solver and the Lagrangian tracking are used in conjunction to determine the arrival rate of ash particles as function of the azimuthal angle of the deposition tube. And the radiative heat transfer is solved by the DO model, as discussed in section 2.2.1. Additionally, the dynamic mesh model is employed to achieve the growth of the ash deposition.

3.1 Lagrangian particle tracking method

The main goal of the Lagrangian particle tracking method in the current work is to determine the arrival rate of the fly ash particles. This is computed by tracking a finite number of Lagrangian particles upstream of the deposition tube. The kinematic equation satisfied by those particles is shown as follow (Yang et al., 2017b):

$$\frac{d\vec{v}_p}{dt} = \frac{18\mu_g}{\rho_p d_p^2}\frac{C_D Re_p}{24}\left(\vec{v}_g - \vec{v}_p\right) + \vec{g}\frac{\left(\rho_p - \rho_g\right)}{\rho_p} + \vec{F} \tag{3.1.1}$$

where the term $\vec{F}$ is a source term that may include the effect of thermophoresis or other minor transportive effect (see section 2.2.2). The thermophoretic force, which is caused by the temperature gradient in the gas that is closed to the solid deposition surface, and this may be neglected when a high deposit surface temperature exists. The term $\frac{18\mu_g}{\rho_p d_p^2}\frac{C_D Re_p}{24}\left(\vec{v}_g - \vec{v}_p\right)$ represents the drag force, which is opposite to the direction of motion whenever the particle velocity is greater than the flue gas velocity, and the second term $\vec{g}\frac{\left(\rho_p - \rho_g\right)}{\rho_p}$ is the gravitational force due to gravity. In an equilibrium state, the pathlines followed by the particles have a tendency to converge to the streamline of the background flow field after a sufficient time has reached.

As discussed in section 2.2.2, the effect of turbulence will not be felt by the particles if the mean velocity of the gas were used to compute the trajectory (note that the typical RANS equations solve for the mean velocity). An additional force, termed turbulent diffusion, is needed, which is computed on the basis of a discrete random walk (DRW) approach. To be more specific, the instantaneous gas velocity $\tilde{u}$ is assumed to be composed of a time-averaged part, say $\bar{u}$, and a fluctuating part, say u'. The DRW treats first that the turbulence is isotropic, which means that the statistical characteristics of the turbulence are uniform in all directions, and there exists a characteristic time, say τ_e, for a turbulent eddy to persist in an episodic manner. Therefore, the following observations can be assumed (ANSYS Inc., 2020):

$$\begin{aligned} \tilde{u} &= \bar{u} + u' && (3.1.2) \\ u' &= \varsigma\left(\sqrt{\bar{u'^2}}\right) = \varsigma\left(\sqrt{2k/3}\right) && (3.1.3) \\ \tau_e &\cong C_L\,(k/\varepsilon) && (3.1.4) \end{aligned}$$

where $\varsigma(x)$ is a pseudo-random number generated from a normal Gaussian distribution with zero mean and standard deviation x. Here, k is the turbulence kinetic energy per unit mass, ε is the energy dissipation rate per unit mass and C_L is a time scale constant. Preliminary studies have revealed that the DRW allows the impacting particles to expand on the two sides of the cylindrical probe to a significant degree and causes the particles to impact on the furnace wall (Yang, 2017). If the turbulence diffusion effect was disabled instead, a significant portion of the particles were observed to concentrate on the symmetry plane in the windward position of the tube and almost no particles were observed to impact on the furnace wall due to the streamline effect.

3.2 Particle sticking model

Sticking may occur when an ash particle arrived at the impaction surface. However, not all impacting particles will adhere to the surface - only a fraction of the particles will do so. Determining whether a particle will adhere to the surface depends on several factors (see section 2.2.3 for a detailed discussion). In this work, a newly proposed model of Yang et al. (2019a) is used, which accounts for the ash chemistry, the particle kinetic energy and the furnace conditions. This model is based on energy conservation principle and is expressed as follows:

$$E_{\text{stick}} = \begin{cases} 1 & \text{if} \quad E^* \leq 0 \\ e^{-9.21 \times E^*(1-f_{\text{melt}})} & \text{if} \quad E^* > 0 \end{cases} \tag{3.2.1a}$$

$$\begin{aligned} E^* = & \frac{1}{4}{d_m}^2 (1-\cos\theta) + \frac{2}{3d_m} \\ & - 0.00536 \times {d_m}^{4.70} \times (1-\cos\theta)^{0.591} - 1 \end{aligned} \tag{3.2.1b}$$

$$d_m = 1 + 0.259 \times We^{0.317} \tag{3.2.1c}$$

$$We = \frac{\rho_p {U_p}^2 D_0}{\gamma_{\text{LV}}} \tag{3.2.1d}$$

where E_{stick} is the sticking efficiency, f_{melt} is the liquid phase fraction (or the melt fraction) of the deposition surface, θ is the contact angle, ρ_p is the particle density, U_p is the normal speed of the particle relative to the impacting surface, D_0 is the characteristic diameter of the ash particle and γ_{LV} is the liquid-vapour surface tension. The quantity E^* in Equation 3.2.1b may be interpreted as the normalized excess energy while d_m is known as the maximum spread ratio. Finally, We is the particle Weber number.

Yang et al. (2019b) validated the model for particle Stokes number up to seven, which is comparable to a utility-scale boiler. The parameters used in the model can be estimated by sampling the bulk ash composition and prescribing a size distribution in the sampled ash content (Mills and Rhine, 1989) while the contact angle is inferred from matching with experimental data. It is worth noting that this sticking model does not directly consider the viscosity of the particle, instead, the viscosity is indirectly transmitted to the model by means of the wetting behaviour (Yang et al., 2019b).

3.3 Deposition growth model

The deposit growth is simulated by means of a node translation on the deposit-flow interface according to the mass that has been collected on each of the faces over an accretion period. ANSYS FLUENT offers the dynamic mesh model to simulate the growth of the ash deposition on the deposit surface. The motion of these nodes are implemented by employing an in-house developed UDF.

As shown in the Figure 3.1, two mesh faces (face a and face b) and three mesh nodes (node $i-1$, i and $i+1$) are distributed on the interface between the flue gas side and the deposit side. The increased thickness of the ash deposition $\Delta\delta_i$ on any face of the interface can be calculated over a time interval Δt as follows:

$$\Delta\delta_i = \frac{\Delta m_i}{\rho_p\left(1-\varepsilon_{\text{deposit}}\right)S} \tag{3.3.1}$$

where Δm_i is the accrued mass on the i-th surface segment over the interval, S is the surface area of this segment and ρ_p is the density of the ash particles. The variable $\varepsilon_{\text{deposit}}$ is the porosity of the ash deposition. Δm_i is calculated by FLUENT during the simulation by assuming that there is a constant stream of Lagrangian particles delivered to the deposition surface (also known as steady tracked), the accrued mass is computed by multiplying the mass flux of the particles with the re-meshing time step. The actual accrued mass is then adjusted by multiplying with the sticking efficiency E_{stick}, which is computed prior to each dynamic re-meshing operation. The deposit properties, such as the porosity, the thermal conductivity and the deposition surface temperature, could have an appreciable effect on the deposition behaviour during the deposit growth (Yang et al., 2017b), which are reflected in the change of the values of the model variables such as the melt fraction, contact angle and the liquid-vapour surface tension. The effect of these variations is not considered in this work and is left for future investigations.

The deposit porosity can be calculated based on the temperature and deposit composition correlation (Yang et al., 2017b; Wang and Harb, 1997; Kær, Rosendahl, and Baxter, 2006; Richards, Slater, and Harb, 1993). Zheng et al. (2020a) and Zheng et al. (2020b) assumed that the porosity of the ash deposit is a linearly decreasing function of the thickness of the ash deposition with an initial porosity value of 0.6 while Zhou and Hu (2021) calculated the deposit porosity by assuming the same initial porosity value along a linear dependence on the volume fraction of the solid and liquid phase. In this thesis, a constant value of $\varepsilon_{\text{deposit}} = 0.6$ may be used (Kær, Rosendahl, and Baxter, 2006). This is a reasonable justification since the deposit temperature and the deposit composition was not observed to change too significantly during the simulation. In reality, however, the porosity of the ash deposition should vary with the deposition growth and therefore a dynamic approach has to be adopted. This may be calculated by a UDF macro and is left for future investigation.

A fixed direction, normal to the initial flow-deposit interface, is constrained on the growth direction of the nodes. At the end of the accretion period, the nodes are relocated along the normal of the cylindrical tube. Let $\left(x_i^t, y_i^t\right)$ denote the position vector of the i-th node on the interface boundary at the time t, then the new position after the node update, namely $\left(x_i^{t+\Delta t}, y_i^{t+\Delta t}\right)$, may be computed by:

$$x_i{}^{t+\Delta t} = x_i{}^t + \Delta\delta_i \cos\theta_i \tag{3.3.2}$$

$$y_i{}^{t+\Delta t} = y_i{}^t + \Delta\delta_i \sin\theta_i \tag{3.3.3}$$

where $\Delta\delta_i$ is calculated from Equation 3.3.1 and θ_i is the azimuthal angle of the i-th node (see Figure 3.2).

The aforementioned node translation strategy is a local scheme in which the update depends only on the local node properties such as the localized

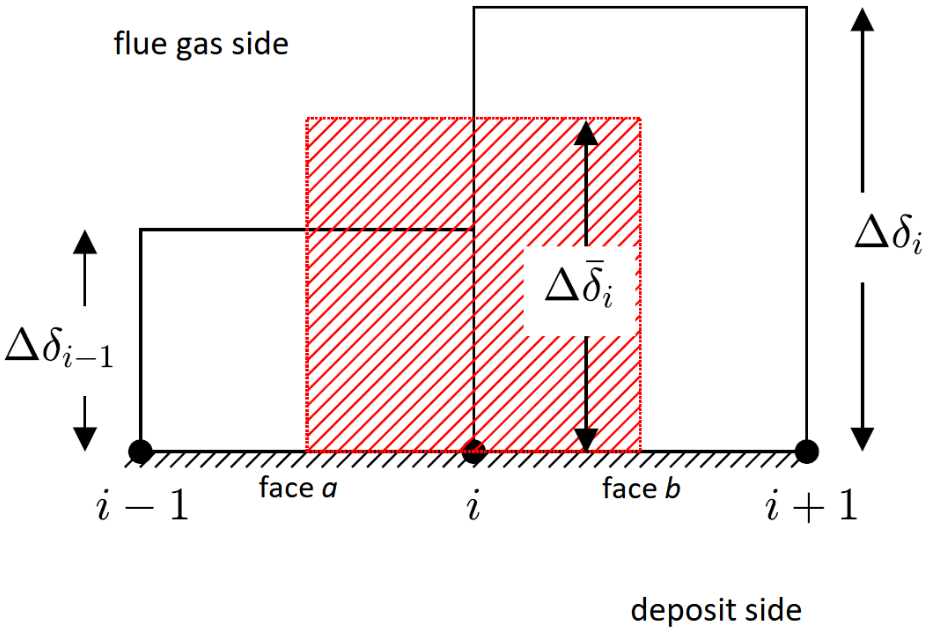

FIGURE 3.1: A schematic diagram on the moving strategy for the moving of the nodes on the interface between the flue gas and the deposit face.

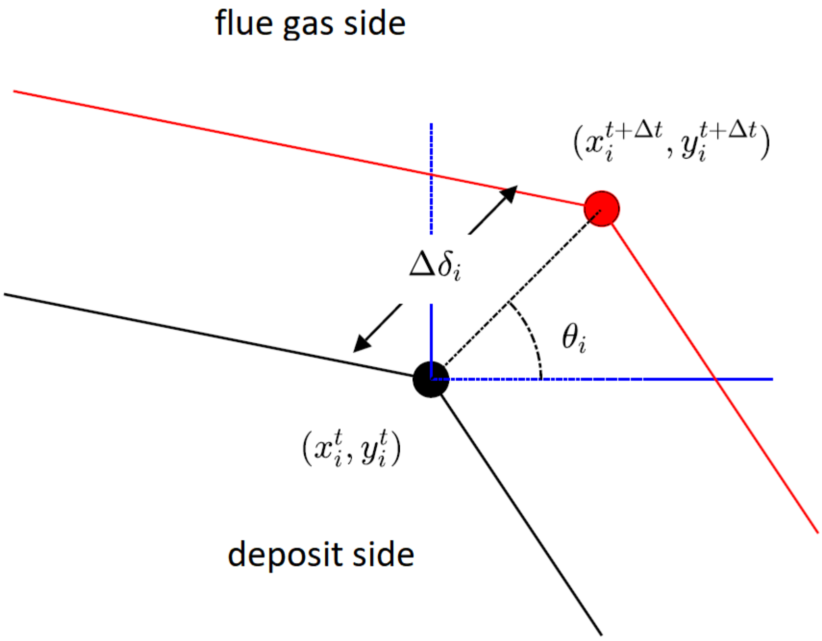

FIGURE 3.2: A schematic diagram on the coordiantes update of node i.

collected deposition mass distribution. However, due to the effect of turbulence diffusion, the mass over a set of neighbouring nodes may show a significant degree of variation, which may cause the mesh to stagger or overlap (García Pérez, Vakkilainen, and Hyppänen, 2015). Schemes that do not include a smoothing procedure may result in the creation of negative volume on one or more interface cells. This is a serious issue in FLUENT as the CFD solver could not handle this numerical instability. Reducing the size of the mesh may help to stabilise the simulation, but it requires a significant cost in computing resources.

Therefore, in order to produce a stable simulation and to allow non-local information to propagate in the update scheme, the average value of the thickness of the ash deposition on the two adjacent faces is used to determine the new coordinates of the nodes. This means that the motion of each node of the interface between the flue gas and the deposit face is calculated from the average collected mass from its two adjacent faces. Shown in the Equation 3.3.4, $\Delta\bar{\delta}_i$ represents the average value of the thickness of ash deposition on the two neighbouring faces; $\Delta\delta_i$ and $\Delta\delta_{i-1}$ are the increased thickness of this two adjacent faces:

$$\Delta\bar{\delta}_i = \frac{\Delta\delta_i + \Delta\delta_{i-1}}{2} \tag{3.3.4}$$

The updated coordinates of the node i are then determined as follows:

$$x_i{}^{t+\Delta t} = x_i{}^t + \Delta\bar{\delta}_i \cos\theta_i \tag{3.3.5}$$

$$y_i{}^{t+\Delta t} = y_i{}^t + \Delta\bar{\delta}_i \sin\theta_i \tag{3.3.6}$$

ANSYS FLUENT uses a combination of *smoothing* and *remshing* operations to establish a consistent mesh in the computational domain. This is applied in the dynamic mesh model to preserve the mesh integrity (ANSYS Inc., 2020). To this ends, the spring-based smoothing method may be selected,

Threshold	Deposit cells	Flue gas cells
Minimum cell size	$\sim \Delta x_1$	$\sim 0.1\Delta x_1$
Maximum cell size	$\sim 2\Delta x_1$	$\sim 200\Delta x_1$
Target cell skewness	0.6	0.5

TABLE 3.1: Approximated thresholds for the local face remeshing algorithm (García Pérez, 2016).

which utilizes the fact that the equilibrium state of a connected network of springs produces a smooth distribution of nodes that minimizes the potential energy of the system. Each spring, which connects two adjacent nodes, is characterized by a spring constant and a characteristic length. Thus, the force produced by the spring follows the Hook's law in which the force is a linear function of the relative displacement of the two connected nodes (ANSYS Inc., 2020). Without loss of generality, the spring length is taken to be zero and the spring factor may be taken to be between 0 and 1. This value also controls the non-local effect of the spring in the network. For example, a value of zero indicates that there is little damping in the system; a small change in the displacement can affect faraway cells, whereas a value of one suggests that the effect localizes to only neighbouring cells (García Pérez, 2016). The walls are not static, the movement of the boundary cells can sometimes result in a large difference between the boundary displacement and the local cell sizes, which then deteriorates the overall quality of the cells in the proximity of the boundary walls. It has been observed that this could lead to divergence problems in the solution.

To alleviate this issue, a local face remeshing procedure can be applied to a localized set of cells. The procedure determines the average size of the cells, if the size is larger than the threshold value, the cells are collapsed, otherwise they are split to maintain a relative uniform size distribution (ANSYS Inc., 2020). The local face remeshing is controlled by adjusting the *Minimum* and *Maximum* Length Scale parameter in the FLUENT solver (ANSYS Inc., 2017).

The dynamic mesh model requires experimenting with the various input parameters in the solver in order to produce a stable simulation case. For the current simulation, the values of those parameters are defined in Table 3.1, where Δx_1 defines the length of the cells adjacent to the interface. Those thresholds are chosen according to the suggestions of García Pérez (2016), where they used a trial-and-error approach to avoid generating poor quality cells during the mesh morphing process. It is important to keep in mind that a finer mesh may produce saw-tooth instabilities (see section 5.2.1), therefore the maximum allowable cell size in the flue gas side should not be too small so as to avoid introducing instabilities into the simulation.

3.4 Summary

The current model is used to predict the ash deposition behaviour in boilers where steady state is assumed. The construction of the model is split into two phases - the gas phase, which solves the field equations of the background gas using the RANS equations, and the discrete phase, which solves the equations of motion of the fly ash particles in a Lagrangian frame. The combination of these two phases determines the deposition behaviour by means of a sticking model where the distribution of the sticking mass flow rate is determined as a function of the azimuthal angle of the deposition tube. Based on this mass flow rate distribution, the geometry of the deposition interface is updated using the dynamic mesh module of FLUENT and the preceding procedure is repeated until the specified time is reached.

Chapter 4

Experimental data

This chapter discusses the experimental facilities that are being used to aid the development and validation of the ash deposition growth models. Ash deposit formation on an uncooled tube for coal air combustion and biomass air combustion in pilot-scale furnace (PACT) has been analysed by deploying the CFD based ash deposition growth model. This pilot-scale furnace in PACT has been chosen for this validation study because there is an extensive volume of experimental data collected over the years and it is an ideal candidate to conduct validation work both on the theoretical and numerical basis.

4.1 Pilot-scale furnace

In order to validate the developed models, the Pilot-scale Advanced Capture Technology (PACT) facilities have been utilized to provide experimental data. UKCCSRC PACT offers a combustion plant that can operate either in air or oxyfuel mode. The experimental setup consists of two modules, the pilot-scale furnace Figure 4.1a and an ash collection measurement system Figure 4.1b. The pilot-scale furnace is a down-fired furnace of a cylindrical shape with a length of 4000 mm and an inner diameter of 900 mm. The furnace is fitted with two swirl burners, one for coal and one for biomass

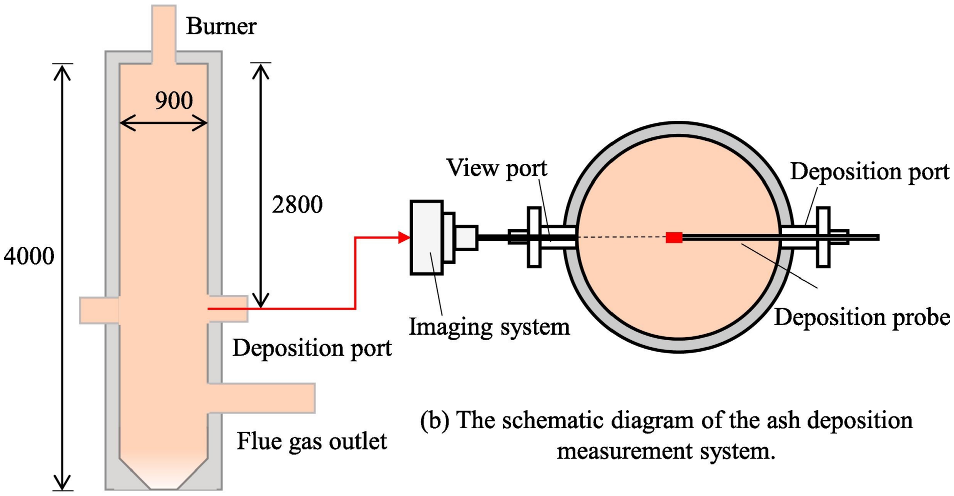

(a) The schematic diagram of the pilot-scale furnace.

(b) The schematic diagram of the ash deposition measurement system.

FIGURE 4.1: The schematic diagram of (a) the pilot-scale furnace (mm) and (b) the ash deposition measurement system (Yang et al., 2019b).

combustion; both of which consist of a primary, secondary and tertiary register. Pulverized fuels and primary oxidizer stream are delivered via the primary register while the rest of the preheated oxidizer are fed through the secondary and tertiary register. In order to achieve a steady stream of gas flow, a stable swirled flame needs to be maintained, which can be achieved by controlling the oxidizer flow rate. Similarly, the swirl intensity is adjusted by controlling the flow rate of the preheated oxidizer in the secondary and the tertiary registers. An excess oxygen level in the flue gas is maintained at 3.5% (dry basis).

Two types of solid fuels are considered in the experiment - the El Cerrejon coal, which is a low-ash and low-sulphur bituminous coal, and the recycled wood for the biomass fuel. The composition of these two solid fuels is critical in identifying the underlying deposition behaviour. A few of those properties are listed in Table 4.1, which shows that the woody biomass contains a significantly higher concentration of volatiles but at a lower fixed carbon content than the El Cerrejon coal. At the same time, inferring from the ultimate analysis, a higher concentration of the oxygen content in the biomass fuel is observed, which could lead to a lower heating value. Both fuels produce approximately the same amount of ash (≈ 3%). The composition of the fly ash, on the other hand, differs quite markedly. For instance, the ash composition due to the coal is mainly composed of silicon, alumina, iron, calcium and sulphur whereas it is silicon and calcium for the woody biomass.

Ash composition(wt.%)	Coal	Biomass	Proximate analysis (wt.%) (as received)	Coal	Biomass
SiO_2	39.9	44.4	Moist.	7.63	5.8
Al_2O_3	16.6	5.8	Vol.	35.5	73.9
Fe_2O_3	10.8	7.6	FC	54.0	17.1
CaO	14.4	29.5	Ash	2.9	3.2
MgO	1.9	4.1	GCV (kJ/kg)	28.7	18.4
K_2O	1.6	2.6	Ultimate analysis (wt.%)		
Na_2O	1.9	1.5	C	80.9	51.9
TiO_2	0.6	0.9	H	5.12	6.0
P_2O_5	0.8	0.6	N	1.65	0.4
SO_3	11.4	3.0	O	11.8	41.7

TABLE 4.1: Fuel properties of the EI Cerrejon coal (Coal) and the recycled wood (Biomass) that were used for the CFD calculations (Yang et al., 2019b).

4.2 Ash deposition measurements

The ash deposition measurement system is responsible to collect information on the deposition behaviour both quantitatively and qualitatively. For this reason, in addition to the sampling sub-module, the system is also fitted with an imaging unit where a detailed sequence of the growth stages can be recorded and to allow shedding events to be determined on the deposit once enough mass is accumulated. The sampling unit consists of an ash deposition probe with a detachable uncooled ceramic coupon at the tip (see Figure 4.1b). The probe is inserted into the middle cross-section of the furnace in order to allow the deposit to settle and to provide a detailed temperature condition for the slagging formation. The exact position of the probe is shown in Figure

4.1a, where it sits at a distance of 2800 mm from the top wall of the furnace. To replicate the real condition in a utility-scaled boiler, the particle Stokes number in the pilot-scale boiler needs to be matched with that of the utility-scaled boiler. However, given the relatively low speed of the exit flue gas in the pilot-scale boiler ($\approx$ 0.5 m/s), it is possible to adjust the outer furnace diameter to compensate for the lower speed. This requires a scaling of (1:20) of the dimension of a real superheater tube, which is difficult to realize in practice. For this reason, the modelled superheater tube is assumed to have a characteristic diameter of 37 mm in this thesis (Yang et al., 2019b).

One of the key parameters for the deposition formation is the *ash deposition rate*, which is defined as the ratio of the deposition mass over the deposition time. The deposition time is a controlled parameter and it can be adjusted for experiment and simulation. In this study, a typical deposition time of four to six hours is used. This will ensure that the deposits have sufficient mass to allow a distinct shape to be distinguished before excessive mass is shed. The ash deposition rate is calculated from the measured mass of ash deposition on the deposition probe during four to six deposition time. The ash deposition rate for coal air combustion case is 6.0 $g/(m^2h)$, while it is 24.2 $g/(m^2h)$ for biomass air combustion (Yang et al., 2019b). Unfortunately, the thickness of the deposition is not measured during the experiments. Readers are referred to the work of Huynh (2018), Yang et al. (2018), and Yang et al. (2019b) for more information on the whole experimental set-up.

Chapter 5

CFD prediction of ash deposition in a pilot-scale furnace

This chapter mainly presents the dynamic ash deposition growth model and the CFD predictions of ash deposition growth for coal air and biomass air combustion in pilot-scale furnace. The dynamic ash deposition growth model is validated through the experimental data. The effects of the flue gas velocity and the deposit shape change are also investigated in this chapter.

5.1 Case settings

5.1.1 Geometry

Base on the experimental facilities discussed in Chapter 4, a two-dimensional (2D) geometry with a tube of diameter 37 mm placed in the central region is considered as the computational domain, which is shown in Figure 5.1. The length and width of this computational domain is both 900 mm, respectively. The tube is surrounded initially with a deposit layer of 1 mm (García Pérez, Vakkilainen, and Hyppänen, 2015). The unstructured mesh is used and the computational domain consists of solid zone and fluid zone. The triangular grids are used in the computational domain to apply the dynamic mesh method, whereas the quadrilateral grids surround the deposit-flow interface

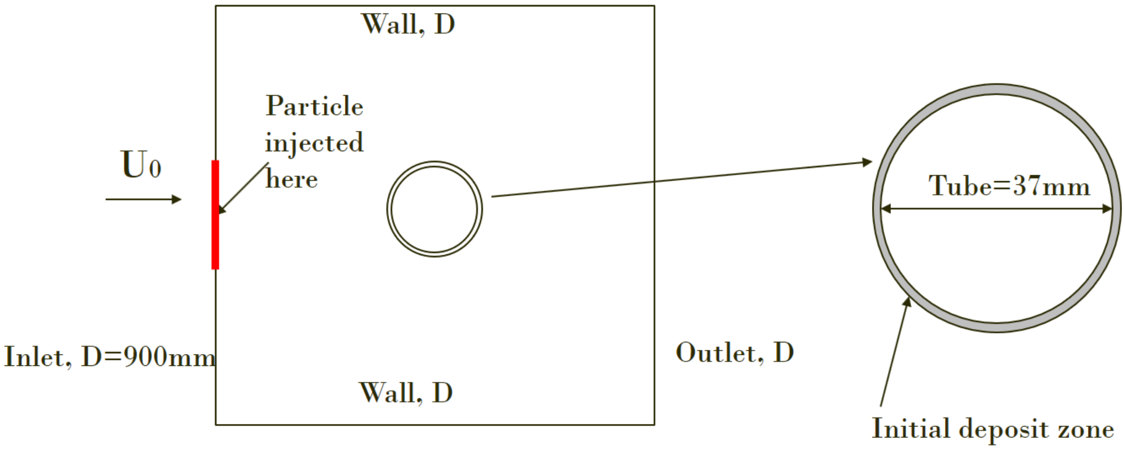

FIGURE 5.1: Schematic diagram of computational domain.

to obtain the accurate resolving of the flow field within the boundary layers of this deposition surface.

5.1.2 Mathematical models and simulation conditions

In order to accurately simulate the ash deposition growth, several mathematical sub-models have been developed and applied in the CFD framework. For instance, the Realizable $k-\epsilon$ model, the Discrete Ordinate model and the Discrete Phase Model (DPM) are used for modelling the turbulence, radiation heat transfer and particle trajectories, as discussed in Chapter 2 and Chapter 3.

The DPM allows the particles' trajectories to be computed and tracked throughout the simulation. This is done in a Lagrangian frame in which the equations of motion are solved on a particle basis. In the deposition experiments, the leeward section of the uncooled tube was initially clean and no ash particle deposits were initiated. Since the tube is uncooled, the temperature difference between the flue gas side and the deposition surface is considered negligible, therefore the effect of thermophoresis is not modelled in this study. However, turbulence diffusion is accounted for by employing the

DRW approach where the instantaneous fluid velocity experienced by the Lagrangian particles is thought to be composed of the mean velocity field and a stochastic field, which is modelled by a Gaussian distribution (see section 3.1 for detail). In the DRW module of FLUENT, a number of parameters can be set, which can drastically affect the predicted particle arrival rate. Following the work of Yang et al. (2019b), a particle size interval of 50 and 10 tries are implemented, these values were found to produce the most reliable results. However, one should note that the fluctuation in the particle arrival rate can be suitably reduced by increasing the particle size interval and number of tries.

The solution procedure first proceeds to compute the mass flux (or the arrival rate) of the ash particles using the DPM. Subsequently, the particle sticking model based on energy conservation is applied to determine the statistical percentage of the mass that will remain on the surface (see section 3.2 for detail). The deposition rate is finally computed as a product between the mass flux and the sticking efficiency.

The sticking model outlined in section 3.2 contains several physical parameters that characterize the ash and surface properties. For example, the ash particle density ρ_p and the liquid-vapour surface tension γ_{LV} need to be estimated, which can be done by analysing the bulk ash composition (Mills and Rhine, 1989). The contact angle, on the other hand, is deduced by matching the ash deposition rate predicted by the model with experimental data. For the cases considered in this section, which concerned with coal/biomass-fired pilot-scale boiler, a value of 160 ° might be used. This assumes that the deposit has a 83% liquid phase content at chemical equilibrium. It should be noted that this number is substituted for the value of f_{melt} in the current model (Yang et al., 2019b).

Since the ash deposition rate is obtained through the above modelling, the deposition growth model can be applied to simulate the growth of the ash deposition on the deposit surface. As discussed in section 3.3, the motion of the nodes in the fluid-solid interface (terms as the deposit surface) is modified by the dynamic mesh model in conjunction with the 'DEFINE_GRID_MOTION' UDF macro. A snippet of the code is shown in Figure 5.2. The line 'r_deposit=0.5*F_UDMI(f, tf, 1)' in the code means that the value that control the node motion is taken to be the average value of the thickness of ash deposition on the two neighbouring faces.

As stated earlier in section 3.3, parameters in the dynamic mesh model have been carefully selected to minimize instability. For example, in the spring-based smoothing method, the spring constant factor is set to 0.1, which is found to produce stable results. As for the remeshing module, the minimum and maximum length scale are set to $4e^{-5}$ m and 0.15 m for the fluid zone while they are 0.0001 m and 0.015 m for the deposit solid zone.

The boundary conditions of the flue gas are determined from the combustion cases (see Table 5.1). The size distribution of the coal ash particles follows the Rosin-Rammler distribution with a mean diameter of 36.86 μm and a dimensionless spread parameter of 1.096. The distribution is computed natively in FLUENT with the input parameters given by Table 5.2. The density of the coal ash particles is deduced based on the composition information in Table 4.1, which is calculated approximately to be 3174 $\mathrm{kg/m^3}$.

The ash particles are assumed to be uniformly distributed at the inlet and they are injected from a section of the inlet boundary spanning 74 mm about the line of symmetry. The reason to limit the injection length is to reduce the particle count since only particles that interact with the tube contribute to the deposit growth. The schematic of the domain is shown in Figure 5.1.

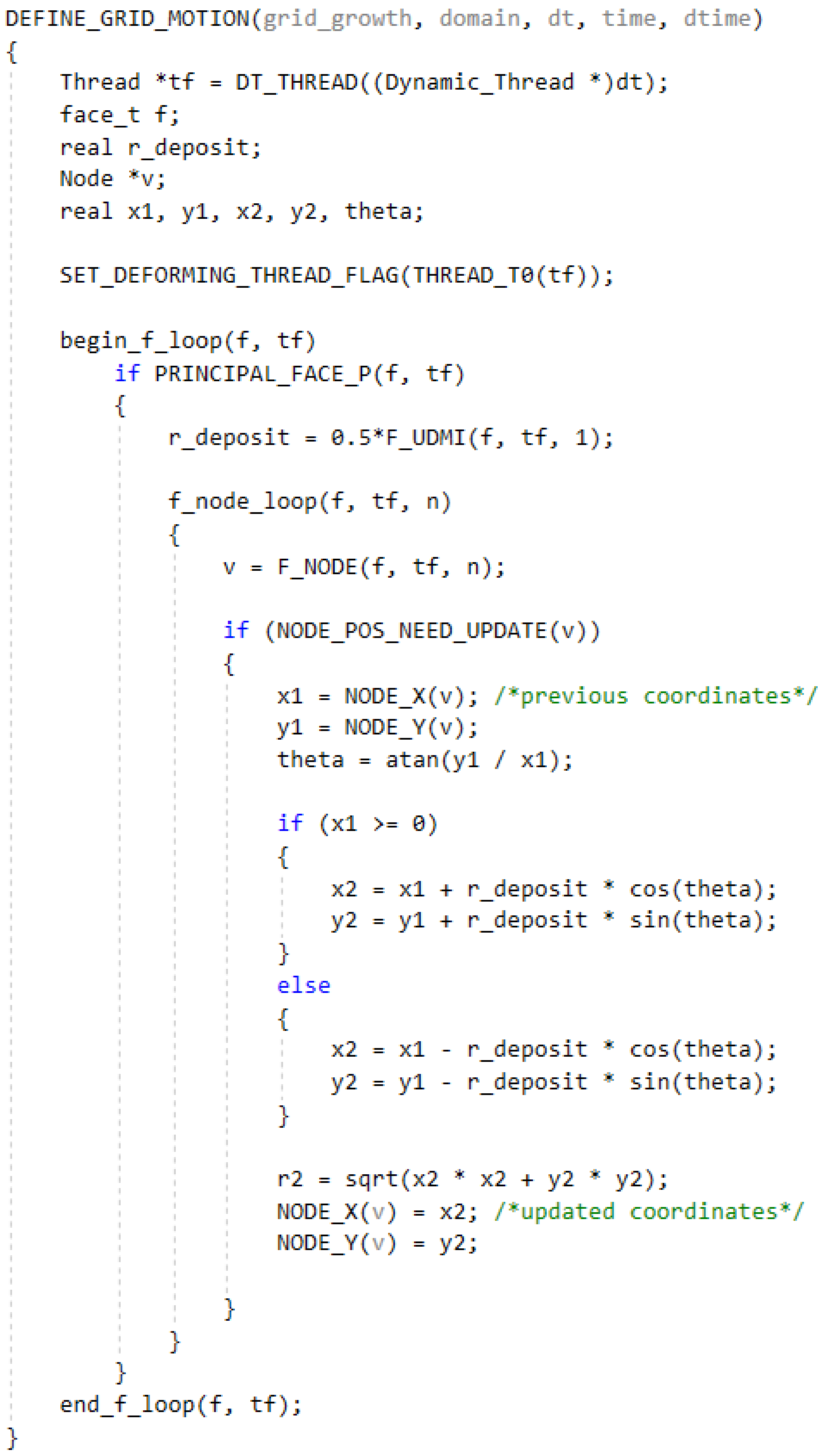

```
DEFINE_GRID_MOTION(grid_growth, domain, dt, time, dtime)
{
    Thread *tf = DT_THREAD((Dynamic_Thread *)dt);
    face_t f;
    real r_deposit;
    Node *v;
    real x1, y1, x2, y2, theta;

    SET_DEFORMING_THREAD_FLAG(THREAD_T0(tf));

    begin_f_loop(f, tf)
        if PRINCIPAL_FACE_P(f, tf)
        {
            r_deposit = 0.5*F_UDMI(f, tf, 1);

            f_node_loop(f, tf, n)
            {
                v = F_NODE(f, tf, n);

                if (NODE_POS_NEED_UPDATE(v))
                {
                    x1 = NODE_X(v); /*previous coordinates*/
                    y1 = NODE_Y(v);
                    theta = atan(y1 / x1);

                    if (x1 >= 0)
                    {
                        x2 = x1 + r_deposit * cos(theta);
                        y2 = y1 + r_deposit * sin(theta);
                    }
                    else
                    {
                        x2 = x1 - r_deposit * cos(theta);
                        y2 = y1 - r_deposit * sin(theta);
                    }

                    r2 = sqrt(x2 * x2 + y2 * y2);
                    NODE_X(v) = x2; /*updated coordinates*/
                    NODE_Y(v) = y2;

                }
            }
        }
    end_f_loop(f, tf);
}
```

FIGURE 5.2: The UDF that controls the motion of the nodes.

Boundary conditions		Coal air case	Biomass air case
Inlet (flue gas presents as mole fraction)	Velocity (m/s)	0.5	0.5
	Temperature (K)	1637	1531
	O_2	0.047	0.035
	H_2O	0.065	0.113
	CO_2	0.133	0.145
	N_2	0.755	0.707
Wall	Temperature (K)	1637	1531
Tube	Adiabatic wall (heat flux = 0)		
Outlet	Pressure outlet		

TABLE 5.1: The flue gas boundary conditions for coal air and biomass air combustion cases in the CFD simulation (Yang et al., 2019b).

Fly ash properties		Coal fly ash	Biomass fly ash
Flow rate (g/s)		0.24	0.31
Rosin-Rammler distribution (µm)	Minimum diameter	1	1
	Maximum diameter	200	200
	Mean diameter	36.86	102
	Spread parameter	1.096	1.174
Density (kg/m^3)		3174	3144
Specific capacity ($J\,kg^{-1}\,K^{-1}$)		1479	1269
Surface tension		0.394	0.411
Contact angle (°)		160	160
Melt fraction		0.83	0.415

TABLE 5.2: Fly ash properties used in the ash deposition model (Yang et al., 2019b).

5.1.3 CFD settings

The commercially available CFD solver, ANSYS FLUENT version 19.2, has been deployed to model the turbulence, radiation heat transfer, particle trajectories and the ash deposition growth. The software is coupled with the User Defined Functions and Memories to model the ash deposition growth process. Since the dynamic mesh model is utilized in the simulation, the transient FLUENT is used instead.

The flow chart of the simulation algorithm is shown in Figure 5.3. A similar quasi-transient calculation concept has been used to integrate the deposition growth model with the CFD framework (Kær, Rosendahl, and Baxter, 2006; Yang, 2017). In each time step, the algorithm proceeds to compute the global gas flow properties, such as the flow velocity, temperature, wall heat flux and etc. Once the velocity fields are known, Lagrangian particles are released from the inlet and are subsequently tracked by computing their trajectories. During this phase, the effects of particle-particle interaction are ignored as well as the influence on the turbulence diffusion due to the particles' presence (i.e. one-way coupling, see section 2.2.2). This is an acceptable compromise provided that the volume fraction of the fly ash particles in the flue gas is relatively low (Greifzu et al., 2016). The sticking procedure applies to a Lagrangian particle on the deposition surface, which determines a percentage of the mass of the particle that will stick to the surface. The remaining mass of that particle is reflected back to the stream. The collective mass on a deposition surface is then used to update the surface node dynamically and a global meshing is subsequently performed.

Due to a large number of cells in the computational domain, it has become a general requirement to utilize the parallelization capability of modern computer to accelerate the solution procedure. In particular, ANSYS FLUENT offers a parallel mode in which the computational domain is split into multiple partitions. Each computing node on the processor is assigned a partition and computations are carried out independently and the node synchronization is relied on the Message Passing Interface (MPI) protocol (ANSYS Inc., 2017). This way, a simulation case can be distributed to multiple processors. To be more exact, in Figure 5.4a, parallel FLUENT uses the Metis partition method as default. The different coloured regions in the domain correspond to the different partitions in parallel FLUENT with 6 processes. Note, however, that the deposit-flow interface is separated in three different partitions and is solved through three different processes. This may result in the erroneous mesh update if the dynamic mesh model was enabled in the simulation. Therefore, it is necessary to use a parallel partition strategy that avoids

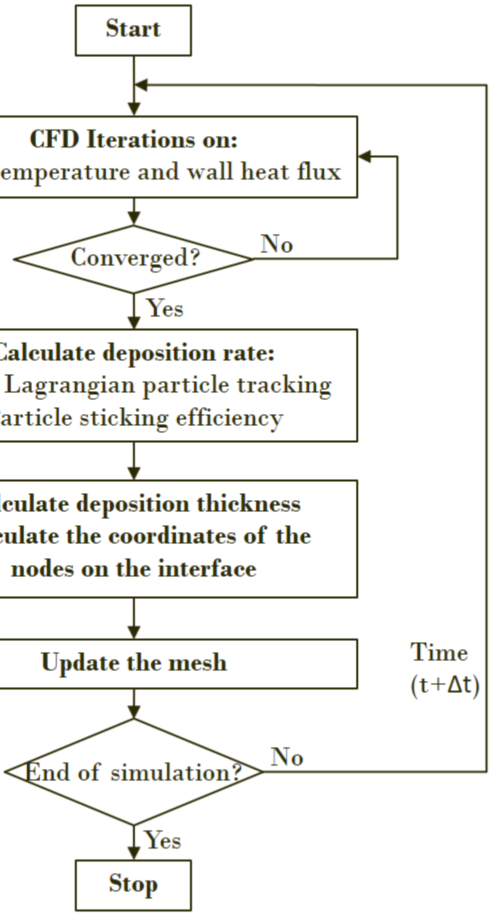

FIGURE 5.3: The algorithm of the ash deposition growth model integration in the CFD framework.

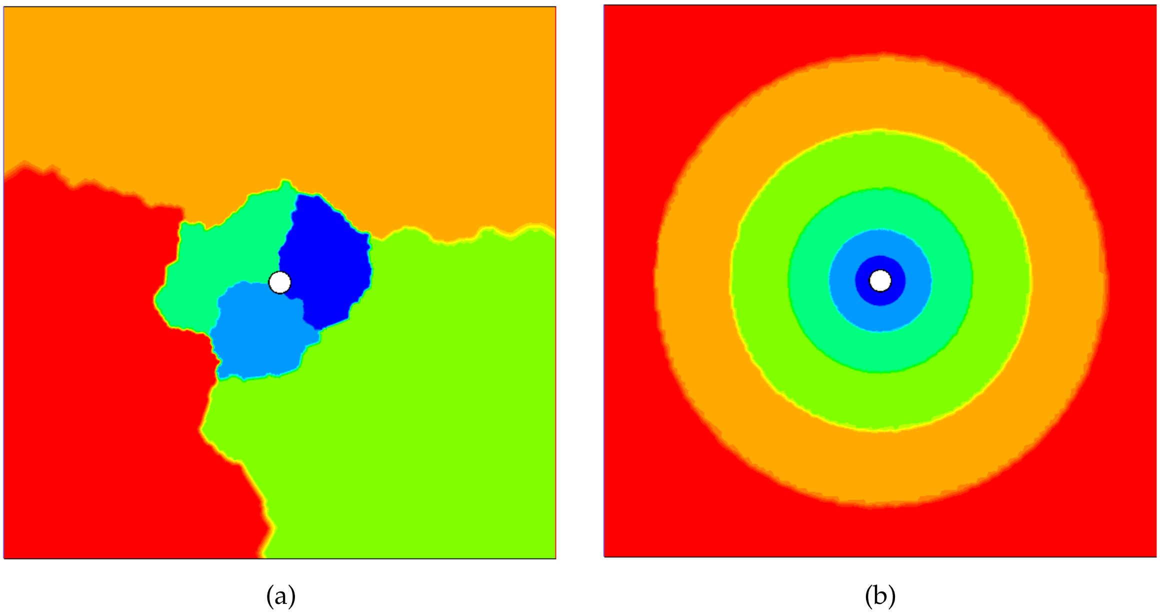

(a) (b)

FIGURE 5.4: The mesh partition in parallel ANSYS FLUENT: (a) Default partitions in parallel Fluent with 6 processes; (b) Modified partitions in parallel Fluent with 6 processes.

this issue. FLUENT has a built-in Polar R-Coordinate partition method, for which the partitions are arranged in a concentric manner as is shown in Figure 5.4b. The Polar R-Coordinate partition method places the deposit-flow interface (known as deposit surface) into the same partition. In doing so, the dynamic mesh could be deployed in the parallel FLUENT mode to properly modify the interface node whilst retaining the same performance acceleration.

5.2 Independence study

5.2.1 Mesh independence

In the simulation, both the accuracy and the efficiency are important factors to take into consideration. The deposition efficiency of the surface can only be accurately predicted when the flow-field near the deposition surface is accurately resolved (Weber et al., 2013a; Zhou and Hu, 2021). In order to resolve the flow-field within the boundary layer near the deposition surface, ten layers of quadrilateral cells with size 0.1 mm were distributed around the tube. Three different meshes are investigated with increasing resolution (Figure 5.5). They are known as the coarse mesh, medium mesh and the fine mesh. In Figure 5.5, the inner red circle represents the uncooled tube while the outer red circle is the deposition surface, which is also known as the interface between the deposit side and the flue gas side. The zone between these two red circles is the initial deposit zone and the rest is the fluid zone. For the coarse mesh, 100 faces on the fluid-solid interface were set and the total number of the cells amounts to 65702. As for the medium mesh, the number of the mesh face on the interface is 200 and the total number of cells is 82978. Finally, the fine mesh contains 124366 cells in total and has 400 mesh faces on the interface.

Sensitivity tests have been investigated on the influence of the different sizes of mesh. In order to get the results quickly and reduce the computational cost, all of the fly ash particles are assumed identical with a constant diameter of 100 µm. The density of the deposition on the tube is set to 400 kg/m^3. For the purpose of the sensitivity tests, it is assumed that all of the arrival ash particles will have a 100% sticking efficiency, so that the impacting particles will contribute 100% of their mass to the node update. In the discussion of Yang et al. (2019b), the effect of the flue gas velocity during the ash deposition formation was investigated. It has been observed that the flue gas velocity is a significant factor in determining the impaction efficiency, which is defined as the ratio between the number of particles delivered to the deposition surface and the total number of particles being released into the gas. For example, Yang et al. (2019b) noted that the impaction efficiency is increased approximately from 3% to 50% for coal ash particles at the two flue speeds 0.5 m/s and 25 m/s, respectively. Hence, in order to observe a more pronounce change of the deposition shape, a reasonable value of the impaction efficiency is required. Presently, this is controlled by adjusting the velocity of flue gas and ash particles to 5 m/s. The effect of the time step size will be discussed later, but for the present cases, the time step size is set to 1s as default and there are 400 time steps in total. 400 seconds of deposition time is simulation during this study.

Figure 5.6 shows the deposition shape after 400s deposition time for the three meshes. The light grey zones represent the grown deposition. The results highlighted a common trend where a dominant growth direction is observed (see Figure 5.6b), which is located at the upstream stagnation position of the deposit surface (i.e. $\alpha = 180°$). All of the cases considered have reached steady state and no instabilities are observed. However, the grown deposition surface in the fine mesh case appears to be not smooth compared to the coarse and medium mesh cases, as is shown in Figure 5.7. It would appear that beyond a certain mesh resolution, saw-tooth instability could propagate throughout the simulation, which may pose a risk for the appearance of negative cell volumes during the mesh update. The appearance of the instability may be attributed to the non-smooth mass flux on the deposit surface, which is determined from the discrete phase. At a certain mesh resolution, this non-smoothness exacerbates the cells to alternate to skew on a particular direction; resulting in a saw-tooth pattern that cannot be smoothed over time. One way to resolve this issue is to employ the mass re-distribution approach, in which the mass of the impacting particle is re-distributed over a section of the interface surface. However, this approach is computational intensive and difficult to implement on parallel FLUENT. For this reason, this approach is not being used in the current study.

Since the tube position at $\alpha = 180°$ is the stagnation point, ash particles are more likely to be transported to this area, which may lead to a higher impaction efficiency around the stagnation region. Among the three cases investigated, the differences in the velocity, pressure and the particle arrival rate are all less than 2%. From Figure 5.7, the largest thickness of the deposition is 2.582 mm, 2.588 mm and 2.588 mm for the coarse, medium and fine mesh, respectively. The y^+ in the coarse mesh is 1.4 and 0.6 for the medium mesh while a value of 0.8 was used for the fine mesh. Simulation times of the coarse and medium mesh simulations are about the same while the time for the fine mesh took three times longer than the other cases. Therefore, it is reasonable to use the medium mesh for subsequent simulations as it reduces the computational cost whilst maintaining an acceptable accuracy.

5.2.2 Time step size independence

As discussed in section 5.2.1, the medium mesh contains 82978 cells and 200 faces on the interface and it balances computational speed and accuracy, thus it is chosen for the following simulations. The sensitivity of the time step size will be investigated in this section. García Pérez, Vakkilainen, and Hyppänen (2015) used a time step of 0.1 ms to predict the deposition shapes in a tube array. Zhou and Hu (2021) chose the time step 0.005 s to investigate the ash deposition behaviour whilst Yang, Zhou, and Wu (2022) set the time step size to be 10 s in the first 3 minutes of the deposition and 30 s in the rest time. Based on the former test cases, for the uniform ash particle size (100 µm), two different time step sizes, 1 s and 0.01 s, have been tested. Figure 5.8 shows the shape of the ash deposition after 400s deposition time. The basic flow variables such as the velocity, pressure and the particle arrival rate, are observed to not deviate much from each other; each with a relative error estimate of less than 1%. To reinforce the sensitivity of the time stepping, the deposition height is investigated between the two cases at the forward stagnation point. It is observed that the largest thickness of the deposition, which is at the forward stagnation point, is 2.588 mm and 2.595 mm for the 1 s and 0.01 s time step size cases, respectively. This is largely consistent with

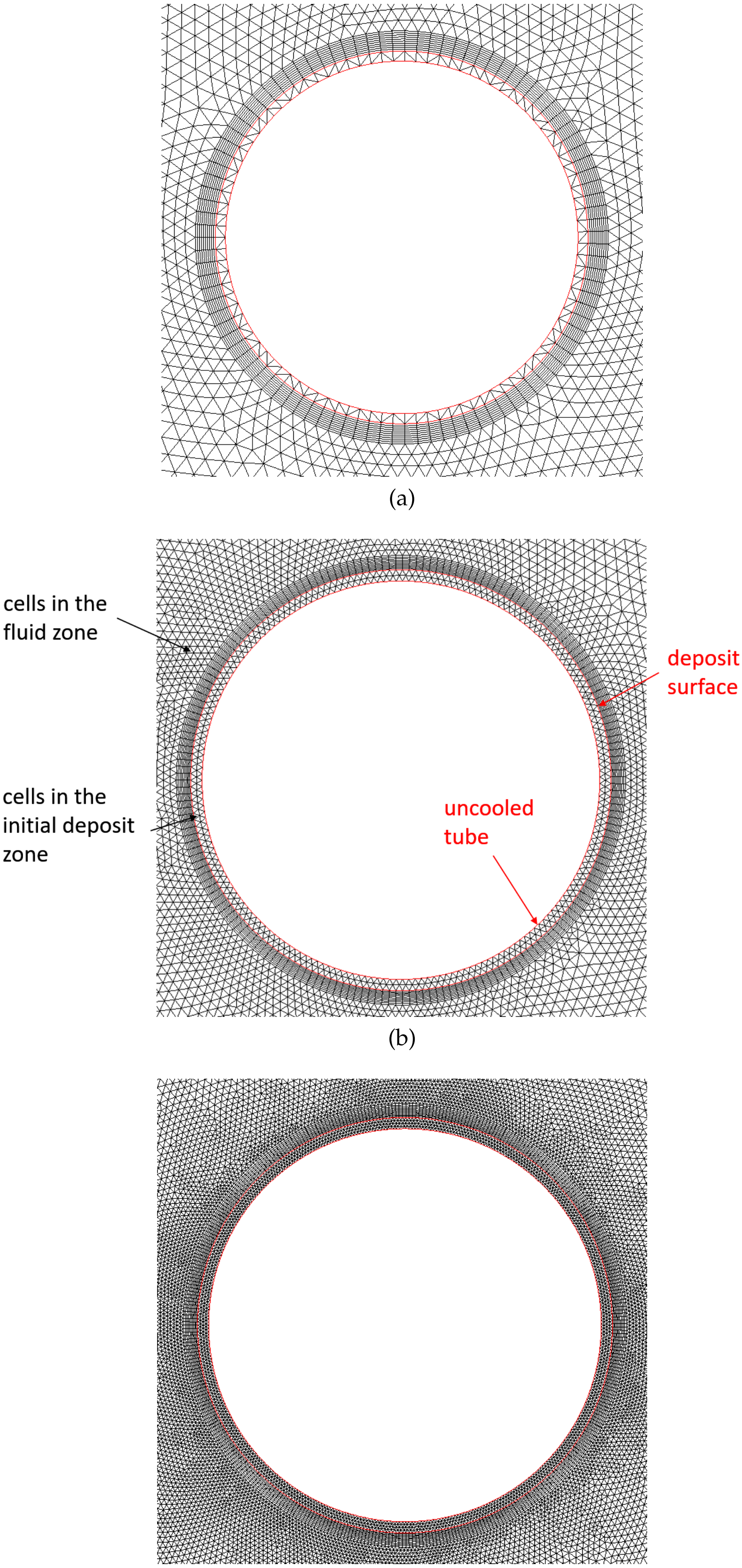

(a)

(b)

(c)

FIGURE 5.5: Different meshes around the tube: (a) Coarse mesh, (b) Medium mesh, (c) Fine mesh.

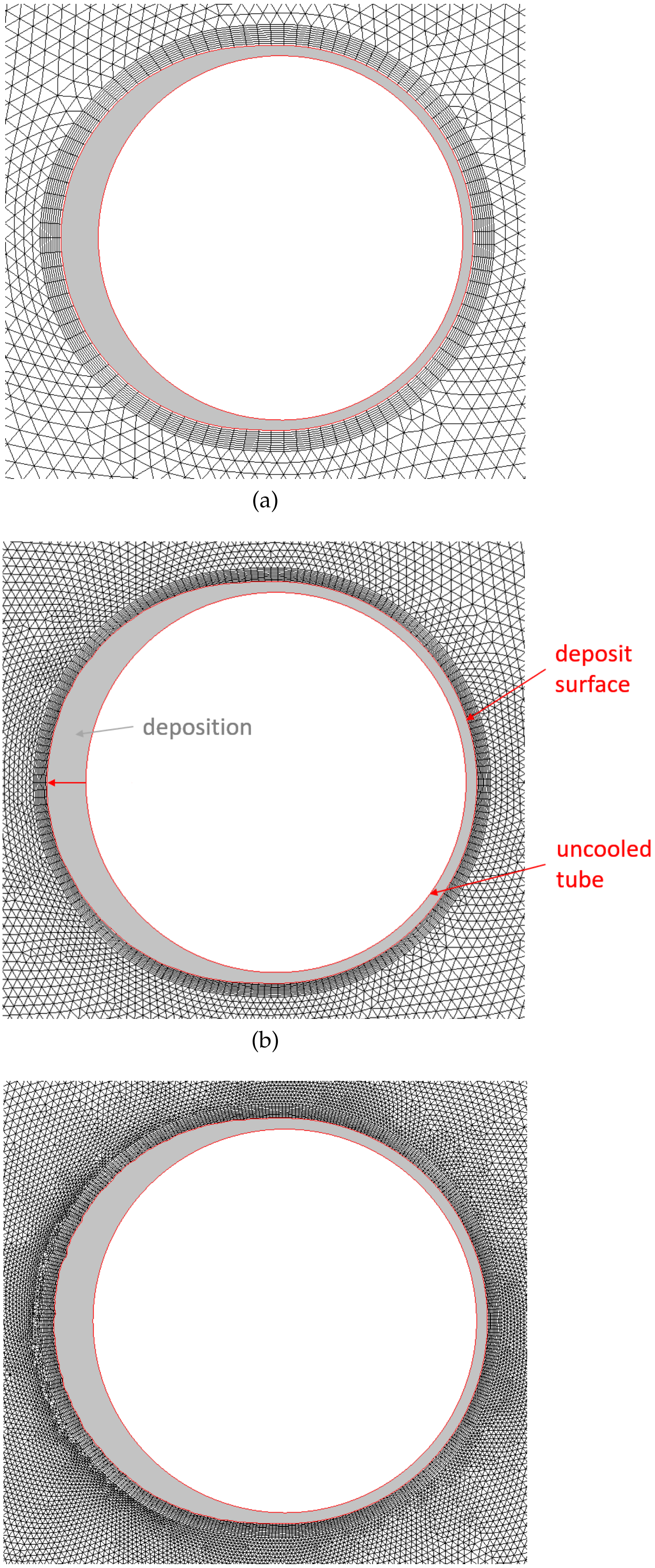

(a)

(b)

(c)

FIGURE 5.6: Simulation results for test cases in different meshes: (a) Coarse mesh, (b) Medium mesh, (c) Fine mesh.

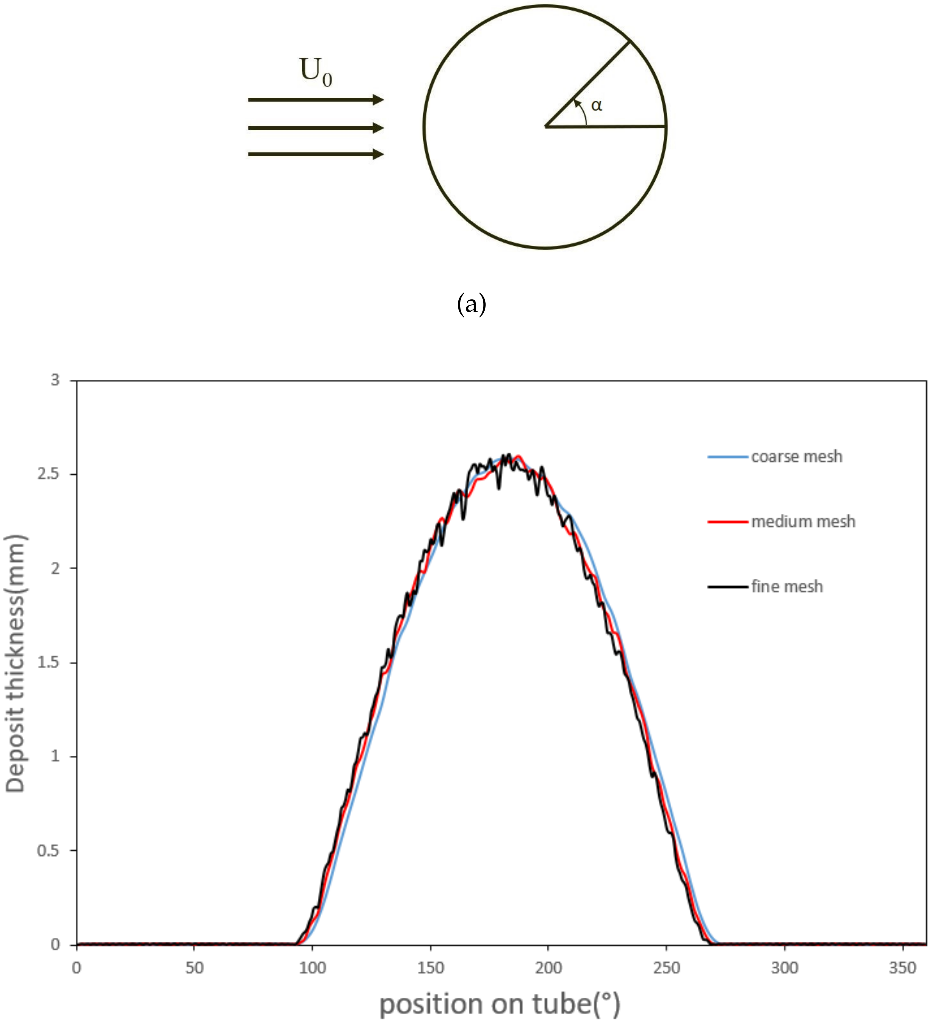

(a)

(b)

FIGURE 5.7: Simulated deposit growth profile on the tube for test cases in different meshes: (a) Referencing for the angle coordinate α for tube; (b) Deposition thickness on the tube.

the observed differences between the flow variables.

In addition to the uniform size distribution of the ash particles discussed previously, time sensitivity tests are also carried out for ash particles that follow the Rosin-Rammler distribution discussed in section 5.1.2. For these set of tests, the same simulation conditions are retained except that the investigated time steps are chosen to be: 0.001 s, 0.01 s and 1 s. Note that an extra case of time step is included (namely 0.001 s), this is necessary since the Rosin-Rammler distribution might produce ash particles with exceptionally small diameters, which may affect the overall deposition behaviour. Figure 5.9 shows the shape of the ash deposition after 400 time steps. The largest thickness of the deposition is 1.522 mm, 1.521 mm and 1.523 mm for the 1 s, 0.01 s and 0.001 s time step size cases, respectively. The deposition height at the forward stagnation point of the tube can be shown to vary within 1% of each other.

This concludes that the quasi-transient simulations are not too sensitive to the choice of the time step size. For this reason, a larger time step may be selected to achieve the same level of accuracy while substantially accelerate the simulation time.

5.3 Case study for coal/biomass deposition

5.3.1 Predicted ash deposition behaviour in PACT

Figure 5.10 shows that the measured deposit is mainly formed at the windward section of the uncooled tube while almost no deposit appears on the leeward section (Yang et al., 2019b). Windward is towards the direction from which the flue gas is coming, while leeward is downwind from this direction. In the pilot-scale furnace, the Reynolds number for the flue gas is about 70 in

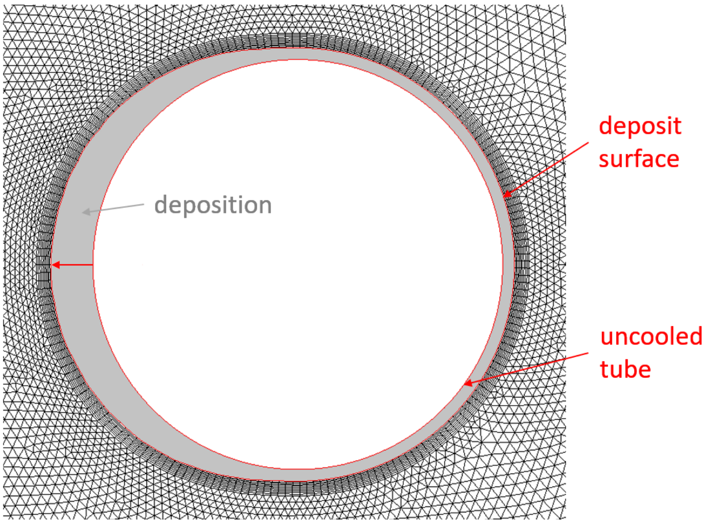

(a)

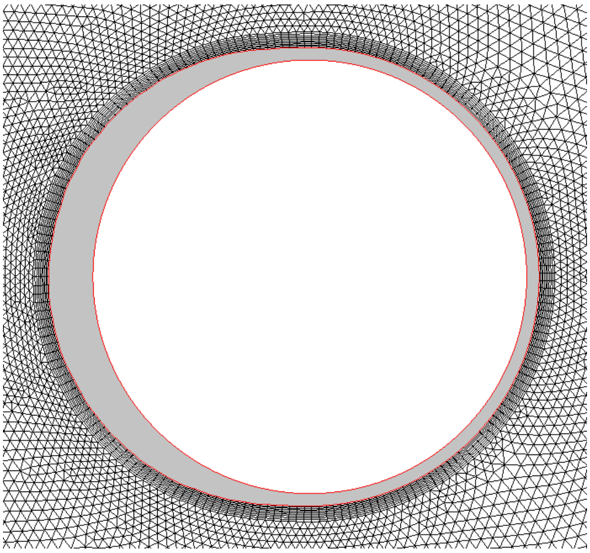

(b)

FIGURE 5.8: Simulation results for test cases in different time step sizes for uniform particles for 400s deposition time: (a) 1 s, (b) 0.01 s.

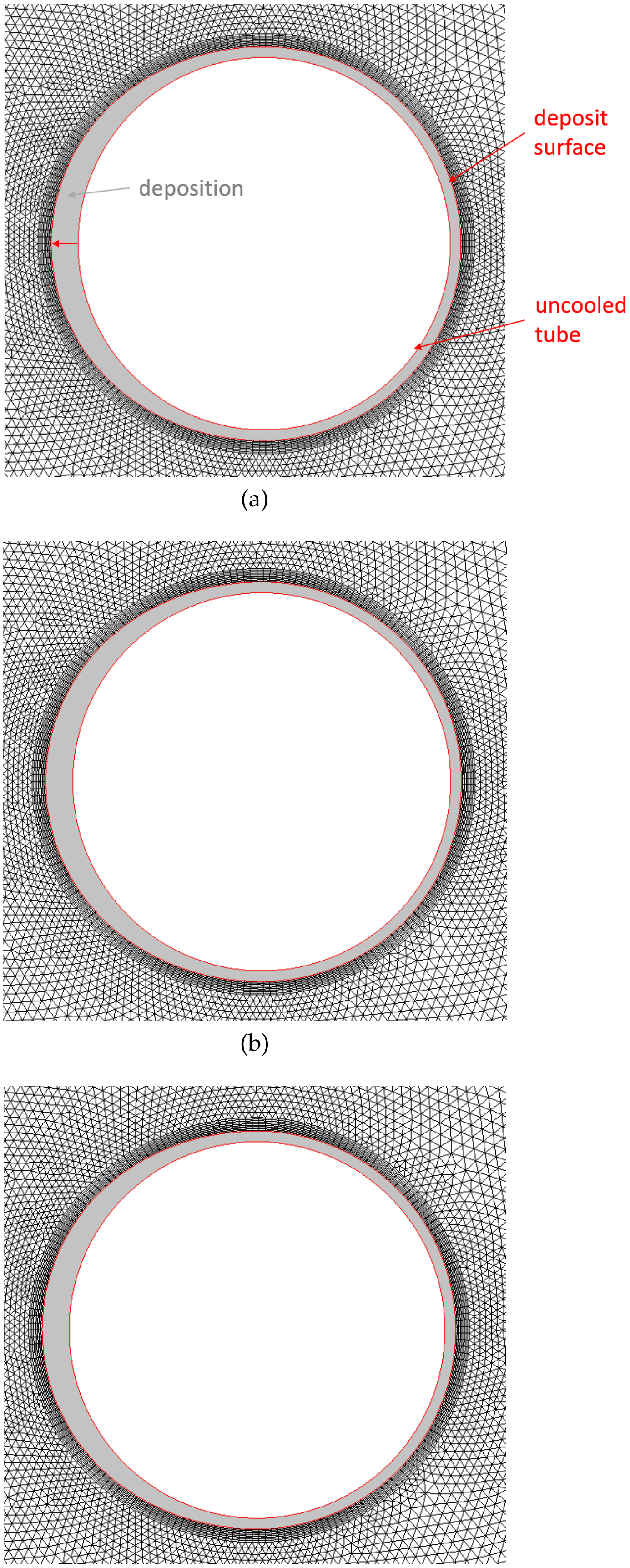

(a)

(b)

(c)

FIGURE 5.9: Simulation results for test cases in different time step sizes for 2R distribution particles for 400s deposition time: (a) 1 s, (b) 0.01 s, (c) 0.001 s.

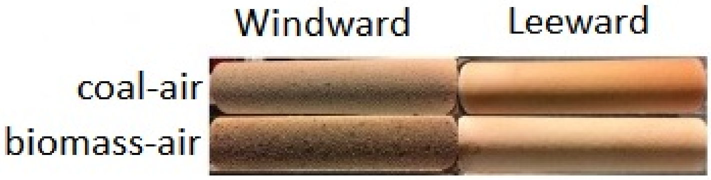

FIGURE 5.10: Deposit images on the tube (Yang et al., 2019b).

the downstream region (Yang et al., 2019b). Hence, both the thermophoretic effect and the eddy impaction are insignificant (Yang et al., 2019b).

Figure 5.11 shows the predicted deposition shape on the tube after six hours for the pilot-scale furnace in PACT. The predicted deposition (light grey zone) surface shows that the deposit shape is not smooth (see Figure 5.11). The reason might be attributed to the small particle Stokes number in the simulation. Furthermore, one may also argue that the current number of the tracked ash particles is not sufficiently large enough to reconstruct a smooth profile. This is consistent with the observation of Yang, Zhou, and Wu (2022), who observed that, by increasing the particle count into the main flow, a substantial improvement on the smoothness of the impaction efficiency distribution can be achieved, which also helps to reduce the error in the predicted deposition thickness. Currently, the effect of the number of tracked ash particles is not investigated further and is left for further work.

The ash deposition rate for coal air combustion case was found to be about 6.0 $g/(m^2h)$ in experiment, while it is about 24.2 $g/(m^2h)$ for recycled wood biomass (Yang et al., 2019b). The predicted ash deposition rate for coal and biomass air combustion cases are 5.5 $g/(m^2h)$ and 25.0 $g/(m^2h)$, respectively. The simulation results for both cases agree with the measured results. The predicted deposition rate is calculated from the multiplied value of the ash particle mass flux, the overall impaction efficiency and the overall sticking efficiency. It can be observed that the ash deposition rate for coal air combustion is much lower than the biomass, which is chiefly because of

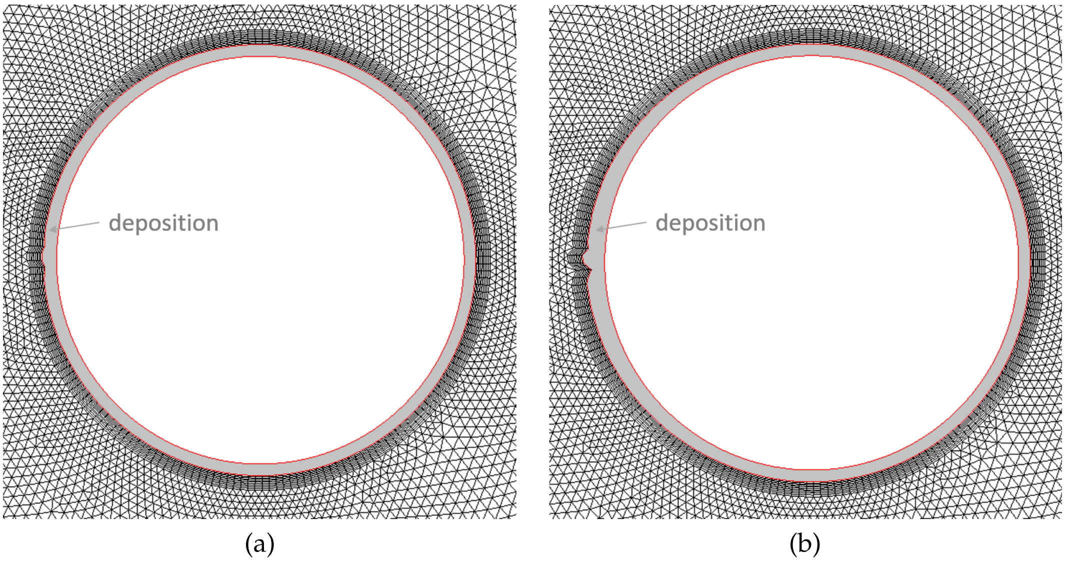

(a) (b)

FIGURE 5.11: Predicted ash deposition on the tube after 6h in PACT: (a) Coal air; (b) Biomass air.

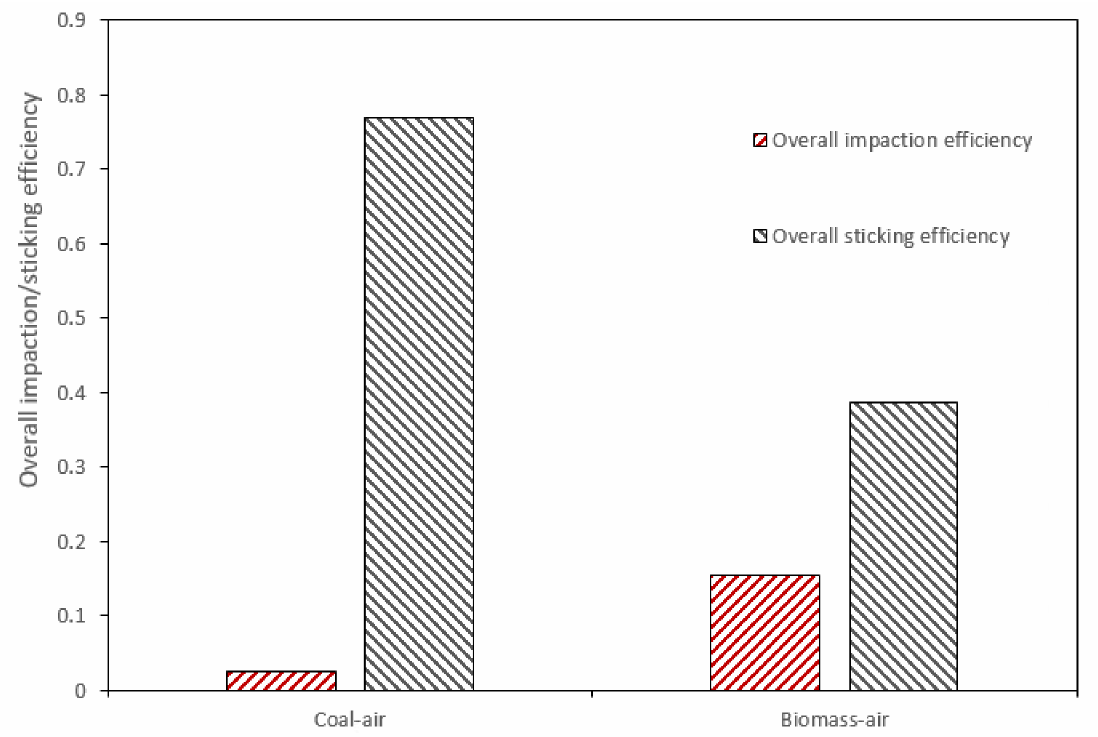

FIGURE 5.12: Predicted overall impaction and sticking efficiency in pilot-scale furnace.

the overall impaction efficiency for coal (2.6%) being much lower than the biomass (15.4%), see figure in Figure 5.12. On the other hand, the overall sticking efficiency for coal has a value of 0.77, which is approximately twice the value of biomass (0.38).

5.3.2 The effect of flue gas velocity

Utility-scale boilers produce a much higher flue gas velocity than pilot-scale furnaces. For instance, a typical flue gas speed produced by an utility-scale boiler is about 20 m/s whereas it is about 0.5 m/s for pilot-scale boilers. This difference in flue gas speed contributes to a large difference in the dimensionless parameters in the system such as the the Reynolds number and particle Stokes number as well as the total kinetic energy. In order to accurately predict the deposition behaviour, one needs to take account of the velocity condition.

Figure 5.13 and Figure 5.14 show the predicted ash deposition (light grey zone) for coal and biomass under different flue gas speeds (0.5 m/s, 15 m/s and 25 m/s). For the coal air combustion case, the change of the deposition shape is seen to be the greatest when the flue gas velocity is 15 m/s. Likewise, the largest deposition shape change corresponds to the flue gas velocity 0.5 m/s for the biomass air combustion case. Figure 5.15b shows the predicted deposition thickness at the tube position $\alpha = 180^\circ$, which matches the deposition shape change in Figure 5.13 and Figure 5.14. Similarly, Figure 5.15a shows the predicted ash deposition rate under different conditions. It is interesting to note that the predicted ash deposition rate for coal increases from 6 to $32 - 42$ g/(m^{2}h) when the flue gas velocity is increased from 0.5 m/s to 25 m/s. The coal air combustion has the highest ash deposition rate at the 15m/s of flue gas velocity. On the other hand, the ash deposition rate decreases from 25 to $3 - 6.7$ g/(m^{2}h) for the biomass air combustion. The

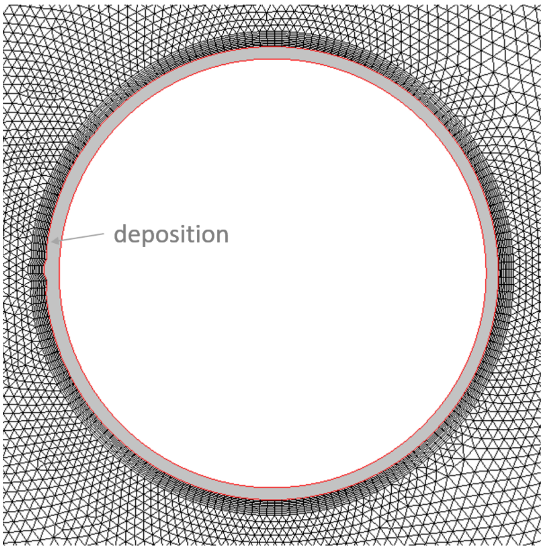

(a) v = 0.5 m/s

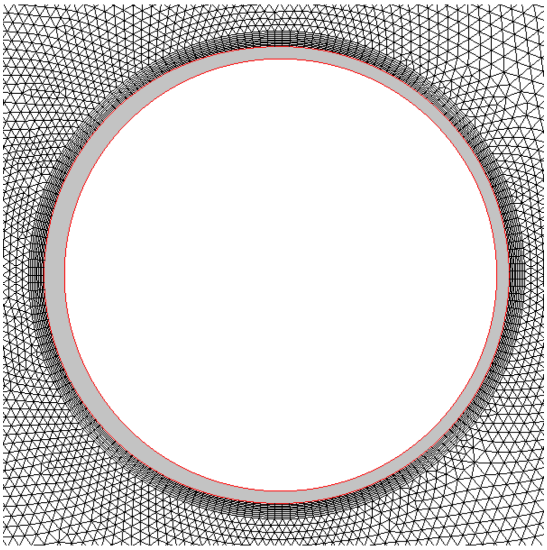

(b) v = 15 m/s

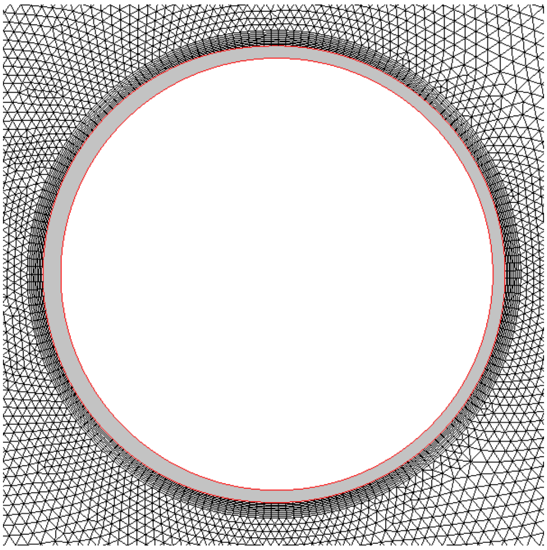

(c) v = 25 m/s

FIGURE 5.13: Predicted ash deposition on the tube for coal air case after 6h under different flue gas velocity.

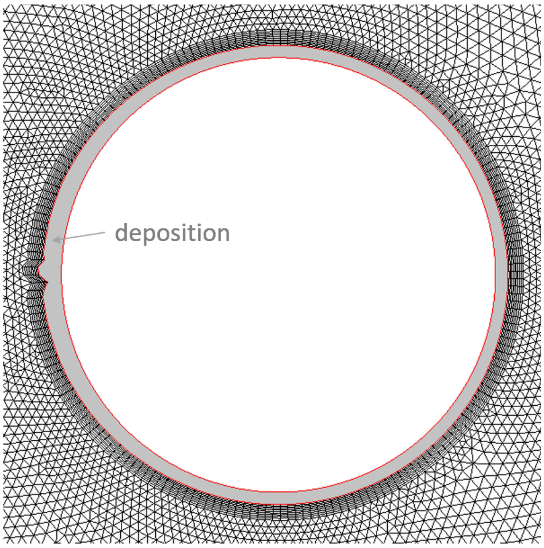

(a) v = 0.5 m/s

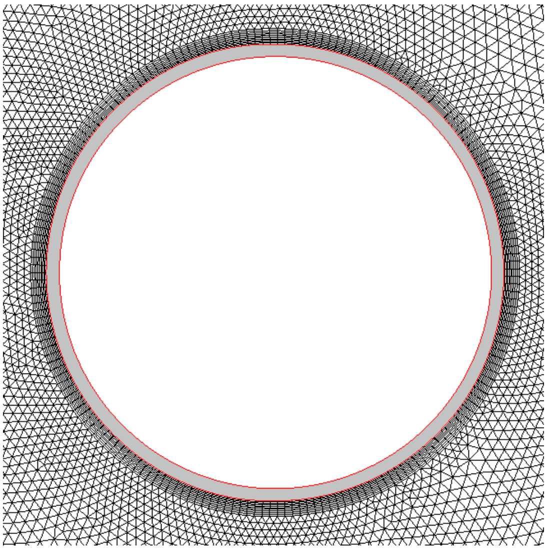

(b) v = 15 m/s

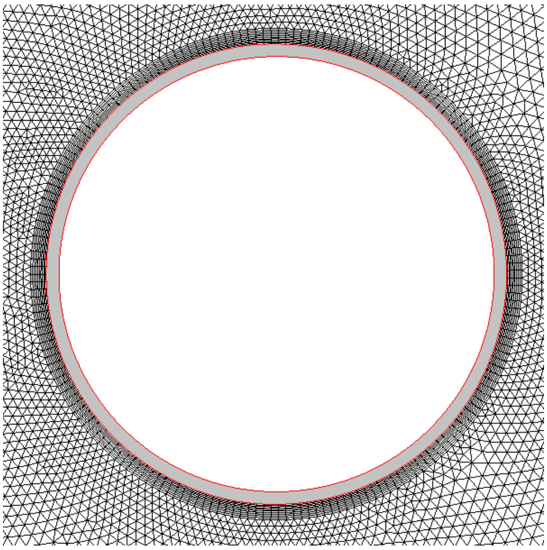

(c) v = 25 m/s

FIGURE 5.14: Predicted ash deposition on the tube for biomass air case after 6h under different flue gas velocity.

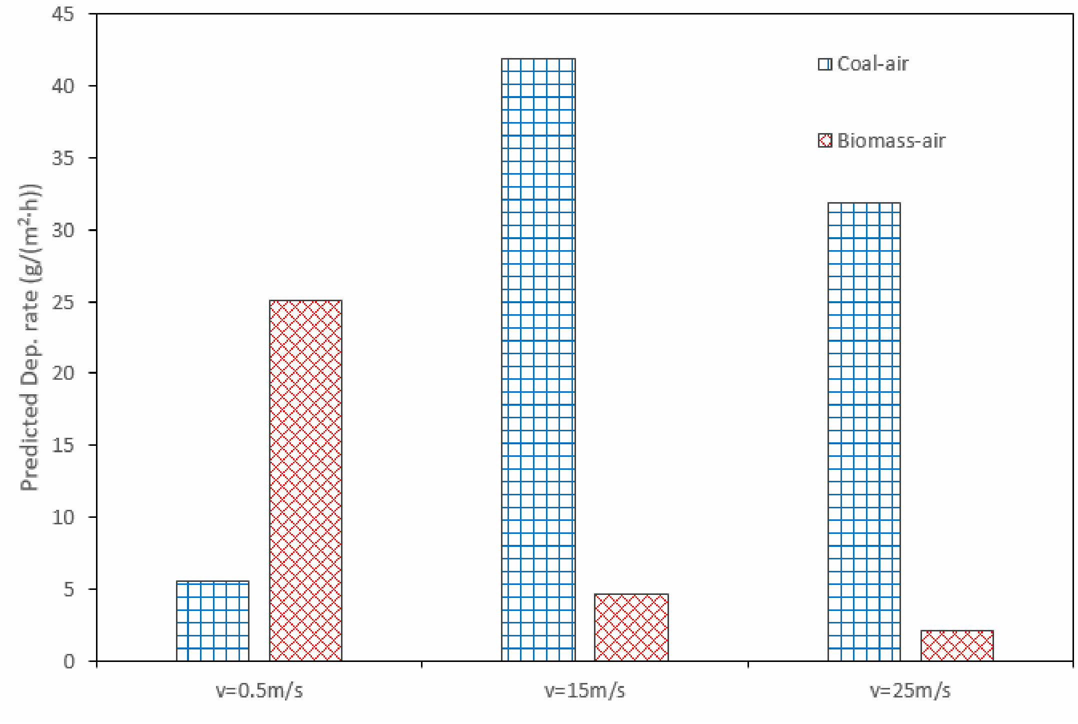

(a)

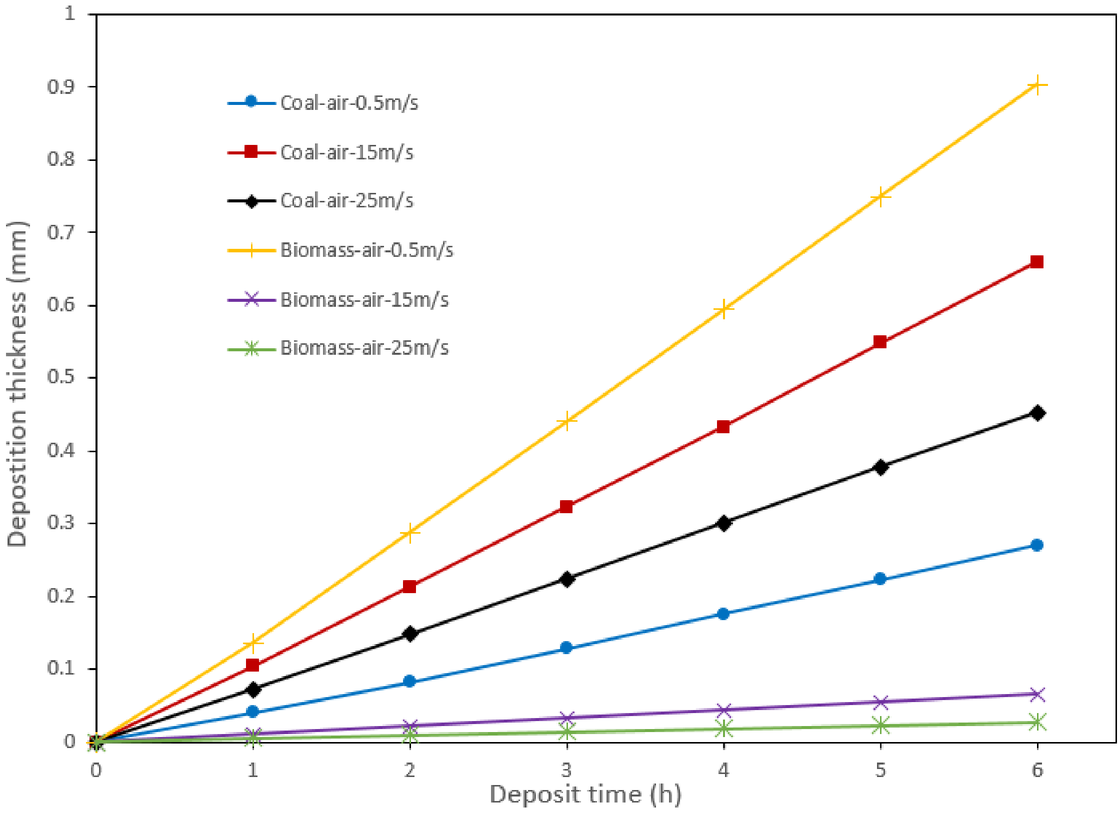

(b)

FIGURE 5.15: (a) Predicted ash deposition rate under different flue gas velocity conditions; (b) Predicted deposition thickness for coal and biomass air cases under different flue gas velocity conditions.

change of the deposition rate leads to the same change trend of the deposition shape. Also, the predicted deposition rates are similar to Yang et al. (2019b)'s predicted results. Furthermore, the trend predicted by the model for coal and biomass deposition rate with the increase of the flue gas velocity is mainly caused by the difference of the fly ash properties produced by the two fuels. As shown in Table 5.2, biomass fly ash particles are more coarse than the coal ash particles. Due to the low flue gas velocity (i.e. 0.5 m/s), the pilot-scale furnace favours the coarse particle deposition. However, with the increasing of the flue gas, the fine particles take the major responsibility to the deposition (Yang et al., 2019b).

The predicted impaction and sticking efficiencies are given in Figure 5.16 for the three speeds considered in this study ($v = 0.5, 15, 25$ m/s). The higher speeds are indicative to the typical velocity conditions in utility-scale boilers. Consequently, those boilers lead a higher particle Stokes number and kinetic energy, which can have a drastic effect on the impaction and sticking efficiencies. For example, the impaction efficiency increases from 2.6% to almost 50% for coal when the flue gas speed goes from 0.5 to 25 m/s. The sticking efficiency, on the other hand, is observed to be decreasing at higher velocities; starting at the maximum of 77% to around 25% at the highest speed. A similar trend is observed for the biomass combustion. This decreasing trend in the sticking efficiency is actually predicted by the sticking model (i.e. Equation 3.2.1), where the higher flue gas speed results in a higher normalized excess energy E^*. If this energy is positive, then the model predicts an exponentially decreasing function of E^* (see Equation 3.2.1b). For the two combustion cases (coal and biomass) considered, the reported results are both consistent with the results of Yang et al. (2019b).

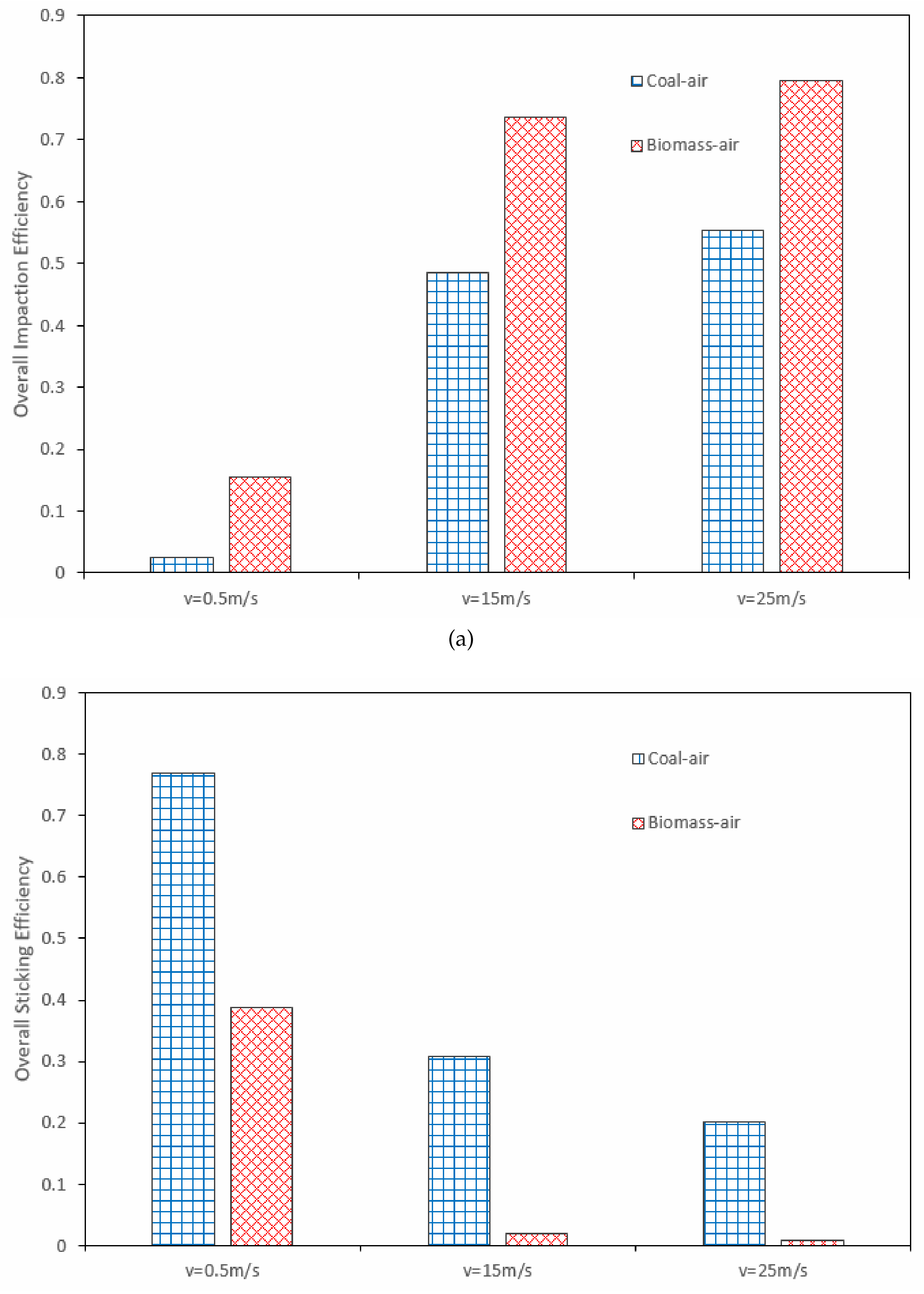

(a)

(b)

FIGURE 5.16: Predicted (a) overall impaction efficiency and (b) overall sticking efficiency under different flue gas velocity conditions.

5.3.3 Prediction of evolution of deposition shape

In utility-scale boilers, the combustion system is intended for long term operations. Thus, understanding the effect of the ash deposition is ever more important. In section 5.3.2, it is observed that the high flue gas velocities in the coal air combustion case lead to the biggest deposit rate under the velocity of 15 m/s. The deposit geometry essentially determines the accurate prediction of the formation process, thus this section examines the evolution of the geometry from an initially clean tube. To this ends, the same boundary conditions are used. Figure 5.17 shows the change of the deposition shape during the 84 hours. The shedding of the deposition (or erosion) is not considered during the simulation.

It is worthwhile to examine some important features about the ash deposition. For instance, it is noted that the predicted deposition rate varies as a function of the azimuthal angle α sampled at three different times (Figure 5.18), however, the averaged predicted deposition rate (defined as the area integral divided by 2π) are around 41 $\mathrm{g}/(\mathrm{m}^2\mathrm{h})$ for all deposition times. It should be noted that most ash particles accumulate at the tube position $\alpha = 180°$ when the deposit grows. And at the deposit time of 84h, there are a few particles transport to the leeward of the tube (position $\alpha = 10°$), which is mainly because the turbulence eddy diffusion effect. The change of the deposition shape results in a change of the velocity distribution around the tube, which is shown in Figure 5.20. Moreover, the predicted sticking efficiency follows a similar trend (shown in Figure 5.19a), and the overall sticking efficiency remains around 30% for the whole 84 hours. Since the calculation of the sticking efficiency is related to the normal velocity of the impacting particles to the deposit face, the average normal velocity is larger at the position $\alpha = 180°$ than it is at $\alpha = 90°$ and $\alpha = 270°$ (Figure 5.19b). The sticking efficiency will decrease with increasing normal velocity magnitude. It is noted that, due to the change of the velocity distribution around the tube from the deposit time 0h to 84h, the average normal velocity of the ash particles at the same tube position (for example, the tube position $\alpha = 130^\circ$) decreases with the deposit time. Thus the sticking efficiency at the same tube position increases with the deposit time. But the arrival rate of the ash particles at the same tube position ($90^\circ - 160^\circ$ and $200^\circ - 270^\circ$) decreases with time. The net effect is that the deposition rate (product between the arrival and sticking efficiency) is observed to be lower than those of earlier times except near the forward stagnation point at which a noticeable increase of deposition rate is found. All of the changes lead to the accumulation of the ash particles at the tube position $\alpha = 180^\circ$ when the deposition time comes to 84h. However, the average rate among the three sampled times is approximately constant and it could be because the temperature remains unchanged when predicting the ash deposition on the uncooled tube.

When modelling the ash deposition on the cooled tube, the mechanisms involved in the ash particles transport to the deposit surface are more complicated than those of the uncooled case. For the prediction of the ash deposition on the uncooled tube discussed earlier, the thermophoresis effect is not taken into consideration. However, this is considered an important mechanism in the presence of a strong temperature gradient. Yang et al. (2017b) considered the alkali vapour condensation and thermophoresis when predicting the ash deposition on the cooled tube, especially at the initial stage when the deposition surface temperature was increasing at a faster rate. Additionally, other deposition properties, like porosity and thermal conductivity, may also vary with the deposition growth (Yang et al., 2017b), which are taken as constant in the current study. In the paper of Yang, Zhou, and Wu (2022), the predicted deposition rate increases with the increasing of deposit time.

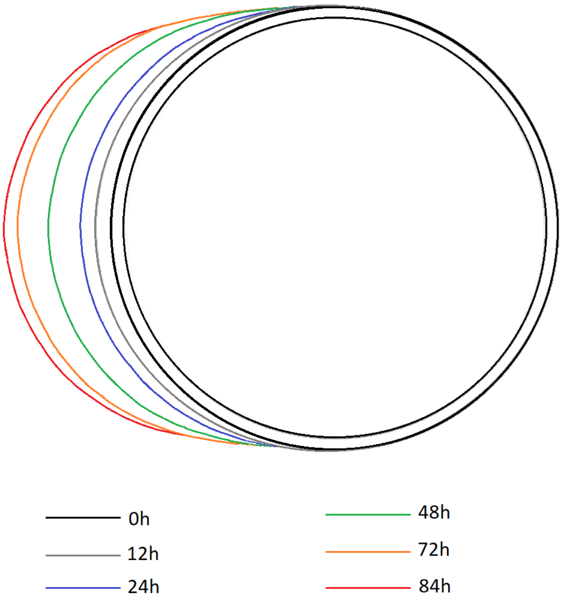

(a)

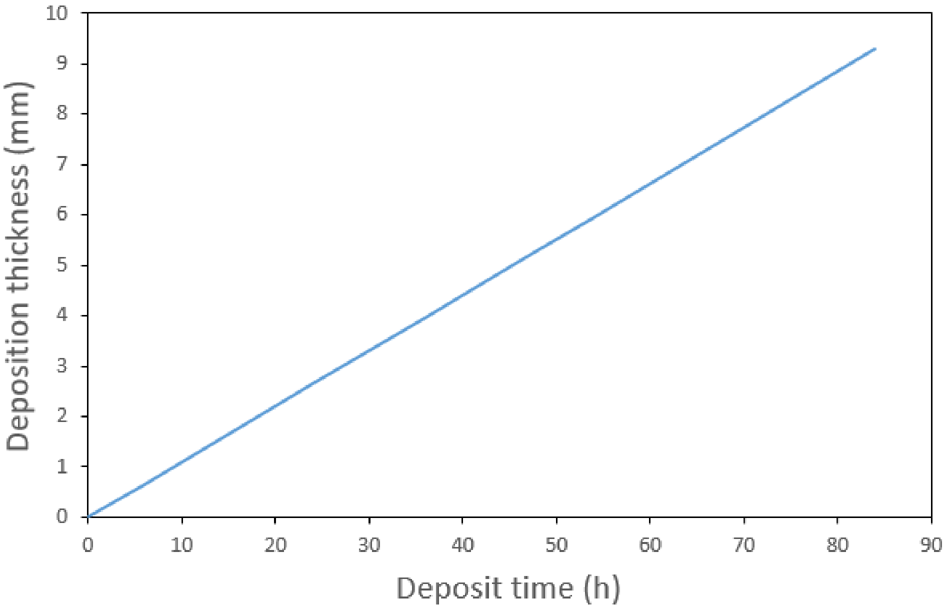

(b)

FIGURE 5.17: Predicted long term ash deposition for coal air case: (a) The change of the deposition shape; (b) The deposit thickness at the tube position $\alpha = 180°$ as a function of the deposition time.

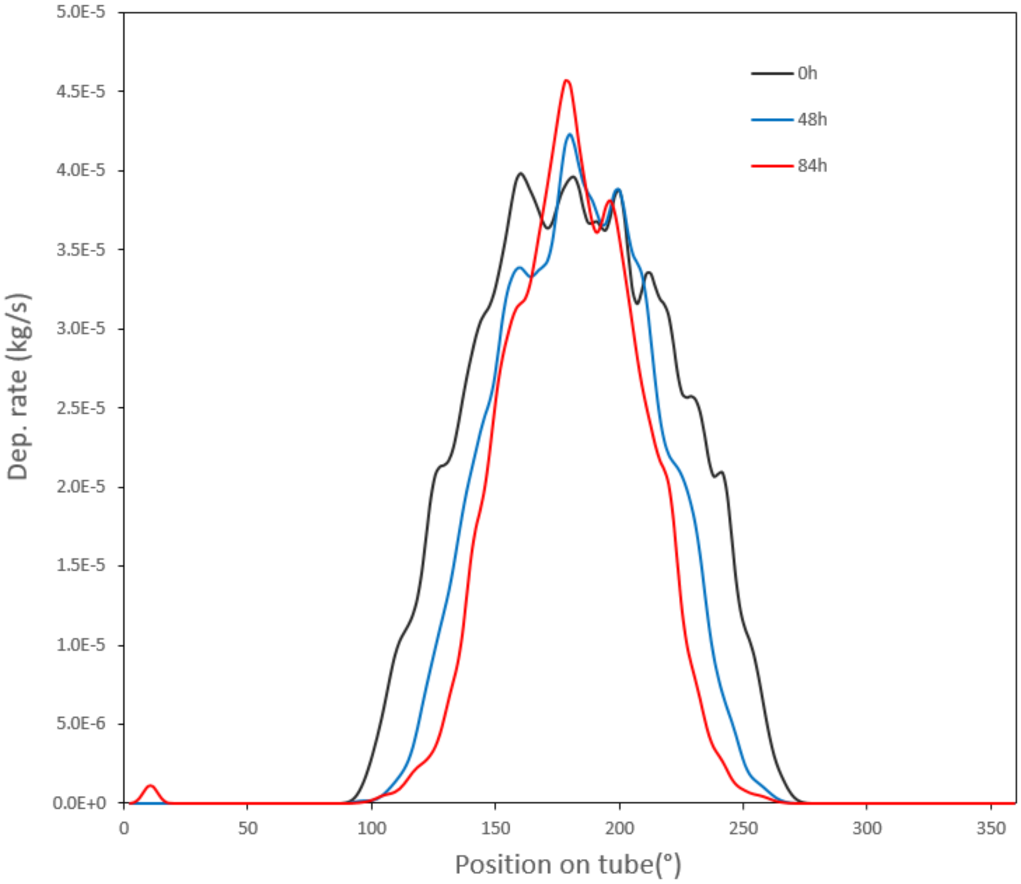

(a)

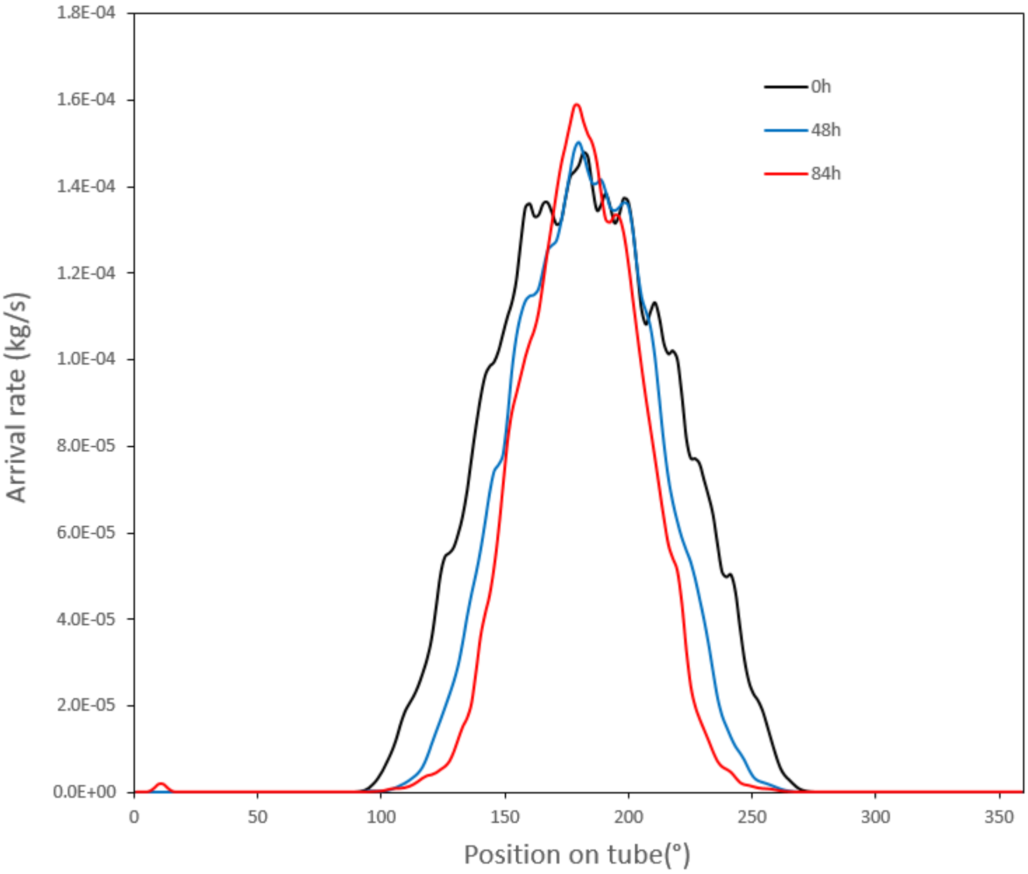

(b)

FIGURE 5.18: Predicted (a) deposition rate and (b) arrival rate on the tube under different deposit time.

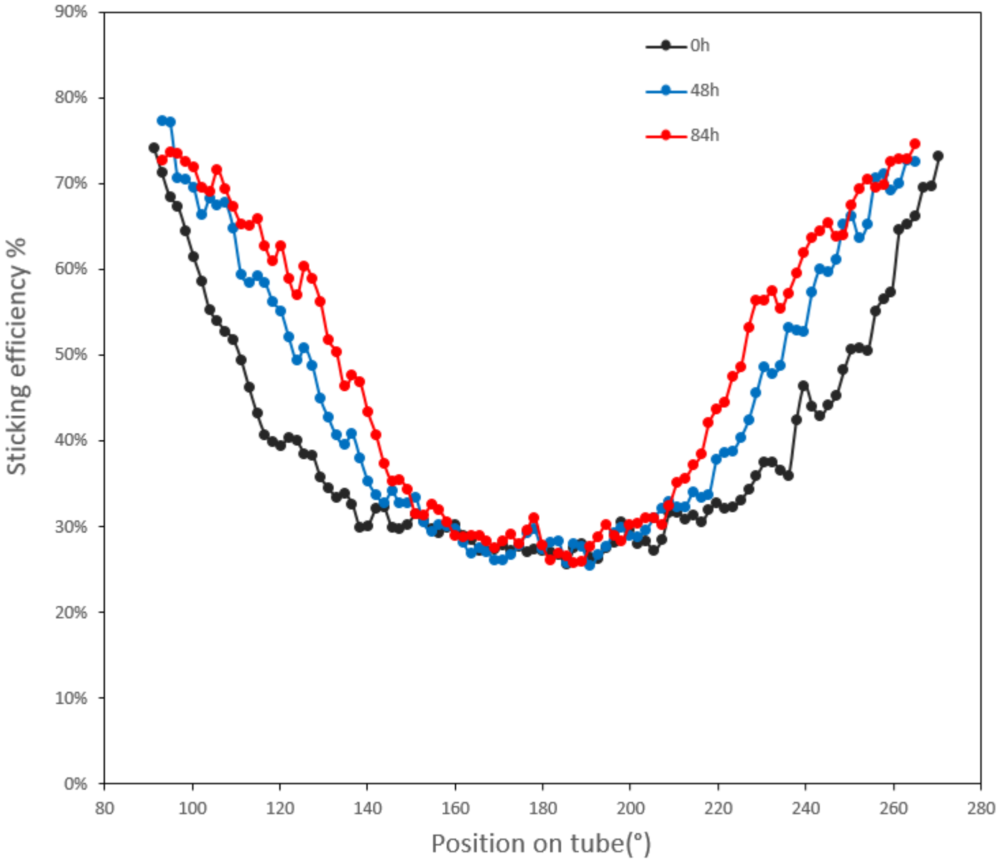

(a)

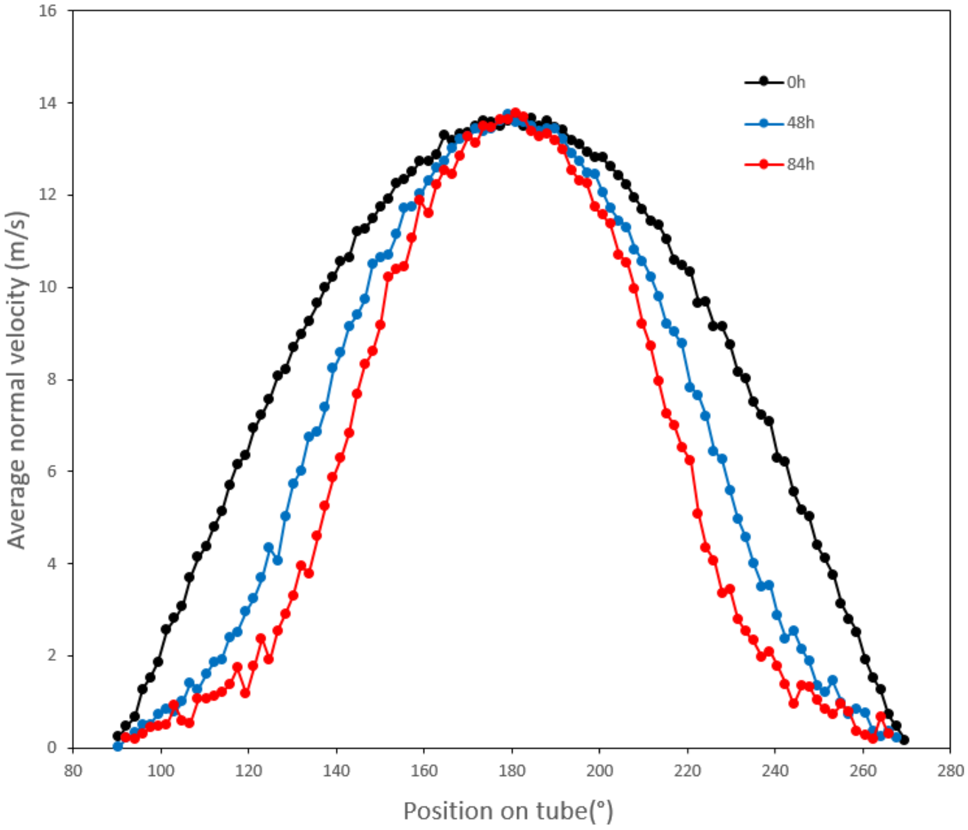

(b)

FIGURE 5.19: Predicted (a) sticking efficiency and (b) average normal velocity on the tube under different deposit time.

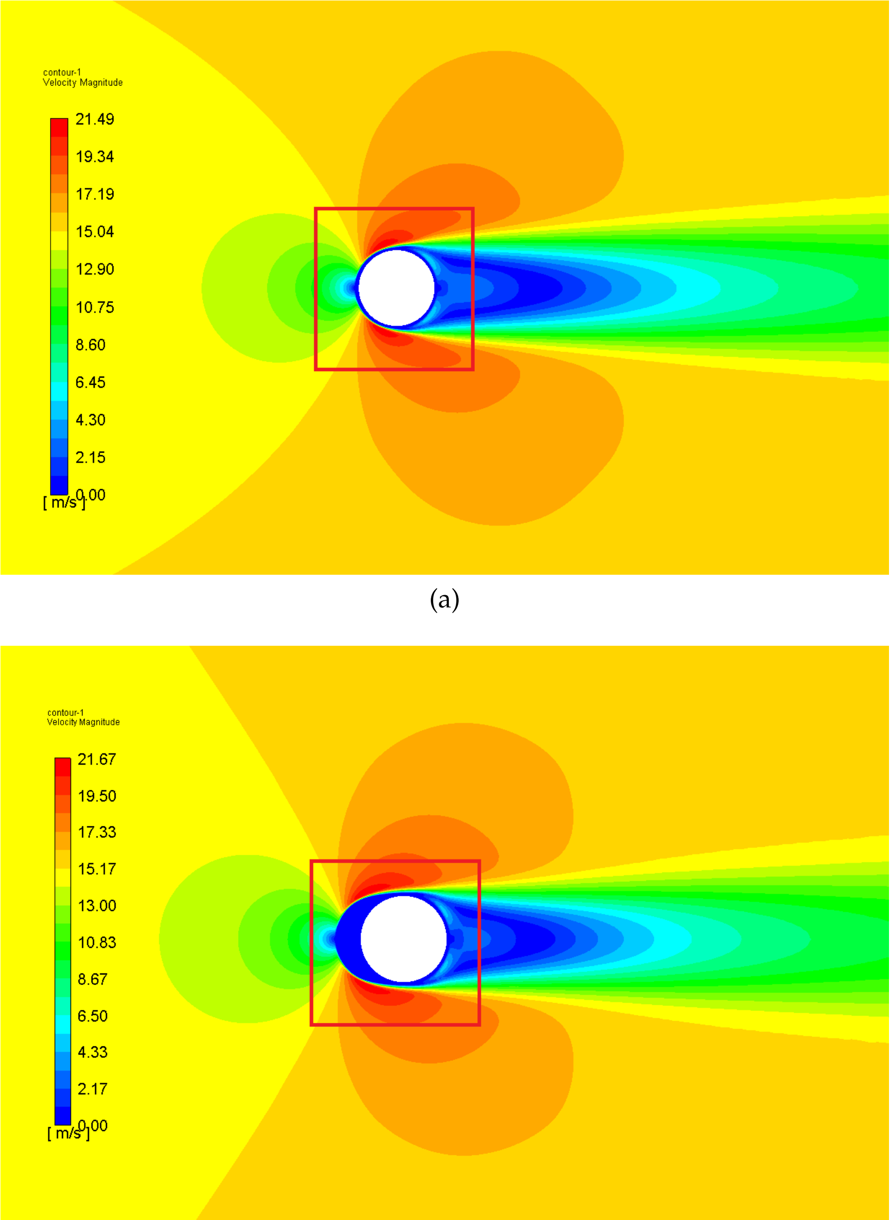

(a)

(b)

FIGURE 5.20: Predicted velocity distribution near the tube: (a) Deposit time for 0h; (b) Deposit time for 84h.

5.3.4 Comparison of the present method and mass re-distribution technique

The mass re-distribution method mentioned in section 2.2.4 is also employed in the same simulation case described in section 5.3.3. Figure 5.21 shows the predicted ash deposition for coal air combustion during the 72h period. It is noted that when the mass re-distribution method was employed, the deposition surface became uneven at a deposit time of 48h. The situation deteriorates when the deposit time is progressed to 72h. This is mainly because of the random turbulence effect on the ash particle motion. In addition, the tracked particle count is not large enough. A given face may not collect any ash particle during a simulation, while the neighbouring faces may have collected several particles. The difference between the collected mass on the neighbouring faces would accumulate as the deposit time increases. Also, the motion of each node on the interface is calculated from the collected mass from one face. Although the mass re-distribution method is used once in the simulation, it is still not enough to obtain a smooth mass distribution. García Pérez, Vakkilainen, and Hyppänen (2015) even used 10 iterations of this mass re-distribution method to have a smooth resulting mass distribution. The uneven deposition surface could increase the risk of negative volume occurring during the simulation, which then causes the failure of the CFD package.

In contrast, the predicted ash deposition surface remains very smooth during the whole 72h when the present method was employed. The reason is that the ash particles are injected at the central region (discussed in section 5.1.2), thus more particles can be tracked in front of the tube, which will reduce the effect of the random turbulence motion. Also, the motion of each node on the interface is calculated from the average collected mass from its two adjacent faces. This could absorb the difference between the collected mass on the neighbouring faces. In addition, the mass re-distribution

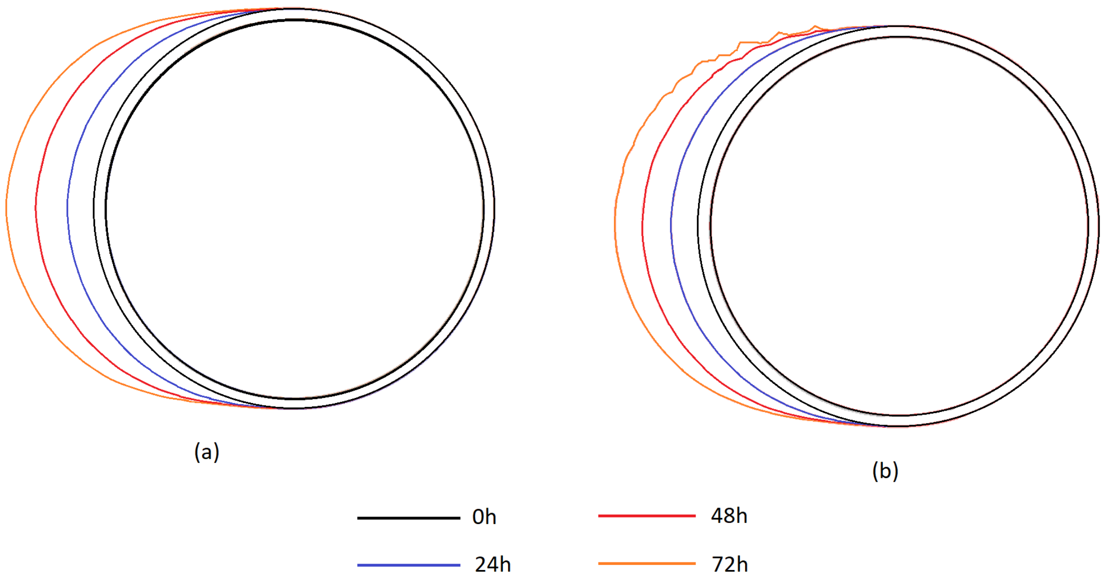

FIGURE 5.21: Predicted long term ash deposition for coal air case through different methods: (a) The present method, (b) The mass re-distribution method.

method cannot be employed in the parallel FLUENT (García Pérez, 2016; García Pérez, Vakkilainen, and Hyppänen, 2015), so it takes three times longer time than the case in which the present method is used. Longer simulation time would cost if several iterations of the mass re-distribution method are employed in the simulation.

5.4 Conclusion

Ash deposition formation for the EI Cerrejon coal (coal) and the recycled wood (biomass) air combustion cases has been investigated through CFD methods in this chapter. A new simulation method, combining with dynamic mesh, discrete phase model and mesh partition method, is developed in the parallel ANSYS FLUENT to simulate the accurate and smooth change of the deposit surface during the ash deposition processes. In the pilot-scale furnace, the predicted deposition rate for the biomass air combustion case is much higher than it is for the coal air combustion. The effect of flue gas velocity is also investigated. The results show that the increase of the flue gas velocity leads to the increase of the ash deposition rate in the coal air combustion case. And the ash deposition rate decreases in the biomass air combustion case with increasing flue gas velocity. The particle impaction efficiency increases from approximately 2.6% to 50% for coal and 15.4% to 75% for biomass while the sticking efficiency decreases from 77% to 25% for coal and 38% to 1% for biomass with the increasing of the flue gas velocity. Additionally, the effect of the deposition shape change has also been investigated. It is noted that due to the change of the velocity distribution around tube caused by the change of the deposition shape, the ash particles accumulate at the tube position $\alpha = 180^\circ$. The average normal velocity of the particles to the face that particles are hitting decreases at position $90^\circ - 160^\circ$ and $200^\circ - 270^\circ$ with the change of the deposition shape, while the sticking efficiency increases. The average predicted deposition rate and overall sticking efficiency remain almost constant is mainly because the deposition temperature remains the same when predicting the ash deposition on the uncooled tube. And this simulation method has more steady simulation smoother change of the deposition shape and takes one third of time when compared to the current mass re-distribution method.

Chapter 6

CFD prediction of the ash deposition growth in Zhundong lignite combustion

This chapter discusses the CFD predictions of the ash deposition growth in the Zhundong lignite combustion by using the dynamic ash deposition growth model discussed in Chapter 3 and Chapter 5. The Zhundong lignite originates mostly from the Xinjiang province in China, and it is one of the low rank coals that is widely being employed in the Chinese power plants. However, this lignite has a serious slagging and fouling problem when burnt in the boilers. In the experiments from Zhou et al. (2013), which concern the measurement of the slagging formation on a 300 kW pilot-scale test furnace, the ash deposit composition is identified to compose mostly of SiO_2, Al_2O_3 and Fe_2O_3, and are regarded to play a crucial role in the deposit formation process. The thickness evolution on the deposition probe is obtained by a digital image technique and is found to vary approximately linearly with respect to time until erosion occurred. This set of information is ideal to carry out a validation calculation of the current method because the experimental thickness measurement is readily available. Note the experimental data from PACT does not contain the thickness measurement.

6.1 Case Settings

Following Yang et al. (2017b), the computational domain is a 2D geometry with a tube of diameter 40 mm placed in the central region as is shown in Figure 6.1. The length of this computational domain is 700 mm with a width of 350 mm (Yang et al., 2017b). The unstructured mesh is used and the computational domain is consisting of solid and fluid zones. Triangular grids are used in the computational domain excluding the deposit-flow region in order to apply the dynamic mesh method. Meanwhile, quadrilateral grids are deployed surrounding the deposit-flow interface in order to accurately resolve the flow field within the boundary layers of this deposition surface. The ash particles are assumed to be uniformly distributed at the inlet and they are injected from a span of 80 mm (twice as the diameter 40 mm of the tube) along the inlet boundary in order to reduce the number of particles.

ANSYS FLUENT version 19.2 has been employed to predict the ash deposition formation of Zhundong lignite combustion. The software is combined with in-house developed UDFs. The realizable $k - \epsilon$ model is incorporated to simulate the effect of turbulence and the Discrete Ordinate model is used for the radiation heat transfer. Finally, the Discrete Phase Model (DPM) is used for the ash particle tracking. The DRW model is also applied to simulate the effect of turbulence on the ash particles. In addition, the particle sticking model and the ash deposition growth model are employed to predict the ash particle sticking behaviour and the ash deposition growth (see Chapter 3 and Chapter 5). The same mesh setting is used as in section 5.2.1 with the medium mesh being selected as a default. The interface contains 200 faces and ten layers of quadrilateral cells with size 0.1 mm are distributed around the tube in the simulation.

The flue gas boundary conditions of the Zhundong lignite combustion

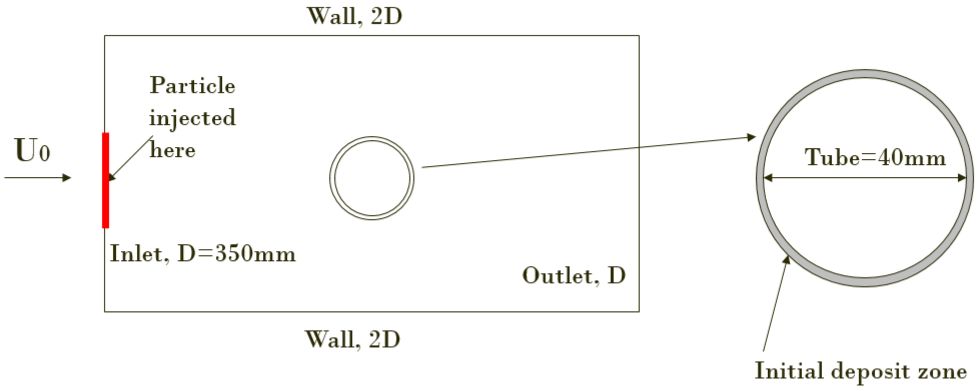

FIGURE 6.1: Schematic diagram of computational domain in Zhundong lignite combustion case (Yang et al., 2017b).

case are shown in Table 6.1. To validate the simulation, the experiment conducted by Zhou et al. (2013) is selected for the validation case. In the experiment, a flow rate of 1.153 g/s was used for the ash particle and they were injected at a speed of 2.8 m/s from an inlet. The ash particle size ranged between 1 µm and 60 µm with a mean diameter of 16 µm and a spread parameter of 0.7 based on the Rosin-Rammler distribution, which indirectly results from the original coal particle size distribution and the ash content (Zhou et al., 2013; Yang et al., 2017b). Table 6.2 is the fuel properties of the Zhundong lignite in the dried basis.

Boundary conditions		Zhundong lignite case
Inlet (flue gas presents as mole fraction)	Velocity (m/s)	2.8
	Temperature (K)	1543
	O_2	0.05
	H_2O	0.026
	CO_2	0.166
	N_2	0.758
Wall	Temperature (K)	1543
Tube	Adiabatic wall (heat flux = 0)	
Outlet	Pressure outlet	

TABLE 6.1: The flue gas boundary conditions for Zhundong lignite combustion cases in the CFD simulation (Yang et al., 2017b).

Ash composition(wt.%)		Proximate analysis (wt.%) (db)	
SiO_2	35.08	Volatiles	32.79
Al_2O_3	14.04	Fixed carbon	52.91
Fe_2O_3	6.07	Ash	12.3
CaO	27.78	HHV (MJ/kg) (db)	54.01
MgO	4.73	Ultimate analysis (wt.%)	
K_2O	0.48	C	64.07
Na_2O	8.31	H	3.58
TiO_2	0.71	O	19.22
SO_3	2.8	N	0.65

TABLE 6.2: Fuel properties of the Zhundong lignite (Zhou et al., 2013).

6.2 Results and discussions

Figure 6.2a shows the ash deposition shape on the tube of the Zhundong lignite after 2h. The inner red circle is the tube and the outer red circle is the deposition surface. The light grey zone is the ash deposition. A smooth deposition surface is observed by using the same simulation methods (discussed in Chapter 3 and Chapter 5). Additionally, Figure 6.2b shows the comparison of the deposit thickness at the tube position $\alpha = 180°$ between the predicted results and the experimental data (Yang et al., 2017b). The blue line corresponds to the predicted result with the porosity parameter $\varepsilon_{\text{deposit}} = 0.6$. For this value of the porosity, the line slightly over-predicts the thickness for times greater than 20 minutes. However, decreasing the porosity parameter to 0.5 results in a much better agreement with the experimental measurements for larger times as indicated by the yellow line in Figure 6.2b. Clearly, the value of $\varepsilon_{\text{deposit}}$ plays an important role in determining the correct thickness distribution of the deposition. In principle, however, the deposit porosity can vary depending on the deposit temperature and its chemical composition. For example, experimental findings suggest that the porosity of the inner layer of potassium salt may be as high as 0.9(Robinson et al., 2001) while a deposit consisting of coarse weakly sintered silicate particles typically has a porosity of around 0.6 (Richards, Slater, and Harb, 1993). Unfortunately, the porosity of the Zhundong lignite is still not well researched in the current literature, therefore an approximate value can only be inferred from other chemicals that share a similar composition at a similar deposition condition. For instance, Table 6.2 shows that the Zhundong lignite ash mainly consists of SiO_2 (accounting approximately 35% of the ash composition), which is chemically similar to the sintered silicate ash particle used in Richards, Slater, and Harb (1993) accounting approximately 37% of the ash content. Thus, it is reasonable to justify the choice for the porosity used in this study as a first approximation. To account for the temperature variation on $\varepsilon_{\text{deposit}}$, a simple correlation based on the ratio of the liquid to the solid volumes can be employed (Kær, Rosendahl, and Baxter, 2006). More specifically, let V_{liquid} and V_{solid} denote the volume of the liquid and solid phase respectively, then the porosity is given as:

$$\varepsilon_{\text{deposit}} = 1 - \left[(1-\varepsilon_0) + \frac{V_{\text{liquid}}}{V_{\text{solid}}} (1-\varepsilon_0) \right] \tag{6.2.1}$$

where ε_0 is the initial deposit porosity. The effect of the deposition temperature is to alter the volume fraction of the liquid and solid phases. The current study assumes that the volume of the liquid phase is negligible compared to the solid phase, which is applicable in high temperature applications. Thus, a constant value can be used instead for the present simulation. The effect of deposition temperature is left for future investigation.

6.3 Conclusion

This chapter presents the dynamic CFD simulation of the ash deposition growth in Zhundong lignite combustion with the new approach discussed

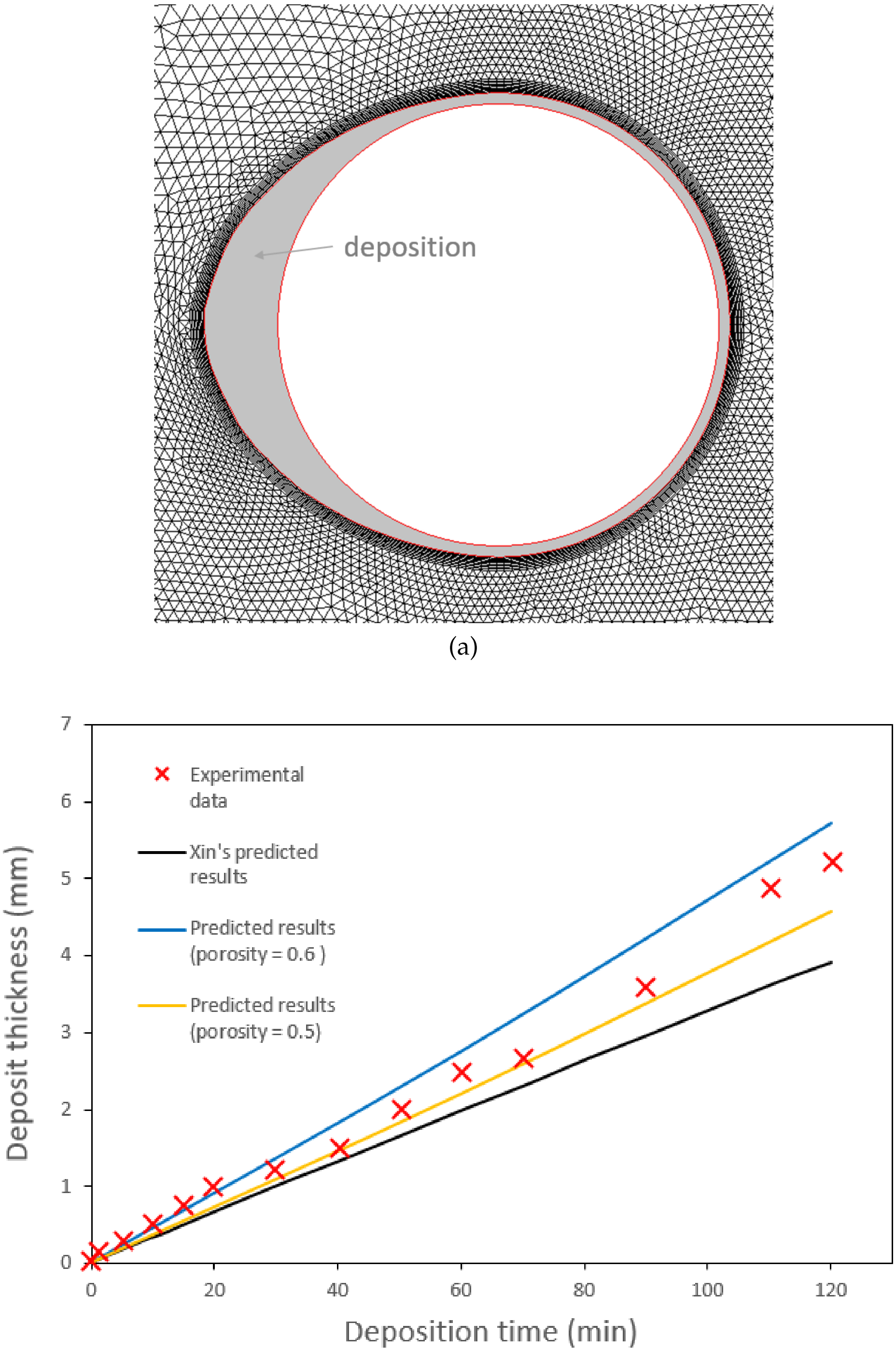

(a)

(b)

FIGURE 6.2: (a) Predicted ash deposition on the tube of Zhundong lignite combustion after 2h; (b) Comparison of the deposit thickness between the predicted results and the experimental data (Yang et al., 2017b) as a function of the deposition time.

in Chapter 3 and Chapter 5. A smooth deposition shape is obtained with the employment of this simulation method. The predicted results is close to the experimental data, although the predicted deposit thickness shows a slightly higher growth rate compared to the experimental data when the $\varepsilon_{\text{deposit}}$ is set as 0.6. However, decreasing the porosity to 0.5 results in a much better agreement with the experimental measurements.

Chapter 7

Conclusions and future work

In the foreseeable future, it is anticipated that the use of pulverized solid fuel will continue to grow. Technologies that utilized pulverized solid fuel as a co-firing fuel will prove indispensable to meet electricity demands as well as to combat the ever-increasing thread of global warming, especially in countries where fossil fuels remain the majority of energy source. However, changing fuel mixture to be used in boiler results in the production of a radical ash deposition behaviour. Thus deposition issues remain the major bottleneck in improving the efficiency of existing combustion system that utilizes solid fuel either in co-firing or coal blending mode. Understanding how such a process evolves is critical in designing, maintaining and operating a sustainable combustion system. However, the ash deposition formation remains a very complex process in the furnace, which involves physical and chemical processes that account for: ash-forming, transporting, sticking and consolidating. Each of which is a non-linear process that requires a careful analysis of the temperature-time history of the fuel particles. For this purpose, the CFD approach is regarded as the most versatile method to simulate those phenomena to a high degree of accuracy.

In CFD methods, it is significant to predict the ash particle impaction and sticking behaviours in order to estimate the ash deposition formation accurately. In this thesis, a new approach has been developed to predict the growth of the ash deposition. The Discrete Phase Model and the Discrete

Random Walk model are employed to track the fly ash particles accurately. The particle sticking model, based on an energy conservation analysis, is developed and proposed. This sticking model takes the the particle properties relevant to the ash chemistry, particle kinetic energy and furnace operating conditions into consideration. In addition, the dynamic mesh model is applied for updating the mesh as the ash deposition grows. This new simulation method is also combined with the mesh partition mesh and developed in the parallel ANSYS FLUENT to simulate the accurate and smooth change of the deposit surface during the ash deposition processes.

Ash deposition formation for the EI Cerrejon coal (coal) and the recycled wood (biomass) air combustion cases has been investigated through CFD methods in Chapter 5. A novel ash deposit growth model is developed to dynamically predict the formation of ash deposition during coal and biomass air combustion. It is noted that the predicted deposit rate matches the experimental data. In the pilot-scale furnace, the predicted deposition rate for the biomass air combustion case is much higher than it for the coal air combustion. The effect of flue gas velocity is also investigated. The results show that the increase of the flue gas velocity leads to the increase of the ash deposition rate in the coal air combustion case. And the ash deposition rate decreases in the biomass air combustion case when increased the flue gas velocity. Additionally, the effect of the deposition shape change has also been investigated. It is noted that due to the change of the velocity distribution around tube caused by the change of the deposition shape, the ash particles accumulate at the tube position $\alpha = 180^{\circ}$. And this simulation method has more steady simulation smoother change of the deposition shape and takes one third of time when compared to the current mass re-distribution method.

Dynamic CFD simulation of the ash deposition growth in Zhundong lignite combustion is presented in Chapter 6. A smooth deposition shape is obtained with the employment of this simulation method. The predicted results is close to the experimental data, although the predicted deposit thickness shows a slightly higher growth rate compared to the experimental data when the $\varepsilon_{\text{deposit}}$ is set as 0.6. However, decreasing the porosity to 0.5 results that the predicted deposit thickness has a slightly lower growth rate compared to the experimental measurements.

7.1 Some recommendations for future work

Currently, the dynamic simulation based on the CFD methods are applied to predict the ash deposit growth on an uncooled tube. The temperature of the deposition surface is treated as the same as that of the furnace temperature. So the effect of the temperature of the deposition surface is not considered. When predicting the ash deposition growth on a cooled tube, the deposit surface temperature would change. Additionally, the porosity of the ash deposition will also change as the deposition grows. Therefore, a further development of dynamic ash deposition growth model is suggested to employed to predict the ash deposition processes on a cool tube and take the change of the temperature of the deposition surface and the porosity of the ash deposition into account.

During the simulation, the numbers of the tracked ash particles are finite. But in a real boiler, the ash particles are assumed to be uniformly distributed. Therefore, the further development of the effect of the numbers of the tracked ash particles is suggested.

For the current ash deposition prediction, 2D geometry is considered. It is important to explore the current ash deposition growth model to 3D geometry, which is more similar to the ash deposition behaviours in the real boilers.

Ash shedding is another significant physical phenomenon in the later stage of the ash deposition formation. But the ash shedding is not considered in the current simulation. Therefore, a further development of the ash shedding sub-model in the ash deposition model is suggested.

Bibliography

Abbasi, Tasneem and S. A. Abbasi (2010). “Biomass energy and the environmental impacts associated with its production and utilization”. In: *Renewable and Sustainable Energy Reviews* 14.3, pp. 919–937. ISSN: 1364-0321. DOI: `10.1016/J.RSER.2009.11.006`.

Ai, Weiguo and John M. Kuhlman (2011). “Simulation of coal ash particle deposition experiments”. In: *Energy and Fuels* 25.2, pp. 708–718. ISSN: 08870624. DOI: `10.1021/EF101294F/ASSET/IMAGES/LARGE/EF-2010-01294F_0008.JPEG`. URL: `https://pubs.acs.org/doi/full/10.1021/ef101294f`.

Akar, Gul et al. (2013). “Characterization of ash deposits from the boiler of Yenikoy coal-fired power plant, Turkey”. In: *International Journal of Coal Geology* 105, pp. 85–90. ISSN: 0166-5162. DOI: `10.1016/J.COAL.2012.12.001`.

ANSYS Inc. (2017). “ANSYS FLUENT User Guide”. In: *ANSYS Fluent User's Guide* 18.2, p. 2974.

— (2020). “ANSYS FLUENT Theory Guide”. In: *ANSYS Inc., USA* 15317.November, pp. 419–541.

Black, Alexander John (2014). “Oxy-fuel combustion for carbon capture using computational fluid dynamics”. PhD thesis.

B.P. Statistical Review (2020). “Stratistical Review of World Energy”. In: *Statistical Review of World Energy* vol. 67, pp. 1–56. ISSN: 0300-3604. URL: `bp.com/statisticalreview`.

Brach, Raymond M and Patrick F Dunn (1992). “A Mathematical Model of the Impact and Adhesion of Microsphers”. In: *Aerosol Science and Technology* 16.1, pp. 51–64. ISSN: 1521-7388. DOI: `10.1080/02786829208959537`. URL: `https://www.tandfonline.com/action/journalInformation?journalCode=uast20`.

Bradley Adams et al. (1985). “Mineral impurities in coal combustion: behavior, problems, and remedial measures”. In: DOI: `10.2172/1015460`. URL: `http://www.osti.gov/servlets/purl/1015460-vxUeVx/`.

Bryers, Richard W. (1996). “Fireside slagging, fouling, and high-temperature corrosion of heat-transfer surface due to impurities in steam-raising fuels”. In: *Progress in Energy and Combustion Science* 22.1, pp. 29–120. ISSN: 0360-1285. DOI: `10.1016/0360-1285(95)00012-7`.

Cai, Yongtie et al. (2018). “Modeling of ash formation and deposition processes in coal and biomass fired boilers: A comprehensive review”. In: *Applied Energy* 230, pp. 1447–1544. ISSN: 0306-2619. DOI: `10.1016/J.APENERGY.2018.08.084`.

Chen, Gang. (2012). *Guo lu yuan li*. Hua zhong ke ji da xue chu ban she. ISBN: 9787560974989.

Chen, Lei, Ph. D. Massachusetts Institute of Technology (2013). “Computational fluid dynamics simulations of oxy-coal combustion for carbon capture at atmospheric and elevated pressures”. PhD thesis. URL: `https://dspace.mit.edu/handle/1721.1/81694`.

Degereji, M. U. et al. (2012). “Prediction of ash slagging propensity in a pulverized coal combustion furnace”. In: *Fuel* 101, pp. 171–178. ISSN: 00162361. DOI: `10.1016/j.fuel.2010.12.038`.

Doshi, V. et al. (2009). “Development of a modeling approach to predict ash formation during co-firing of coal and biomass”. In: *Fuel Processing Technology* 90.9, pp. 1148–1156. ISSN: 0378-3820. DOI: `10.1016/J.FUPROC.2009.05.019`.

Falcone, S. K. et al. (1984). "Mineral transformations during ashing and slagging of selected low-rank coals". In: *Annual meeting of the American Nuclear Society*. URL: `https://www.osti.gov/biblio/5141881`.

Fei, Yang (2015). "Computational Fluid Dynamics and Process Co-simulation Applied to Carbon Capture Technologies". PhD thesis.

Garba, Mohammed Umar (2012). "Prediction of ash deposition for biomass combustion and coal/biomass co-combustion". PhD thesis. Leeds University Library, pp. 130–140. URL: `http://etheses.whiterose.ac.uk/4373/1/PredictionofAshDepositionforBiomassCombustionandCoal%26BiomassCo-combustion.pdf`.

Garba, M.U. et al. (2013). "Modelling of deposit formation and sintering for the co-combustion of coal with biomass". In: *Fuel* 113, pp. 863–872. ISSN: 0016-2361. DOI: `10.1016/J.FUEL.2012.12.065`.

García Pérez, Manuel (2016). "Modeling the effects of unsteady flow patterns on the fireside ash fouling in tube arrays of kraft and coal-fired boilers". PhD thesis. ISBN: 9789523350007.

García Pérez, Manuel, Esa Vakkilainen, and Timo Hyppänen (2015). "2D dynamic mesh model for deposit shape prediction in boiler banks of recovery boilers with different tube spacing arrangements". In: *Fuel* 158, pp. 139–151. ISSN: 00162361. DOI: `10.1016/j.fuel.2015.04.074`.

— (2016). "Fouling growth modeling of kraft recovery boiler fume ash deposits with dynamic meshes and a mechanistic sticking approach". In: *Fuel* 185, pp. 872–885. ISSN: 00162361. DOI: `10.1016/j.fuel.2016.08.045`.

Greifzu, Franziska et al. (2016). "Assessment of particle-tracking models for dispersed particle-laden flows implemented in OpenFOAM and ANSYS FLUENT". In: *Engineering Applications of Computational Fluid Mechanics* 10.1, pp. 30–43. ISSN: 1994-2060. DOI: `10.1080/19942060.2015.1104266`. URL: `https://www.tandfonline.com/doi/abs/10.1080/19942060.2015.`

1104266https://www.tandfonline.com/doi/full/10.1080/19942060.2015.1104266.

Hansen, Lone A., Flemming J. Frandsen, and Kim Dam-Johansen (2005). "Ash Fusion Quantification by Means of Thermal Analysis". In: *Impact of Mineral Impurities in Solid Fuel Combustion* July 2016, pp. 181–193. DOI: 10.1007/0-306-46920-0_12.

Huang, L. Y. et al. (1996). "Prediction of ash deposition on superheater tubes from pulverized coal combustion". In: *Fuel* 75.3, pp. 271–279. ISSN: 00162361. DOI: 10.1016/0016-2361(95)00220-0.

Huynh, Hung Ngoc (2018). "Radiation Simulation for Air and Oxy-fuel Combustion using Computational Fluid Dynamics". PhD thesis.

Kær, S. K., L. A. Rosendahl, and L. L. Baxter (2006). "Towards a CFD-based mechanistic deposit formation model for straw-fired boilers". In: *Fuel* 85.5-6, pp. 833–848. ISSN: 0016-2361. DOI: 10.1016/J.FUEL.2005.08.016.

Leppänen, A. et al. (2014). "Numerical modeling of fine particle and deposit formation in a recovery boiler". In: *Fuel* 129, pp. 45–53. ISSN: 00162361. DOI: 10.1016/j.fuel.2014.03.046.

Li, Bingzhi, Anders Brink, and Mikko Hupa (2009). "CFD investigation of deposition in a heat recovery boiler: Part II - Deposit growth modelling". In: *Progress in Computational Fluid Dynamics* 9.8, pp. 453–459. ISSN: 14684349. DOI: 10.1504/PCFD.2009.027763.

— (2013). "CFD investigation of slagging on a super-heater tube in a kraft recovery boiler". In: *Fuel Processing Technology* 105, pp. 149–153. ISSN: 0378-3820. DOI: 10.1016/J.FUPROC.2011.08.007.

Li, Gengda et al. (2015). "Fine particulate formation and ash deposition during pulverized coal combustion of high-sodium lignite in a down-fired furnace". In: *Fuel* 143, pp. 430–437. ISSN: 00162361. DOI: 10.1016/j.fuel.2014.11.067. URL: http://dx.doi.org/10.1016/j.fuel.2014.11.067.

Lokare, Shrinivas S. et al. (2006). "Investigation of ash deposition rates for a suite of biomass fuels and fuel blends". In: *Energy and Fuels* 20.3, pp. 1008–1014. ISSN: 08870624. DOI: `10.1021/EF050410E/ASSET/IMAGES/LARGE/EF050410EF00012.JPEG`. URL: `https://pubs.acs.org/doi/full/10.1021/ef050410e`.

Loo, Sjaak van and Jaap Koppejan (2012). *The handbook of biomass combustion and co-firing*. Taylor and Francis, pp. 1–442. ISBN: 9781136553783. DOI: `10.4324/9781849773041/HANDBOOK-BIOMASS-COMBUSTION-CO-FIRING-JAAP-KOPPEJAN-SJAAK-VAN-LOO`. URL: `https://www.taylorfrancis.com/books/mono/10.4324/9781849773041/handbook-biomass-combustion-co-firing-jaap-koppejan-sjaak-van-loo`.

McKendry, Peter (2002). "Energy production from biomass (part 1): Overview of biomass". In: *Bioresource Technology* 83.1, pp. 37–46. ISSN: 09608524. DOI: `10.1016/S0960-8524(01)00118-3`.

McLennan, A. R. et al. (2000). "An experimental comparison of the ash formed from coals containing pyrite and siderite mineral in oxidizing and reducing conditions". In: *Energy and Fuels* 14.2, pp. 308–315. ISSN: 08870624. DOI: `10.1021/EF990092H/ASSET/IMAGES/LARGE/EF990092HF00005.JPEG`. URL: `https://pubs.acs.org/doi/full/10.1021/ef990092h`.

Mills, Kenneth C. and Jeffrey M. Rhine (1989). "The measurement and estimation of the physical properties of slags formed during coal gasification: 2. Properties relevant to heat transfer". In: *Fuel* 68.7, pp. 904–910. ISSN: 0016-2361. DOI: `10.1016/0016-2361(89)90128-2`.

Mu, Lin, Liang Zhao, and Hongchao Yin (2012). "Modelling and measurements of the characteristics of ash deposition and distribution in a HRSG of wastewater incineration plant". In: *Applied Thermal Engineering* 44, pp. 57–68. ISSN: 1359-4311. DOI: `10.1016/J.APPLTHERMALENG.2012.03.039`.

Mueller, Christian et al. (2005). “Deposition behaviour of molten alkali-rich fly ashes—development of a submodel for CFD applications”. In: *Proceedings of the Combustion Institute* 30.2, pp. 2991–2998. ISSN: 1540-7489. DOI: `10.1016/J.PROCI.2004.08.116`.

Płaza, Piotr Patryk (2013). “The Development of a Slagging and Fouling Predictive Methodology for Large Scale Pulverised Boilers Fired with Coal / Biomass Blends By”. In: *Cardiff School of Engineering* July 2013, p. 227.

Richards, Galen H., Peter N. Slater, and John N. Harb (1993). “Simulation of Ash Deposit Growth in a Pulverized Coal-Fired Pilot Scale Reactor”. In: *Energy and Fuels* 7.6, pp. 774–781. ISSN: 15205029. DOI: `10.1021/EF00042A012/ASSET/EF00042A012.FP.PNG_V03`. URL: `https://pubs.acs.org/doi/abs/10.1021/ef00042a012`.

Robinson, Allen L et al. (2001). “Experimental Measurements of the Thermal Conductivity of Ash Deposits: Part 2. Effects of Sintering and Deposit Microstructure”. In: DOI: `10.1021/ef0000375`. URL: `https://pubs.acs.org/sharingguidelines`.

Rushdi, A. et al. (2005). “Mechanistic prediction of ash deposition in a pilot-scale test facility”. In: *Fuel* 84.10, pp. 1246–1258. ISSN: 0016-2361. DOI: `10.1016/J.FUEL.2004.08.027`.

Saidur, R. et al. (2011). “A review on biomass as a fuel for boilers”. In: *Renewable and Sustainable Energy Reviews* 15.5, pp. 2262–2289. ISSN: 13640321. DOI: `10.1016/j.rser.2011.02.015`. URL: `http://dx.doi.org/10.1016/j.rser.2011.02.015`.

Smith, I. W. (1982). “The combustion rates of coal chars: A review”. In: *Symposium (International) on Combustion* 19.1, pp. 1045–1065. ISSN: 0082-0784. DOI: `10.1016/S0082-0784(82)80281-6`.

Srinivasachar, S. et al. (1992). "A fundamental approach to the prediction of coal ash deposit formation in combustion systems". In: *Symposium (International) on Combustion* 24.1, pp. 1179–1187. ISSN: 0082-0784. DOI: `10.1016/S0082-0784(06)80139-6`.

Taha, Taha J. et al. (2013). "CFD modeling of ash deposition for co-combustion of MBM with coal in a tangentially fired utility boiler". In: *Fuel Processing Technology* 114, pp. 126–134. ISSN: 0378-3820. DOI: `10.1016/J.FUPROC.2013.03.042`.

Thy, Peter et al. (2006). "Compositional constraints on slag formation and potassium volatilization from rice straw blended wood fuel". In: *Fuel Processing Technology* 87.5, pp. 383–408. ISSN: 03783820. DOI: `10.1016/j.fuproc.2005.08.015`.

Tortosa Masiá, A. A. et al. (2007). "Characterising ash of biomass and waste". In: *Fuel Processing Technology* 88.11-12, pp. 1071–1081. ISSN: 03783820. DOI: `10.1016/j.fuproc.2007.06.011`.

Vassilev, Stanislav V. et al. (2010). "An overview of the chemical composition of biomass". In: *Fuel* 89.5, pp. 913–933. ISSN: 00162361. DOI: `10.1016/j.fuel.2009.10.022`. URL: `http://dx.doi.org/10.1016/j.fuel.2009.10.022`.

— (2013). "An overview of the composition and application of biomass ash. Part 1. Phase-mineral and chemical composition and classification". In: *Fuel* 105, pp. 40–76. ISSN: 00162361. DOI: `10.1016/j.fuel.2012.09.041`. URL: `http://dx.doi.org/10.1016/j.fuel.2012.09.041`.

Versteeg, H K et al. (2007). *An Introduction to Computational Fluid Dynamits Second Edition*. ISBN: 13: 9780131274983.

Walsh, Peter M. et al. (1990). "Deposition of bituminous coal ash on an isolated heat exchanger tube: Effects of coal properties on deposit growth". In: *Progress in Energy and Combustion Science* 16.4, pp. 327–345. ISSN: 03601285. DOI: `10.1016/0360-1285(90)90042-2`.

Wang, Huafeng and John N. Harb (1997). "Modeling of ash deposition in large-scale combustion facilities burning pulverized coal". In: *Progress in Energy and Combustion Science* 23.3, pp. 267–282. ISSN: 03601285. DOI: `10.1016/s0360-1285(97)00010-5`.

Weber, Roman et al. (2013a). "Fly ash deposition modelling: Requirements for accurate predictions of particle impaction on tubes using RANS-based computational fluid dynamics". In: *Fuel* 108, pp. 586–596. ISSN: 0016-2361. DOI: `10.1016/J.FUEL.2012.11.006`.

Weber, Roman et al. (2013b). "On predicting the ash behaviour using Computational Fluid Dynamics". In: *Fuel Processing Technology* 105, pp. 113–128. ISSN: 03783820. DOI: `10.1016/j.fuproc.2011.09.008`. URL: `http://dx.doi.org/10.1016/j.fuproc.2011.09.008`.

Wieland, Christoph et al. (2012). "Evaluation, comparison and validation of deposition criteria for numerical simulation of slagging". In: *Applied Energy* 93, pp. 184–192. ISSN: 0306-2619. DOI: `10.1016/J.APENERGY.2011.12.081`.

Yang, Xin (2017). "Development of Ash Deposition Prediction Models through the CFD Methods and the Ash Deposition Indice". PhD thesis. URL: `http://etheses.whiterose.ac.uk/17127/`.

Yang, Xin, Hao Zhou, and Hao Wu (2022). "CFD modelling of biomass ash deposition under multiple operation conditions using a 2D mass-conserving dynamic mesh approach". In: *Fuel* 316, p. 123250. ISSN: 0016-2361. DOI: `10.1016/J.FUEL.2022.123250`.

Yang, Xin et al. (2016). "Predicting ash deposition behaviour for co-combustion of palm kernel with coal based on CFD modelling of particle impaction and sticking". In: *Fuel* 165, pp. 41–49. ISSN: 00162361. DOI: `10.1016/j.fuel.2015.10.056`. URL: `http://dx.doi.org/10.1016/j.fuel.2015.10.056`.

Yang, Xin et al. (2017a). “Ash deposition propensity of coals/blends combustion in boilers: A modeling analysis based on multi-slagging routes”. In: *Proceedings of the Combustion Institute* 36.3, pp. 3341–3350. ISSN: 15407489. DOI: 10.1016/j.proci.2016.06.060. URL: http://dx.doi.org/10.1016/j.proci.2016.06.060.

Yang, Xin et al. (2017b). “Understanding the ash deposition formation in Zhundong lignite combustion through dynamic CFD modelling analysis”. In: *Fuel* 194, pp. 533–543. ISSN: 00162361. DOI: 10.1016/j.fuel.2017.01.026. URL: http://dx.doi.org/10.1016/j.fuel.2017.01.026.

Yang, Xin et al. (2018). “Prediction of the radiative heat transfer in small and large scale oxy-coal furnaces”. In: *Applied Energy* 211, pp. 523–537. ISSN: 0306-2619. DOI: 10.1016/J.APENERGY.2017.11.070.

Yang, Xin et al. (2019a). “Prediction of particle sticking efficiency for fly ash deposition at high temperatures”. In: *Proceedings of the Combustion Institute* 37.3, pp. 2995–3003. ISSN: 1540-7489. DOI: 10.1016/J.PROCI.2018.06.038.

Yang, Xin et al. (2019b). “Understanding the effects of oxyfuel combustion and furnace scale on biomass ash deposition”. In: *Fuel* 247, pp. 36–46. ISSN: 0016-2361. DOI: 10.1016/J.FUEL.2019.03.031.

Zbogar, Ana et al. (2009). “Shedding of ash deposits”. In: *Progress in Energy and Combustion Science* 35.1, pp. 31–56. ISSN: 03601285. DOI: 10.1016/j.pecs.2008.07.001. URL: http://dx.doi.org/10.1016/j.pecs.2008.07.001.

Zevenhoven, Maria, Patrik Yrjas, and Mikko Hupa (2010). *Ash-Forming Matter and Ash-Related Problems*. John Wiley and Sons, Ltd, pp. 493–531. DOI: 10.1002/9783527628148.hoc068. URL: https://onlinelibrary.wiley.com/doi/full/10.1002/9783527628148.hoc068https://onlinelibrary.wiley.com/doi/abs/10.1002/9783527628148.hoc068https://onlinelibrary.wiley.com/doi/10.1002/9783527628148.hoc068.

Zheng, Zhimin et al. (2020a). “Dynamic simulation on ash deposition and heat transfer behavior on a staggered tube bundle under high-temperature conditions”. In: *Energy* 190, p. 116390. ISSN: 0360-5442. DOI: `10.1016/J.ENERGY.2019.116390`.

Zheng, Zhimin et al. (2020b). “Simulating growth of ash deposit in boiler heat exchanger tube based on CFD dynamic mesh technique”. In: *Fuel* 259, p. 116083. ISSN: 0016-2361. DOI: `10.1016/J.FUEL.2019.116083`.

Zhou, Hao and Shihao Hu (2021). “Numerical simulation of ash deposition behavior with a novel erosion model using dynamic mesh”. In: *Fuel* 286, p. 119482. ISSN: 0016-2361. DOI: `10.1016/J.FUEL.2020.119482`.

Zhou, Hao et al. (2013). “Experimental Measurement of the Effective Thermal Conductivity of Ash Deposit for High Sodium Coal (Zhun Dong Coal) in a 300 KW Test Furnace”. In: DOI: `10.1021/ef4012017`. URL: `https://pubs.acs.org/sharingguidelines`.

Zhou, Hao et al. (2019). “Simulation of ash deposition in different furnace temperature with a 2D dynamic mesh model”. In: *Journal of the Energy Institute* 92.6, pp. 1743–1756. ISSN: 1743-9671. DOI: `10.1016/J.JOEI.2018.12.006`.